Université de Montréal

Structural and Biochemical Characterization of the Organomercurial Lyase MerB

Par

Haytham Mohamed Gamaleldin Wahba Abdelgawwad

Département de Biochimie

Faculté de Médecine

Thèse présentée à la Faculté de Médecine

en vue de l'obtention du grade de PhD en biochimie

June, 2016

Université de Montréal
Faculté des études supérieures

Cette thése intitulée:
Structural and Biochemical Characterization of Organomercuriallyase MerB

Présentée par:
Haytham Mohamed Gamaleldin Wahba Abdelgawwad

a été évaluée par un jury compose des personnes suivantes:

Joelle Pelletier, président-rapporteur
James Omichinski, directeur de recherche
Stephen Michnick, membre du jury
Ann M. English, examinateur externe
Rémy Sauvé, représentant du doyen de la FES

Résumé

Le mercure est présent dans l'environnement à cause de phénomènes naturels (volcans) ou des activités humaines (combustion de combustibles fossiles). Le mercure existe sous forme de mercure élémentaire (Hg^0), ionique (Hg^{II}) ou organique tel le méthylmercure (MeHg). Ces diverses formes sont en flux constant les uns avec les autres dans le cycle biogéochimique naturel. De par leur grande hydrophobicité et leur capacité à pénétrer les membranes biologiques, les composés organomercuriels contituent la forme la plus toxique de mercure retrouvée dans l'environnement Des niveaux élevés de MeHg ont d'ailleurs été détectés dans la chaire de poissons de nombreuses régions du monde. Conséquemment, une consommation de produits de la mer contaminés représente un grave danger pour la santé humaine.

Certaines bactéries isolées à partir d'environnements contaminés par le mercure ont évolué vers un système qui leur permet de convertir efficacement les composés mercuriels présents autant sous forme ionique qu'organique en un mercure élémentaire moins toxique. Cette résistance au mercure s'explique par l'acquisition d'un élément génétique connu sous le nom d'opéron mer. L'opéron mer code entre autre pour deux enzymes importants : la lyase organomercurielle MerB et la réductase mercurielle MerA. MerA catalyse la réduction du Hg^{II} conduisant à la formation du mercure élémentaire Hg^0 qui est un composé volatile et moins toxique. MerB, quant à elle, catalyse la protonolyse de la liaison carbone-mercure de composés organomercuriels pour produire un composé réduit de carbone et du mercure ionique (Hg^{II}). Au vu des effets des organomercuriels et de la réduction de Hg^{II}, MerA et MerB sont considérés comme des enzymes clés pouvant servir à la biorestauration des cours d'eau contaminés par les organomercuriels. Une compréhension claire des détails mécanistiques de la façon dont MerA et MerB fonctionnent ensemble au niveau atomique est donc cruciale dans la mise en œuvre de biotechnologies implicant l'opéron mer dans les efforts de bioremédiation.

Dans cette étude, nous avons utilisé la résonance magnétique nucléaire (RMN)et la cristallographie aux rayons X pour caractériser la structure et le mécanisme enzymatique de MerB de *E. coli*. Sur la base d'études structurales précédentes de MerB de *E. coli*, trois résidus (Cys96, Asp99 et Cys159) ont été identifiés comme constituant la triade catalytique nécessaire au clivage de la liaison carbone-Hg. En guise de suivi aux études antérieures, mon projet consiste

d'abord à utiliser la cristallographie aux rayons X afin de définir les rôles de Cys96, Asp99 et Cys159 dans la liaison du substrat et dans le clivage.

Deux approches ont été mises en œuvre pour atteindre cet objectif. Tout d'abord, les mutants MerB ont été testés pour définir le rôle des résidus catalytiques. Deuxièmement, les inhibiteurs de MerB et d'autres substrats non organicomercuriels potentiels ont été utilisés pour explorer le site actif de MerB.

Une sérine se retrouve à la position de Asp99 dans quatre variants de MerB répertoriés chez les bactéries. Pour mieux comprendre le rôle de Asp99, nous avons comparé la sérine présente dans le variants MerB de *Bacillus megaterium* (MerB2) et introduit un variant D99S à la protéine MerB du type sauvage d'*E. coli* (MerB D99S). Nous avons pu constater que la forme purifiée de MerB D99S se caractérisait par une couleur rose après avoir visualisé sa structure cristalline aux rayons X, révélant la présence d'un métal lié au niveau de son site actif. Les analyses par spectrométrie de masse à plasma à couplage inductif (ICP-MS) et par fluorescence des rayons X indiquèrent que MerB D99S se liait au cuivre au niveau du site actif. En outre, les analyses par résonance paramagnétique électronique (EPR) et des études de RMN ont identifié la forme Cu^{II} du cuivre. L'addition de substrats organomercuriels a pu déplacer le Cu^{II} entrainant ainsi une diminution de l'activité catalytique de MerB D99S. En revanche, MerB2 n'a pu être co-purifié avec le cuivre, bien que la structure aux rayons X du complexe MerB2-Hg soit pratiquement identique à la structure du complexe MerB D99S-Hg. Ceci suggère que le résidu Asp99 est essentiel au clivage des liaisons carbone-Hg de composés organiques du mercure et dirige la spécificité de la liaison au métal. De plus, la liaison cuivre-MerB D99S propose un lien possible entre l'évolution de MerB et son homologue structural, la protéine NosL.

Dans la seconde approche, nous nous sommes intéressés au site actif de MerB en testant sa liaison à des composés organostanniques et à des composés organoplombiques avec un inhibiteur de MerB connu sous le nom de triéthylétain (TET) qui se lie au résidu Asp99 sans s'associer aux cystéines du site actif. Une liaison similaire a été observée avec un autre inhibiteur à savoir le triméthylplomb (TML). Quant au diméthylétain (DMT), il inhibe MerB à l'aide d'un mécanisme alternatif en se liant d'abord à Asp99 puis à Cys96 conduisant à un changement critique dans le site actif perturbant ainsi l'interaction π-cation entre Trp95 et Arg155. D'autres inhibiteurs comme le diéthylétain (DET) et le diéthylplomb (DEL) ont été caractérisés comme étant un substrat de MerB où les deux groupes éthyle ont été clivés pour donner les produits ioniques Sn^{IV}

Pb^{IV} qui se lient au site actif de manière similaire à Hg^{II}. DMT, DET et DEL présentent une affinité pour la liaison à MerB supérieure à celle de son substrat initial MeHg. Ces résultats suggèrent que les composés organomercuriels ne sont pas les seuls substrats pour MerB et Asp99 est le premier résidu à se lier aux composés organométalliques suivis de la liaison à Cys96 et Cys159.

Ces observations suggèrent un agrandissement de l'éventail d'applications possibles pour MerB dans la bioremédiation de certains sites contaminés par des composés organométalliques tels les organoplombiques et organostanniques.

Mot-clé: Organomercuriallyase, Merb, Organoplombiques. Organostanniques, Protéine de liaison cuivre, Carbone liaison métallique clivage, Méthylmercure, Organomercuriels, Biorestauration, Résonance magnétique nucléaire, La cristallographie aux rayons X.

Abstract

Mercury is introduced into the environment from either natural occurrences (volcanoes) or from human activities (combustion of fossil fuels). Mercury exists as elemental mercury (Hg^0), ionic mercury (Hg^{II}) or organic mercury like methylmercury (MeHg) and these forms are in constant flux with each other as part of the natural biogeochemical cycle. Organomercurial compounds like MeHg are the most toxic form because of their hydrophobicity and their ability to efficiently permeate membranes and bioaccumulate in organisms. High levels of MeHg have been found in fish in many areas around the world, and therefore human consumption of contaminated seafood represents a serious danger for human health. Bacteria isolated from mercury-contaminated environments have evolved a system that allows them to efficiently convert both ionic and organic mercury compounds to the less toxic elemental mercury. The mercury resistance is due to the acquisition of a transferable genetic element known as the *mer* operon. The *mer* operon encodes for several proteins including two enzymes, the organomercurial lyase MerB and the mercuric ion reductase MerA. MerB catalyzes the protonolysis of the carbon-mercury bond of organomercurial compounds to produce a reduced-carbon compound and inorganic ionic mercury Hg^{II}. MerA catalyzes the reduction of Hg^{II} to elemental mercury Hg^0, which is volatile and less toxic. Due to their ability to cleave MeHg and reduce the resulting Hg^{II} product, MerB and MerA are considered crucial to bioremediation efforts to clean up MeHg from contaminated waterways. A clear understanding of the mechanistic details of how MerB and MerA function together at the atomic level is crucial for appropriate utilization of the *mer* system in bioremediation efforts. We have been using nuclear magnetic resonance (NMR) spectroscopy and X-ray crystallography to structurally and mechanistically characterize *E. coli* MerB. Based on previous structural studies of *E. coli* MerB, three residues (Cys96, Asp99 and Cys159) have been identified as a catalytic triad which is required for carbon-Hg bond cleavage. As a follow up to the earlier studies, my project involves using X-ray crystallography to define the roles of Cys96, Asp99 and Cys159 in substrate binding and cleavage.

Two different approaches were implemented to fulfill this goal. Firstly, MerB mutants were tested to define the role for the catalytic residues. Secondly, MerB inhibitors and other potential non-organomercurial substrates were used to probe MerB active site. The Cys,-Asp-Cys catalytic triad found in *E.coli* MerB is conserved in all MerB variants except four variants where aspartic

acid is replaced by a serine. To understand the role of Asp99, we compared a serine-containing MerB variant (*Bacillus megaterium* MerB2) and an *E. coli* MerB mutant (MerB D99S) to wild type *E. coli* MerB. Interestingly, the purified MerB D99S protein was found to contain a pink color. X-ray crystal structure indicated the presence of a bound metal in the active site of MerB D99S. Analysis by inductively coupled plasma mass spectrometry (ICP-MS) and X-ray fluorescence indicated that MerB D99S binds copper in the active site. Further, electron paramagnetic resonance (EPR) and NMR studies identified the copper as Cu^{II}. Addition of organomercurial substrate displaces bound Cu^{II} but MerB D99S shows diminished catalytic activity. In contrast, MerB2 did not co-purify with copper although the X-ray structure of MerB2-Hg complex is virtually identical to the structure of the MerB D99S-Hg. This suggests that the aspartic acid residue is crucial for the cleavage of carbon-Hg bonds of organomercurials as well as metal-binding specificity. Furthermore, the binding of copper to the MerB D99S protein suggests a possible evolutionary link between MerB and its structural homolog, the copper-binding protein NosL. In the second approach, we probed the active site of MerB through testing its binding to organotin and organolead compounds. The known MerB inhibitor triethyltin (TET) binds to Asp99 without binding to any of the active site cysteines. A similar binding has been observed with trimethylead (TML). Dimethyltin (DMT) inhibits MerB using an alternative mechanism. It first binds to Asp99 then Cys96, which induces a dramatic change in the active site by disrupting a cation-π interaction between Try95 and Arg155. In contrast, diethyltin (DET) and diethylead (DEL) were found to be substrates for MerB, where both ethyl groups were cleaved and the Sn^{IV} and Pb^{IV} products bound to the active site in a similar manner to Hg^{II}. DMT, DET and DEL show higher binding affinity to MerB than its initial substrate MeHg. These results suggest that organomercurials may not be the only substrates for MerB and Asp99 is the first residue to bind to organometals followed by subsequent binding to Cys96 and Cys159. In addition, these observations suggest that there are other possible applications for employing MerB in bioremediation of organolead and organotin contaminated sites while other organometals may have implications when using MerB in bioremediation systems.

Keyword: Organomercuriallyase, MerB, Organolead. Organotin, Copper binding protein, Carbon metal bond cleavage, Methylmercury, Organomercuriels, Bioremédiation, Nuclear magnetic resonance, X ray crystallography.

Table des matiéres

Liste des figures

Liste des abréviations

B. megaterium	*Bacillus megaterium*
B. subtillis	*Bacillus subtillis*
Bacillus sp.	*Bacillus species*
C. butyricum	*Clostridium butyricum*
C159	Cysteine 159
C96	Cysteine 96
Cu	Copper atom
D99	Aspartic acid 99
DEL	Diethyl lead
DML	Dimethyl lead
DMT	Dimethyltin
DPTA	Diethylenetriaminepenta-acetic acid
DTT	Dithiothreitol
E. coli	*Escherichia coli*
EDTA	Ethylenediaminetetraacetic acid
EPR	Electron paramagnetic resonance
EtHg	Ethylmercury
EXAFS	Extended X ray absorption fine structure
FAD	Flavin adenine dinucleotide
GSH	Glutathione
Hg	Mercury atom
Hg^0	Elemental mercury
$HgCl_2$	Mercuric chloride
Hg^I	Mercury I
Hg^{II}	Mercury II
HgO	Mercuric oxide
HgS	Mercuric sulfide
HSQC	Heteronuclear single quantum correlation
ICP-MS	Inductively coupled plasma mass spectrometry
IPTG	Isopropyl β-D-1-thiogalactopyranoside

ITC	Isothermal titration calorimetry
LB	Luria Bertani broth
MeHg	Methylmercury
MerA	Organomercurial reductase
merA	MerA gene from mer operon
MerB	*E. coli* Organomercurial lyase
merB	MerB gene from mer operon
MerB2	Organomercurial lyase 2
MerP	Periplasmic mercury transporter from mer operon
merP	MerP gene from mer operon
MerR	regulator for the mer operon
merR	MerR gene from mer operon
MerT	Mercury transporter from mer operon
merT	MerT gene from mer operon
MR-SAD	Molecular replacement - single anomalous dispersion
NADPH	Nicotinamide adenine dinucleotide phosphate
NMerA	N-terminal MerA
NMR	Nuclear magnetic resonance
NOS	Nitrous oxide reductase gene cluster
NosL	L protein from the nitrous oxide reductase (*nos*) operon
PCMB	*p*-Chloromercuribenzoate
PDB	Protein Data Bank
PHMSA	*p*-hydroxymercuric sulphonic acid
PMA	Phenylmercuric acetate
RMSD	Root mean square deviation
RNAP	RNA polymerase
SAD	Single anomalous dispersion
TBT	Tributyltin
TBT	Tetrabutyltin
TBTO	Tributyltin oxide
TEL	Triethyl lead

TETA	Triethyltin acetate
TEVT	Triethylvinyltin
TML	Trimethyl lead
TMTF	Trimethyltin fluoride
TPT	Triphenyltin
TTEL	Tetraethyl lead
TTET	Tetraethyltin
TTML	Tetramethyl
TTMT	Tetramethyltin
TVT	Tetravinyltin
UNEP	United Nation Environmental Program
UV-Vis	Ultraviolet–visible

Remerciements

First, I would like to express my sincere appreciation and thank to my supervisor Professor James Omichinski. I appreciate his contribution of time and ideas, which made my Ph.D. experience productive. He always has time to join his group frequently in the lab to give advice and share ideas. His priceless guidance helped me in all the time of research and writing of this thesis. I learned a lot from his advice on both research as well as on my career. I would like to thank Professor Omichinski also for his supportive funding in my final 2 years. I have been incredibly fortunate to have a chance to join his group. I would like to thank Professor Jurgen Sygusch for his guidance in X ray data collection strategy and processing and for giving me the opportunity for X ray data collection in National Synchrotron Light Source (NSLS-I). Without his precious support it would not be possible to conduct this research. I would like also to thank Professor Pawel Grochulski at University of Saskatchewan for allowing us to use the Macromolecular X ray crystallography facility at Canadian light source. Many thanks to Professor Pascal Legault and Professor Jacques Archambault; the members of my thesis committee, for their valuable and brilliant comments and insightful questions. Their advice, suggestions and contributions were essential for this study to be accomplished. I would like to thank each member of Omichinski group, specially Mathieu Lussier Price, Julien Lafrance-Vanasse, Laurent Cappadocia and Normand Cyr. They taught me about protein purification and several other biochemical tools during my first days in the lab. They shared their time and expertise unselfishly. The training I have received from them was essential to accomplish my study. I would like to thank also Ahmed Mansour for his contribution to this project during his intern in Omichinski lab. I gratefully acknowledge the funding sources that made my Ph.D. work possible. I was funded by Egyptian Ministry of Higher Education for my first 4 years. Special thanks to all members of Egyptian Bureau of cultural and educational Affairs in Montreal for all the support they provided during my travel and study. I am grateful to my parents and my brothers for all their love and encouragement to pursue my dreams. I have been so blessed to be joined with my wonderful wife who motivated and helped me throughout my PhD studies. Her faithful support, encouragement and patience was what sustained me throughout. She is definitely an important part of this effort. Words cannot express how grateful I am to my lovely wife.

Chapter 1: Introduction

1.1 Different forms of mercury and their toxicity

Due to its unique and attractive properties, humans have extensively employed elemental mercury and mercury-containing compounds in industry and innovation for several centuries. One drawback to the extensive application of this metal in the environment is that exposure to relatively low levels of mercury compounds is often accompanied by a potentially high risk of toxicity to either humans or other animal species. In the environment, mercury exists in many different chemical forms and the toxic effects of mercury vary according to the type of mercury present. The four main forms of mercury are Hg^0 (elemental or metallic mercury), Hg^I (mercurous), Hg^{II} (mercuric) and organomercurial compounds. Although all four forms of mercury are toxic to some degree, organomercurial compounds are generally considered to be the most toxic form followed by the three ionic forms of mercury, in the order $Hg^{II} > Hg^I > Hg^0$ (Bernhoft 2012, Syversen & Kaur 2012).

1.1.1 Metallic Mercury

Hg^0 is the only heavy metal that is known to exist in the liquid state at room temperature, but it is highly volatile. Given the high reactivity of mercury with cellular components, exposure to Hg^0 vapours through direct inhalation has been linked to several adverse effects since Hg^0 is the form of mercury most commonly encountered in the environment. Following inhalation, Hg^0 quickly enters the blood stream via the lungs and is distributed quickly throughout the entire body since it diffuses readily through cell membranes (Hursh *et al.* 1976). Acute exposure to high concentrations of Hg^0 induces bronchitis leading to dyspnea (Garnier *et al.* 1981). In contrast, chronic exposure to lower levels of Hg^0 vapours is known to produce neurological dysfunction accompanied by tremors and memory loss (Smith *et al.* 1983). Although Hg^0 represents the least toxic form of mercurial compounds, the risk to humans is the highest due to its common use in a number of industrial applications including gold mining as well as its continual persistence in the atmosphere from natural occurrences.

1.1.2 Mercurous and Mercuric Mercury

Following elemental mercury, ionic mercury salts are the next most common form of mercury compounds found in the environment and there are two oxidation states for ionic mercury salts, which are often referred to as mercurous (Hg^{I}) or mercuric (Hg^{II}). The most widely used form of Hg^{I} is as a chloride salt Hg_2Cl_2. Hg_2Cl_2 was used extensively in numerous pharmaceutical preparations up until the 1950s, and is commonly known by its trade name calomel. Although it is poorly absorbed from the intestine, long-term exposure to calomel can lead to systemic pain and discoloration of the skin. This condition is known as pink disease (acrodynia) and the mortality rate from calomel poisoning in Britain reached 1 in 10 in 1940s. Once its toxic side effects were recognized, the use of calomel in medical preparations was discontinued (Warkany 1966). Similarly, the most commonly employed Hg^{II} salt is the chloride salt $HgCl_2$, which was used extensively as either a preservative or as an antiseptic in numerous drug preparations. In particular, $HgCl_2$ was the treatment of choice for syphilis for decades before the discovery of antibiotics. As a medical treatment, $HgCl_2$ was either applied topically to infected areas or ingested as an oral medication, but its extensive use led to numerous health complications. The primary side effect following acute exposure to high levels of $HgCl_2$ is necrosis of the gut mucosa, which produces bloody diarrhea and eventually leads to either septic shock or even death in certain circumstances (Barnes *et al.* 1980). Following chronic exposure to $HgCl_2$, Hg^{II} accumulates in the kidney causing glomerulonephritis, renal tubular necrosis and ultimately renal failure (Taugner *et al.* 1966). After exposure to $HgCl_2$, Hg^{II} is transported through binding to the sulfhydryl group of glutathione. In a similar manner, Hg^{II} also targets the sulfhydryl group present in cysteine residues in cellular proteins and in many cases this can result in either a decrease or loss of cellular functions. For example, Hg^{II} accumulation in the renal tubule is the result of its ability to form a complex with the cysteine-rich protein metallothionein. In the case of metallothionein, each molecule of metallothionien has the capacity to bind several molecules of Hg^{II} and this explains how Hg^{II} is concentrated in the kidney and the resultant renal damage (Satoh *et al.* 1997, Zalups 2000).

1.1.3 Organomercurial compounds

Despite the fact that organomercurials have not been as widely used as other mercury species, they are responsible for a considerable number of human toxicities with methylmercury (MeHg) and ethylmercury (EtHg) being the two most common forms linked directly to human toxicities. Before its toxic side effects were recognized, MeHg was used extensively as a pesticide. However, MeHg is also found naturally in the environment as many microorganisms have evolved specific enzymes that convert Hg^{II} into MeHg, including several different bacterial species (Ullrich *et al.* 2001, Clarkson 2002). Although the exact physiological reason for why these microorganisms convert Hg^{II} into MeHg is currently unknown, it serves as a continual source for introducing it into the environment. Due to its lipophilicity, MeHg has the capacity to bioaccumulate within the food chain and through this mechanism represents a constant concern to human health. The most common form of human exposure to MeHg comes from eating seafood (fish and shellfish) containing elevated levels of MeHg. Following the consumption of contaminated food, MeHg is efficiently absorbed from the intestinal tract and distributed to fat tissue throughout the body (Leaner & Mason 2002).

MeHg is the ultimate neurotoxic agent due to its ability to effectively target the neurological system. Unlike other forms of mercury, MeHg efficiently crosses the blood-brain barrier (BBB) and the brain levels of MeHg are 3-6 times higher than circulating blood levels following acute exposure (Aschner & Clarkson 1989). MeHg has also been shown to target other organs, including the liver and kidney as well as being transported through the placenta to the brain of the fetus (Syversen & Kaur 2012). Once absorbed, MeHg has a high tendency to bind sulfhydryl groups present in cysteine residues in proteins in a similar manner to Hg^{II}. The resulting cysteine-Hg-Me complex mimics the neutral amino acid methionine and this facilitates MeHg entry into the cell through the large neutral amino acid carrier (Yin *et al.* 2008). On the other hand, MeHg can be transported from the cell either through complex formation with the sulfhdryl group of GSH or via passive diffusion (Ballatori & Clarkson 1982). Unlike the ionic forms of mercury where symptoms usually disappear when exposure ceases, exposure to MeHg

leads to persistent neurological symptoms and symptoms of neurotoxicity appear rather late after exposure to MeHg. It normally takes several weeks before the symptoms appear, but once they start they propagate very rapidly and the latency period appears to be independent of the level of exposure. The reason and mechanism for this latent period following exposure to MeHg is a challenging mystery that has yet to be answered by the scientific community (Clarkson & Magos 2006).

In addition to MeHg, a number of other organomercurials have been used as antimicrobial agents, but their use is also now limited due to their toxicity. Following MeHg, EtHg ranks second in terms of human exposure to organomercurial compounds, with the most common use of EtHg being as a preservative in vaccine preparations. In humans, the biodistribution of EtHg is very similar to MeHg, but EtHg has a much shorter biological half-life. Unlike MeHg, which mainly affects the central nervous system, exposure to high levels of EtHg causes mainly kidney toxicity (Dorea *et al.* 2013). In addition to EtHg, other organomercurial compounds have been used as antiseptics and antifungals, including merbromine and phenylmercury. Although these compounds have a significantly lower toxicity profile in comparison to either MeHg or EtHg, the usage of any mercury-containing compound encountered general scepticism from the public due to the stigma associated with other mercury containing compounds.

In general, human exposure to the different forms of mercurial compounds through ingestion, inhalation or skin contact leads to variations in the toxicity profile. These variable toxicity profiles following exposure to mercurial compounds is attributed to their different chemical properties that lead to variations in their absorption, distribution and metabolism in humans.

1.2 Occurrences and sources of mercury in environment

Mercury is a naturally occurring element that can be introduced into the environment as a result of either natural causes or human activities. Human activities are responsible for approximately two thirds of the total mercury emission to the environment and the

remaining one third is attributed to natural processes like volcanic eruptions, forest fires and rock weathering. To determine the difference between natural sources and anthropogenic contribution to environmental mercury levels over the last several hundred years, the deposition of mercury in the ice core of a Wyoming glacier was measured in 1991 and 1998. The results showed that naturally released mercury produces a constant background level in the atmosphere independent of human activities. However, with the beginning of the industrial revolution in the nineteenth century, the levels of mercury increased dramatically from human activities as depicted in **Figure 1** (Schuster *et al.* 2002).

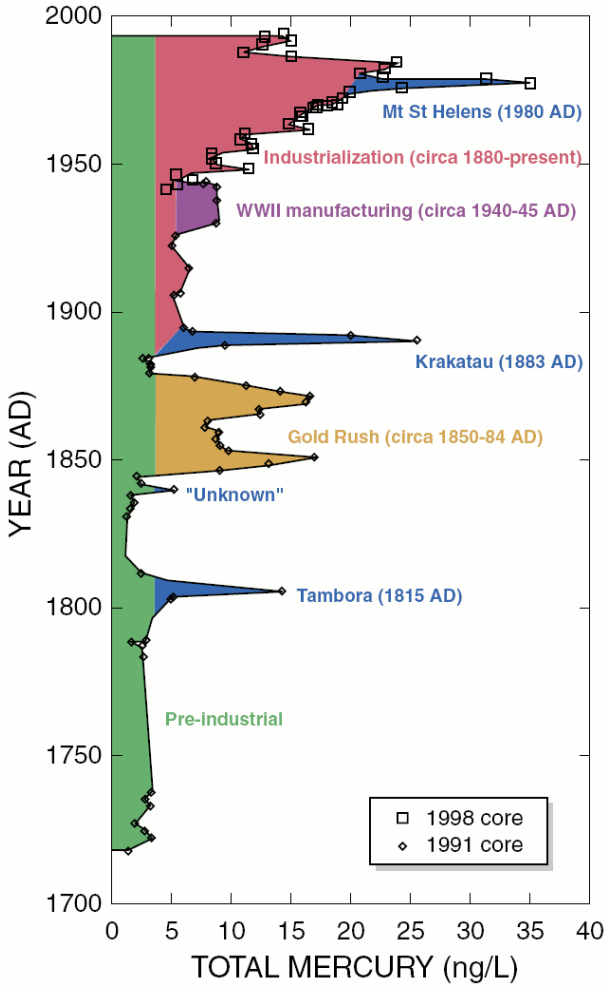

Figure 1: Ice core record of atmospheric mercury deposited at Wyoming's Upper Freemont Glacier over the last 270 years. The ice core covering the period between 1720-1945 was collected in 1991 and it is represented by ◊, and the ice core collected in 1998 by □ covers the

years between 1945-1993. The green area represents the natural background of mercury deposition, where the preindustrial deposition rates until 1880 can be extrapolated to present time (4 ng/L) to illustrate the increases during the last 100 years (in red) and decreases in the past 20 years. The blue color shows the deposition rates corresponding to natural events like volcanic eruptions. The orange area reflects the elevated levels of mercury that are associated with the gold rush period in the United States (US). The pink area represents the increase in global environmental level of mercury after the beginning of the industrial period around 1880 (anthropogenic events). The figure is adapted from (Shuster *et al*. 2002).

1.2.1 Natural sources

Different forms of mercury exist naturally in the earth's crust, atmosphere and oceans. Several natural processes are responsible for mobilizing mercury from the earth's crust and introducing it to the atmosphere and oceans as mentioned above. The most abundant form of mercury in the earth's crust is mercuric sulfide (HgS), which is commonly known as cinnabar ore. In nature, mercuric containing rocks are subjected to natural weathering factors that convert the naturally occurring Hg^{II} into the more volatile Hg^{0}, which is then readily emitted to the atmosphere. Similarly, volcanic eruptions play an important role in mobilizing mercury from the earth's crust into the atmosphere as Hg^{0} (Nriagu & Becker 2003). Following its release into the atmosphere, Hg^{0} is converted through an uncharacterized oxidative process to inorganic forms such as mercuric oxide (HgO). The resulting inorganic mercuric compounds are then deposited, and they return back through rainwater to the earth's surface, where they accumulate in aquatic sediments. After deposition of Hg^{II} either in marine or fresh water sediments, select microorganisms convert Hg^{II} to MeHg through an enzymatically catalyzed biomethylation reaction (Mason & Sheu 2002). Following the biomethylation reaction, MeHg readily bioaccumulates in marine species and in particular fish. In the absence of mercury pollution associated with human activities, only low levels of MeHg will accumulate, but this has changed dramatically due to human activities, which has resulted in a biomagnification of MeHg in the food chain (**See Figure 2 for a schematic of the mercury geochemical cycle**) (Morel *et al.* 1998, Selin 2009).

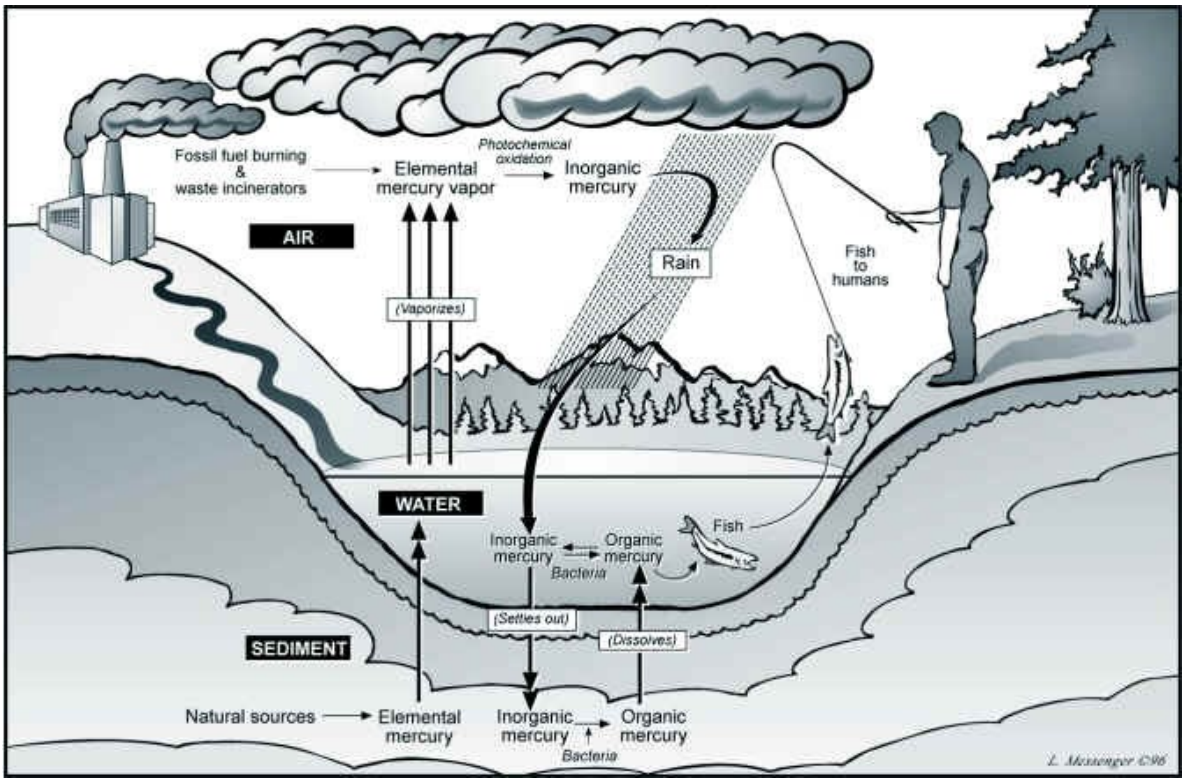

Figure 2: Biogeochemical cycle of mercury species in the environment. Mercury is introduced into environment as a result of natural (degassing from rock, soil and water surface and volcanic eruptions) and anthropogenic activities (gold mining, fossil fuel combustion). Hg^0 is released into the atmosphere, where it circulates for up to 1 year and becomes widely distributed. Hg^0 undergoes a slow photochemical oxidation, which converts it to inorganic mercury. The resultant inorganic mercury travels back to the earth's surface in rain, which leads to it being deposited in aquatic systems and soil. The soil-deposited inorganic mercury can be released into the atmosphere as the results of forest fires, whereas aquatic-deposited inorganic mercury is converted to MeHg by select microorganisms. The MeHg is absorbed by plankton, and the plankton are consumed by higher organisms and this leads to bioaccumulation in fish, which represent an important food source for humans. The figure is adapted from University of Wisconsin-Eau Claire (2014) Mercury in the Environment and Water Supply.url: https://people.uwec.edu/piercech/Hg/mercury_water/cycling.htm. (Last accessed on 30 March 2016)

1.2.2 Human activities (Anthropogenic sources)

Human activities have greatly amplified the rate of mobilization of mercury from the earth's crust since the beginning of the industrial revolution. Humans have released tremendous amounts of mercury during the second half of nineteenth century when cinnabar ore was heavily mined to be used to prepare Hg^0. The Hg^0 prepared from the mining of cinnabar ore has been used for gold extraction around the world. Using Hg^0 in gold mining can result in a significant release of Hg^0 into the atmosphere as was seen following the gold rush period in the United States in the nineteenth century (**Figure 1**). Similarly, coal and fossil-fuel burning for power generation and oil refining are another major source of anthropogenic emission of mercury into the atmosphere because mercury exists naturally in both coal and fossil-fuels (Mason *et al.* 1994). There are numerous other sources of mercury that result from human associated activities and many products contain mercury like batteries, fluorescent lamps, thermometers and blood pressure gauges. The improper handling of mercury-contaminated waste from these consumer products represents another important mechanism for introducing mercury species into the environment and mercury emissions to the atmosphere from such human activities was estimated at 1960 tonnes in 2010 (UNEP 2013).

In addition to releasing inorganic mercury species into the atmosphere, human activities are also responsible for the introduction of several forms of synthetically generated organomercurial compounds. Up until the 1960s, the chloro-alkali industry was the main source for contaminating aquatic systems through the direct release of MeHg as waste. This industry used mercury sulfate cells as catalysts to produce caustic soda, and MeHg was produced as a side product; consequently thousands of tons of MeHg were dumped through waste-water into aquatic systems as a by-product. Since MeHg has the capacity to bioaccumulate in the marine food chain, its lethal effect in humans was readily manifested through the consumption of contaminated seafood (Morel *et al.* 1998). The first unprecedented outbreak of MeHg toxicity was in Minamata, Japan in 1956 due to persistent MeHg release into Minamata Bay from a local chloro-alkali factory**.** In this dramatic incident, thousands of cases of MeHg toxicity were reported due to the consumption of

MeHg contaminated fish from Minamata Bay and MeHg toxicity is now commonly referred to as Minamata disease (Dltri & Dltri 1978, Dltri 1991). A second major outbreak of MeHg poisoning occurred in Iraq in 1972 following the consumption of contaminated bread. The contaminated bread was prepared from wheat seeds treated with MeHg as a fungicidal agent that were originally intended for agricultural purposes and not for human consumption. Thousands of people developed symptoms highly similar to toxicity after consumption of MeHg contaminated fish (Bakir *et al.* 1973, Greenwood 1985).

After the Minamata Bay and Iraq incidents, several governmental regulations came into effect to prevent or at least minimize the risk of toxicity caused by organomercurial compounds. In Japan, a comprehensive mercury-control plan was implemented to reduce mercury production and usage. Mercury extraction from mines was completely stopped by 1974. The chloro-alkali industry developed mercury-free catalysts and mercury use in lamps, batteries and medical equipment were greatly reduced. On the other hand, the use of MeHg as an antifungal agent in agriculture was discontinued globally after the outbreak in Iraq. Although Europe and North America did not experience any significant mercury toxicity outbreaks, several safety measures were implemented to prevent the risk of mercury toxicity. In the USA, fishing is prevented in over three thousand mercury-contaminated lakes (Berlin *et al.* 2007). In Ontario, Canada, three first nation communities suffered from symptoms of Minamata disease in 1970 after eating local fish contaminated with mercury. Due to the increased concern over the possibility of mercury contamination, the government of Canada launched several projects to monitor and control mercury pollution throughout the country. By 1995, all chloro-alkali factories using mercury cells were closed, but this occurred only after large quantities of MeHg had already been discharged into waterways around cities like Sarnia, Hamilton and Cornwall (Mailman *et al.* 2006, Saint-Amour *et al.* 2006, Depew *et al.* 2013).

Despite considerable efforts to minimize anthropogenic mercury emissions through strict emission standards, there is still a high load of previously emitted mercury in the ecosystem, and it will take decades to diminish mercury levels to safe standards in several highly contaminated areas. Furthermore, the growing industrial sectors in Asia, especially

China, are introducing and mobilizing considerable amounts of mercury into the environment, due to the absence of strict emission standards (UNEP 2013). In addition, it appears that levels of MeHg in arctic marine life has been increasing over the last several years, and it has been suggested that this is correlated with global warming and increased melting of the polar ice cap (Schartup *et al.* 2015). Taken together, mercury still represents an important global threat to human health and current efforts to reduce anthropogenic emission and release are not enough to reduce the risk of toxicity. Thus, remediation efforts for cleaning up existing areas of mercury contamination are required to control mercury pollution and avoid future outbreaks of mercury poisoning.

1.2.3 The chemistry of MeHg and organomercurials

In contrast to many other organometallic compounds, organomercurial compounds are typically stable in aqueous solutions. This stability is not due to the strength of the carbon-Hg (15-20 kcal/mole) since carbon-Cd and carbon-Zn bonds (the other members of the group 12 metals) are stronger and organozinc and organocadmium compounds are unstable in aqueous solutions (Mason & Benoit 2003). Rather, the stability of metal-carbon bonds in an aqueous solution is connected to bond polarity. Carbon-metal bonds are polarised ($M^{\delta+}$ - $C^{\delta-}$) as a result of the difference in electronegativity between the carbon atom and the metal. For example, carbon-Cd and carbon-Zn bonds are more polarized than carbon-Hg bond, carbon-Pb and carbon-Sn bonds and this is consistent with their relative stability in aqueous solutions. Whereas organocadmium and organozinc compounds are rapidly degraded in an aqueous environment, organomercury, organotin and organlead compounds are often very stable (Mason & Benoit 2003).

In general, organomercurial ions (RHg^{+}) and mercuric ions show similar reactivity patterns, and both have a strong preference for binding to thiols. Given their strong affinity for thiol-containing compounds, organmercurial compounds such as MeHg are generally thought to exert their toxic effect though the binding to cysteine residues present in proteins. However, organomercurial compounds differ from mercuric ions in that they typically bind to only one thiol ligand as opposed to two due to the stability of carbon-Hg bond. However, studies with model organic compounds indicate that it is possible to cleave

carbon-Hg bonds when more than one sulfur ligand is bound to the mercury atom. The binding of a second sulfur ligand increases the polarization of carbon-Hg bond ($Hg^{\delta+}$-$C^{\delta-}$) and creates a low energy pathway leading to cleavage of the carbon-Hg bond (Mason & Benoit 2003).

1.3 Remediation of mercury contaminated sites

1.3.1 Physical or chemical remediation

Due to the toxicities associated with all forms of mercury compounds, many efforts have been undertaken to remediate mercury-contaminated sites by either stabilizing the mercurial compounds in contaminated sites to prevent them from spreading into the environment or by completely removing them from contaminated soil. The current remediation technologies can be classified as being either non-biological or biological, with the two non-biological methods being either chemical or physical remediation (Wang *et al.* 2004, Wang *et al.* 2012). Within the chemical remediation methods, the most common approaches involve immobilization or stabilization techniques. In these cases, mercury-contaminated waste or soil is chemically treated with either sulphur-containing ligands or reducing agents to minimize mercury mobility. By forming thiol complexes that are both stable and insoluble, it prevents the mercury from leaching into the surrounding environment. Addition of sulphur-containing ligands such as colloidal sulfur to mercury-contaminated soil or waste precipitates the mercury as HgS, which has decreased solubility and lower volatility (Kot *et al.* 2007, Liu *et al.* 2008). In general, the materials employed in immobilization techniques are commercially available and inexpensive. Thus, they are often an attractive option to governmental organizations trying to minimize the potential toxic effects of mercury contamination at the lowest possible cost. However, the mercury is not removed from the contaminated site and this is a major disadvantage of these chemical remediation methods since it does not completely remove the potential risk. In addition, these methods increase the volume of waste and it is important to continually monitor the immobilized mercury in these contaminated sites. To overcome the disadvantage associated with chemical treatments, physical remediation methods have also been developed to eliminate mercurial compounds from contaminated sites using a thermal desorption

technique (Massacci *et al.* 2000). In the thermal desorption process, the soil is heated in a closed system to collect volatilized mercury and its compounds. The relative volatilization rates of mercury compounds are as follows: $Hg^0 \approx (CH_3)_2Hg > Hg_2Cl_2 > HgCl_2 > HgS > HgO$. Heating the soil to between 600-800 °C removes all mercury compounds from contaminated soil, which can then be subsequently condensed for safe disposal. Mercury is removed very efficiently using this approach. For example, heating contaminated soil from a chloro-alkali plant in Sweden at 500 °C for 20 min removed 99% of the total mercury content in the soil. However, the danger of using this technique lies in changing the soil properties due to the very high temperatures required. Raising the soil temperature will definitely alter the levels of other soil contents such as bacteria, trace elements and nutrients such as nitrogen, phosphorus and potassium. To counter the adverse effects of these elevated temperatures on the soil, a new approach using lower temperatures for longer periods of time has succeeded in removing mercury and maintaining the overall quality of the soil (Kucharski *et al.* 2005). Although this method is both safe and efficient, the high cost is a major disadvantage. In addition, it is often very difficult to access the soil under aquatic systems and this represents an important source contributing to the build up of mercury contamination.

1.3.2 Biological remediation (Bioremediation)

In an attempt to avoid using costly and inefficient chemical and physical remediation methods, considerable effort has been devoted to identifying efficient biological methods for remediating mercury-contaminated sites. The discovery of mercury-resistant bacteria isolated from mercury-contaminated sites represented a promising step in developing such bioremediation strategies (Summers 1986, Osborn *et al.* 1997). Select bacterial strains are resistant to mercury containing-compounds due to the presence of a set of genes known collectively as the *mer* operon. The genes present in the *mer* operon encode for a set of proteins that enable the bacteria to detoxify mercury compounds and convert them to the more volatile and less toxic elemental mercury. The proteins expressed from the *mer* operon include two enzymes, the organomercurial lyase MerB and the organomercurial reductase MerA. In resistant bacteria, MerB cleaves the carbon-mercury bond of

organomercurial compounds (**Figure 3**) and produces an organic moiety (CH_4 in the case of MeHg) and ionic Hg^{II}. The resultant Hg^{II} is then transferred directly to MerA, which reduces it to Hg^0 (**Figure 4**) (Ji & Silver 1995). The resultant Hg^0 is less toxic than either Hg^{II} or R-Hg, and the highly volatile Hg^0 can be readily expired by the bacteria. Although the concept of using these mercury-resistant bacteria represents an attractive method for cleaning up mercury-contaminated sites, the major limitation is the small biomass associated with the bacteria. In efforts to use mercury-resistant bacteria on a larger scale, attempts have been made to develop bioreactors (Wagner-Dobler *et al.* 2000). In these bioreactors, the mercury-resistant bacteria are immobilized on a solid support. This allows mercury-contaminated wastewater to be inoculated in the bioreactor for sufficient time periods to allow the bacteria to detoxify either organomercurial compounds or Hg^{II}. Bioreactors have been used for cleaning mercury-contaminated wastewater, but they are not suitable for remediating mercury-contaminated soil. In an attempt to address this limitation, MerA and MerB encoding genes were introduced into genetically modified plants to enable them to detoxify mercury-contaminated soil.

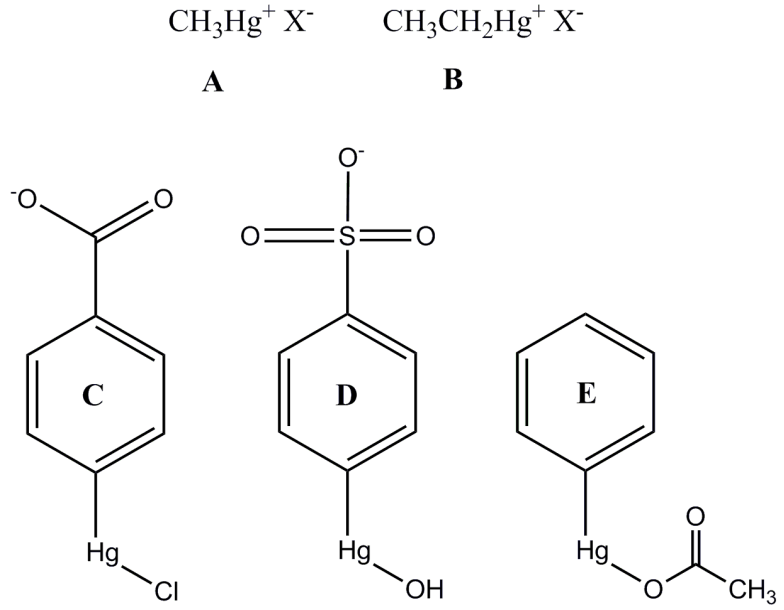

Figure 3: Structures of important organomercurial compounds. Structure of methylmercury; MeHg (A), Ethylmercury; EtHg (B), *p*-chloromercuric benzoic acid PCMB (C), p-hydroxymercuric sulphonic acid PHMSA (D) and phenylmercuric acetate PMA (E). X^- is the counter ion typically Cl^- or Br^-.

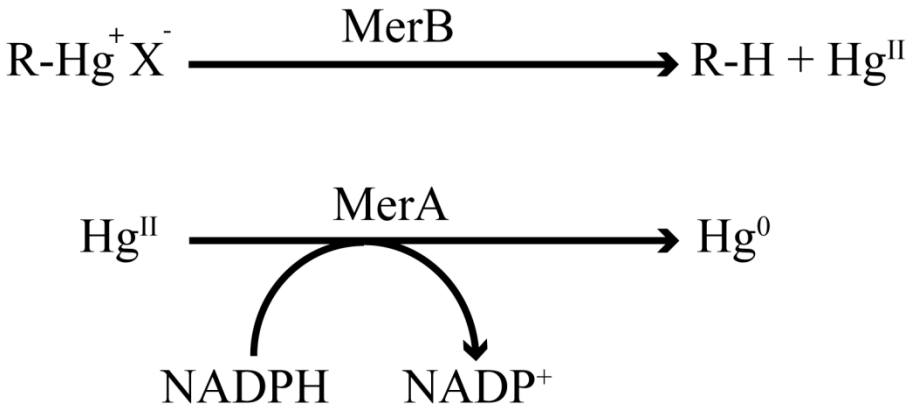

Figure 4: Reactions catalyzed by MerB and MerA.

Bacteria isolated from mercury-contaminated sites have been shown to possess the MerA and MerB enzymes. MerB cleaves carbon-Hg bonds in organomercurial compounds to yield a hydrocarbon moiety and Hg^{II} products. The resultant Hg^{II} is subsequently reduced by MerA enzyme and this produces the volatile and less toxic Hg^0. R represents the alkyl or aryl group bound to the mercury atom, whereas X represents the counter ion such as chloride.

1.3.3 Phytoremediation

In an attempt to develop a method that uses the two enzymes of the *mer* system to remediate contaminated soil, several groups have inserted MerA and MerB into different plant species (Meagher 2000, McGrath *et al.* 2006, Omichinski 2007). This technique is commonly known as phytoremediation and these systems have proven to be very successful in controlled trials. The advantage of phytoremediation systems is that the roots of the plant are able to extract subsurface mercury contamination and transport the mercury compounds to all sections of the plant. Inserting the MerA gene into the *Arabidopsis thaliana* genome allows for the efficient expression of MerA throughout the plant. The net result is that this significantly increases the plant's capacity to grow in Hg^{II}-containing media in comparison with the wild-type plant. The volatilization of Hg^0 from the plant was detected in parallel to a decrease in the Hg^{II} content in the growth media (Rugh *et al.* 1996, Lyyra *et al.* 2007). In addition, Arabidopsis plants expressing both MerB and MerA are able to grow in media containing significant levels of organomercurial compounds as they were able to convert the organomercurial compounds and expel Hg^0. Plants expressing only the MerB gene were

able to grow in organomercurial-containing media, but they showed a decrease in survival relative to plants expressing both MerA and MerB due to the accumulation of Hg^{II} (**Figure 5**) (Bizily *et al.* 2000, Bizily *et al.* 2003). Given the success in *Arabidopsis thaliana,* the MerA and MerB genes have now been successfully introduced into several additional plant species with larger biomass such as yellow poplar trees and tobacco plants (Merkle 2006, Hussein *et al.* 2007, Ruiz & Daniell 2009, Nagata *et al.* 2010). By creating a variety of mercury-resistant plant species that can grow in different environments and geographical locations, it will be possible in the future to select the most suitable plant species to fit the conditions present in a mercury-contaminated site. Moreover, employing mercury-resistant plants for cleaning up contaminated areas has several advantages since it presents a low cost and an environmentally friendly/green technology. In addition their large biomass and their ability to penetrate deep into the soil with their roots allows for the hyper-accumulation of mercury from contaminated soil. Thus, phytoremediation presents several advantages over physical and chemical remediation strategies for cleaning up mercury-contaminated areas. To optimize these phytoremediation technologies, there is a crucial need to obtain a comprehensive understanding of the catalytic mechanisms of MerA and MerB as well as how other components of the *mer* system function.

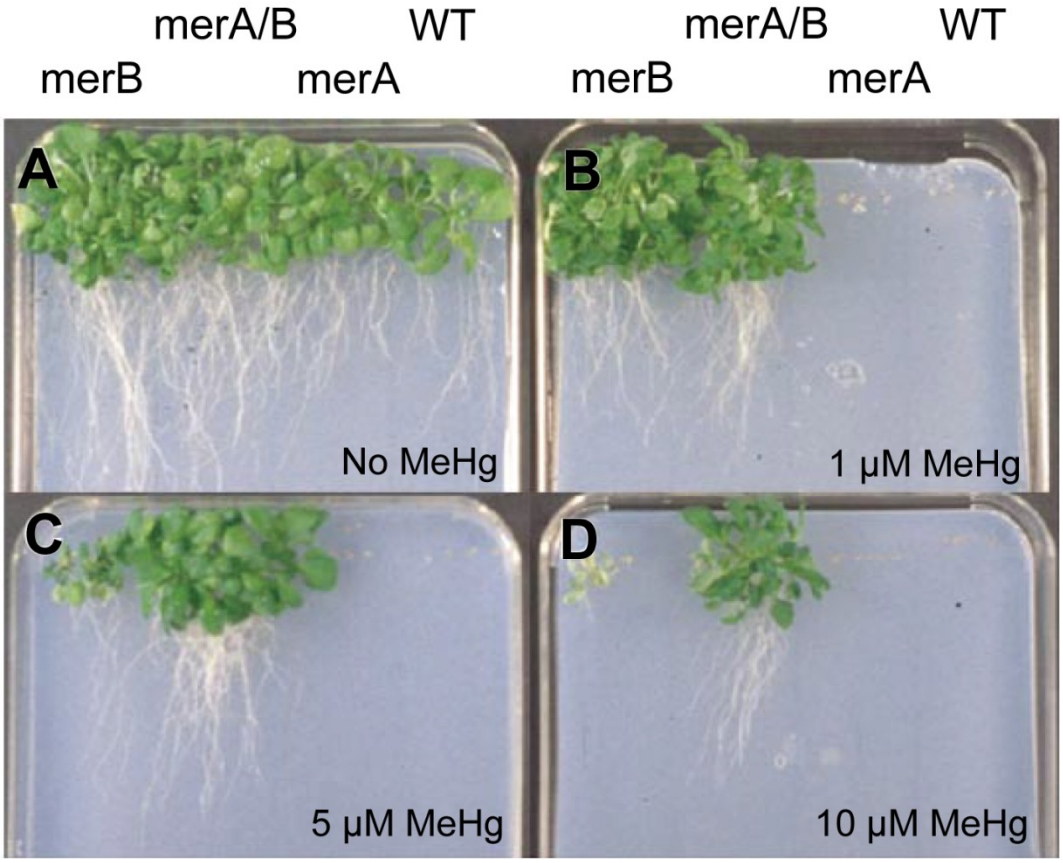

Figure 5: Resistance of transgenic plant to methylmercury chloride.

Growth of transgenic plants expressing the *merB*, *merA/B* or *merA* gene in comparison with wild-type *Arabidopsis thaliana* plants. The seeds for the various plants were germinated in growth media with MeHg concentrations of 0, 1, 5, 10 µM in A, B, C and D, respectively. **A)** In the absence of MeHg, all plants display regular growth behaviour indicating that merA and/or merB-containing plants grow normally. **B)** In 1 µM MeHg, both the merB and merA/B plants grow near normally whereas the merA and wild-type plants fail to germinate and grow. **C)** In 5 µM MeHg, the merA/B plants grow more efficiently than the merB plants, whereas both merA and WT seeds fail germinate. **D)** Although their growth is inhibited, merA/B plants still display resistance to 10 µM MeHg whereas the merB plants could germinate but they did not grow. Adapted from (Bizily *et al.* 2000); courtesy of Dr. Richard Meagher, University of Georgia.

1.4 The Mer system

The unique ability to grow in the presence of toxic concentrations of both inorganic mercury and organomercurial compounds has been observed for a wide range of gram-negative and gram-positive bacteria isolated from mercury-contaminated sites (Miller 1999). This resistance to mercurial compounds by these bacteria is attributed to the presence of a set of genes known as the *mer operon,* which is present on a transferable genetic element such as a plasmid or transposon. The genes of the *mer* operon encode for a set of proteins that function to detoxify and eliminate the mercurial compounds from the bacteria. The proteins of Mer system participate together to convert the highly reactive and highly toxic inorganic and organomercurial compounds to the less toxic and volatile Hg^0, which is readily expired by the cell. The gene contents of *mer* operon vary between the different strains of mercury-resistant bacteria, but the most common genes loaded on *mer* operons include *merR* which encodes for the transcriptional regulatory protein MerR, *merP* which encodes for the periplasmic Hg^{II} transporter protein MerP, *merT* which encodes for the membrane Hg^{II} transporter protein MerT, *merA* which encodes for the ionic mercuric reductase MerA and *merB* which encodes for the organomercurial lyase MerB (**Figure 6**). The proteins expressed from the *mer* operon represent the components of the Mer system (**Figure 7**) (Barkay *et al.* 2003). In the presence of ionic mercury, the transcriptional regulatory protein MerR induces the expression of the *mer* operon. When both MerA and MerB are expressed from the *mer* operon, the mercury resistance is classified as broad spectrum since the bacteria have the capacity to detoxify both ionic mercury and organomercurial compounds. However, when MerA is the only enzyme expressed by the *mer operon*, the resistance is classified as narrow spectrum because the bacteria are only able to detoxify ionic mercury and not organomercurial compounds (Nascimento & Chartone-Souza 2003).

All proteins of the Mer system contain critical cysteine residues that are essential for binding mercury and limiting damage to cellular proteins. Following exposure to Hg^{II}, the MerP protein traps Hg^{II} in the periplasmic space by coordinating it through the sulfhydryl groups of two cysteine residues. Next, MerP directly transfers the Hg^{II} to the sulfhydryl

groups of two cysteine residues on MerT, located on the periplasmic side of the inner membrane. MerT functions by transporting Hg^{II} from the two cysteine residues on the periplasmic side to two cysteine residues on the cytosolic side of the inner membrane. Once bound to the two cysteine residues on the cytosolic side of the inner membrane, the Hg^{II} is directly transferred from MerT to two cysteines located near the amino-terminal end of the mercuric reductase MerA, which reduces Hg^{II} to the volatile Hg^{0}. The volatile Hg^{0} is subsequently expired by the bacteria with minimal damage to other cellular proteins. In the case of organomercurial compounds, they have the capacity to diffuse directly through the bacterial membrane into the cytosol. Once in the cytosol, the organomercurial compounds bind to key cysteine residues present in the active site of the organomercurial lyase MerB. MerB functions by cleaving the carbon-Hg bond to generate an organic moiety (methane in the case of MeHg) and Hg^{II}. The Hg^{II} product remains bound in the active site of MerB until the resultant MerB-Hg^{II} complex directly transfers the Hg^{II} to two cysteine residues of MerA without releasing it into the cytosol where it could damage other cellular proteins. As is the case following exposure to ionic mercury, MerA reduces the Hg^{II} to Hg^{0} as the final detoxification step. The direct transfer of mercury between proteins of the Mer system guarantees inaccessibility of the reactive mercury species to sulfhydryl groups of cellular protein (Barkay *et al.* 2003). Given the uniqueness of the system, each Mer protein has been biochemically characterized in attempts to define their exact role in mercury detoxification. The following section will describe the functional roles of the critical components of the Mer system, which carry out regulation, transport and catalysis.

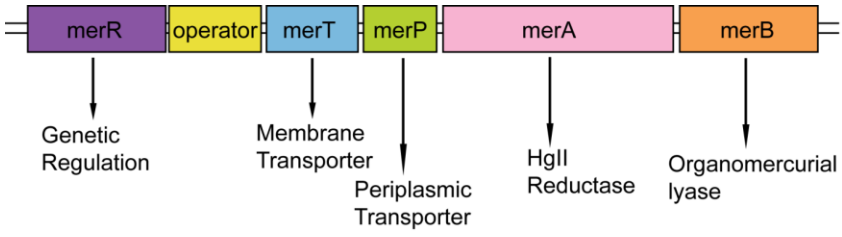

Figure 6: The *mer* operon

The common components of mer operon include the regulator (*merR*), transporters (*merP* and *merT*), mercuric reductase (*merA*) and organomercurial lyase (*merB*).

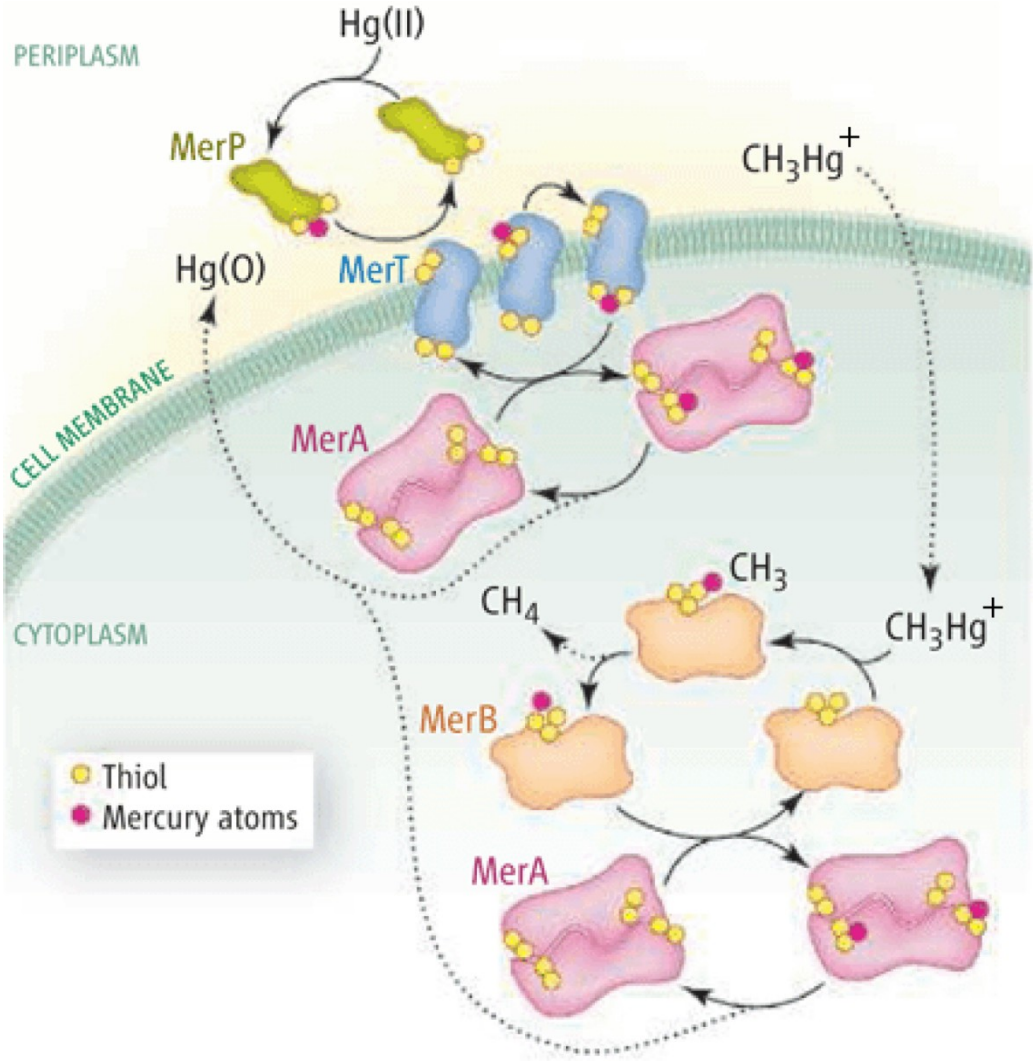

Figure 7: The proteins of the Mer system.

MerP binds Hg^{II} in periplasmic space for transfer to MerT. MerT transports Hg^{II} from the periplasm to the cytosolic side of the inner membrane. On the cytosolic side of the inner membrane, Hg^{II} is transferred from MerT to MerA. In the cytosol, MerA reduces Hg^{II} to Hg^0, which is volatile and is released from the cell. The hydrophobic MeHg passes directly through the membrane without the need for a dedicated transport system. MeHg binds to MerB, which cleaves the carbon-Hg bond to generate methane and Hg^{II}. The Hg^{II} remains bound to MerB until it is transferred to MerA for the final detoxification step to the volatile and less toxic Hg^0. All proteins and enzymes of the Mer system possess thiol functional groups enabling them to bind mercury with high affinity. This figure was adapted from (Omichinski 2007).

1.4.1 Regulation

MerR regulates expression of the *mer* operon and the mechanism of regulation is unique in comparison with other prokaryotic transcriptional regulatory systems. The majority of prokaryotic transcriptional regulators function either as activators by recruiting RNA polymerase (RNAP) to the DNA promoter to initiate gene expression or as repressors by inhibiting recruitment of RNAP (Lee *et al.* 2012). In contrast, MerR functions as both a transcriptional activator and a transcriptional repressor (Shewchuk *et al.* 1989, Brown *et al.* 2003). In the case of the *mer* operon, RNAP forms a stable complex with the DNA promoter, but MerR is also bound to the promoter in the absence of ionic mercury and the mercury-free form of MerR blocks transcription. Binding to ionic mercury induces a significant structural change in the MerR protein. The conformational change in MerR also results in a conformational change in the associated DNA promoter, and this leads to the formation of an RNAP–promoter complex capable of expressing the downstream genes. This unique dual function of MerR as both a repressor and activator represents a novel transcriptional regulatory family (Ansari *et al.* 1992, Condee & Summers 1992, Parkhill *et al.* 1993, Ansari *et al.* 1995, Kulkarni & Summers 1999). MerR is a member of a family of regulators that function as repressors in their apo-form, but as activators in their metal-bound form. Other important members of this family include CueR, ZntR and PbrR, which regulate the expression of dedicated efflux pumps for Cu, Zn and Pb, respectively. There are 4 other metalloregulatory families and they are the ArsR, DtxR, Fur and NikR families. These proteins differ from the MerR family of regulators in terms of their mechanism of regulation. For more information about their mechanism of regulation see (Pennella & Giedroc 2005).

Structural and biochemical studies have provided a detailed description of the activation/repression steps of MerR regulation of the *mer* operon and this includes recent X-ray crystal structures of MerR in both its free and mercury-bound form (Chang *et al.* 2015). Typically, the bacterial RNAP associates with DNA promoters by binding to the (-10 and -35) elements (upstream of transcription site), which are separated by 17 base pairs (bp) (Lee *et al.* 2012). In case or the *mer* promoter, the -10 and -35 elements are separated

by 20 bp so there are three additional bps in comparison with the typical bacterial promoter region. In the apo (metal-free) form, two identical MerR subunits arrange in an anti-parallel manner to form a functional homodimer. The two helix-turn-helix DNA-binding domains of the apo- MerR dimer bind to the *mer* promoter between the -10 and -35 RNAP recognition elements. The binding of the apo-MerR between -10 and -35 elements twists the promoter in a way that allows the RNAP to bind only to the -35 element and not to the -10 element.

This RNAP–*mer* promoter–apoMerR complex suppresses transcription of the *mer* operon. Mercury is chelated in a trigonal planar coordination state by two cysteine residues (Cys114 and Cys123) near the C-terminus of one subnunit of the MerR homodimer and one cysteine residue (Cys79) near the N-terminus of the second subunit of the homodimer. Thus, binding of two atoms of Hg^{II} induces significant structural rearrangements in the regions around the two Hg-binding sites. Due to the near proximity of Hg-binding site to the DNA-binding domain in MerR, the structural rearrangement of the Hg^{II}-binding sites induces a dramatic conformational change in the DNA-binding domains of the MerR homodimer and this plays an essential role in modulating the conformation of the operator DNA. The conformational change induced by the Hg^{II}-MerR complex leads to an untwisting of the DNA promoter and a shortening of the distance between the -35 and -10 elements, which allows the pre-associated RNAP to now bind to both the -35 and the -10 elements and initiate transcription of the *mer* genes (Chang *et al.* 2015). The mechanism of allosteric Hg^{II} binding to MerR allows for an instantaneous response of the *mer* operon to the presence of Hg^{II} in the cell through the immediate transcription of the *mer* genes, which are required for the transport and detoxification of mercurial compounds.

1.4.2 Transport

The two most common Hg^{II} transport proteins expressed from the various *mer* operons are MerP and MerT. MerP is a 72 amino acid protein that is secreted in the periplasmic space following its synthesis. NMR solution and X-ray crystal structures of apo- and Hg^{II}-bound MerP reveal that MerP is a monomer that binds a single Hg^{II} ion (Steele & Opella 1997, Qian *et al.* 1998). MerP consists of a common βαββαβ structural fold with the two α

helices overlaying a four-strand antiparallel β sheet. Two critical cysteine residues located within a CxxC motif bind to Hg^{II} in a linear-coordination geometry. In general, MerP functions as a Hg^{II} scavenger in the periplasmic space and after binding Hg, it transfers it to MerT, a 116-residue protein located in the inner membrane of the bacteria cell, for transport into the cytosol (Serre *et al.* 2004). In contract to MerP, there are currently no high-resolution structures of MerT. However, based on biochemical and biophysical studies, the secondary structure of MerT is predicted to consist of 3 α-helices embedded in the inner membrane with two pairs of highly conserved cysteine residues located on either side of the inner membrane (Brown *et al.* 1991). The first pair is located in the helix near the N-terminus and they face the periplasmic side of the membrane. The second pair of cysteine residues is located between the second and third helix, and they are facing the cytosolic side of the inner membrane. The current working model is that Hg^{II} is transferred from the two cysteine residues of MerP to the cysteine pair of MerT on the periplasmic side. Then, there is a second transfer to the cysteine pair of MerT on the cytosolic side (Morby *et al.* 1995, Brown *et al.* 2002). Once transferred to the cytolsolic side, the Hg^{II} is again directly transferred to MerA in the cytosol for reduction to Hg^0 (Rossy *et al.* 2004). This final transfer involves two cysteines located in the N-terminal domain of MerA and this domain of MerA is structurally homologous to MerP (Ledwidge *et al.* 2010). The Hg^{II} transport system used by mercury-resistant bacteria is a unique system in comparison to other toxic metal transport systems found in prokaryotic organisms. The majority of bacterial metal detoxification systems function by promoting efflux of the metal ion from the periplasmic back to the extracellular environment, which prevents the reactive metals from entering the cell (Silver & Phung 2005, Hobman & Crossman 2015). In contrast, the Mer system imports the toxic Hg^{II} into the cell, where it is converted to the less toxic Hg^0. MerP and MerT transport the toxic Hg^{II} inside the cell and enhance mercury resistance by delivering the toxic Hg^{II} to MerA for reduction to the less toxic Hg^0.

1.4.3 Detoxification enzymes

1.4.3.1 MerA

All known *mer* operons encode for MerA, an enzyme that plays a key role in mercury detoxification by reducing Hg^{II} to Hg^{0}, and several biochemical and structural studies have contributed to our understanding of the mechanistic details of Hg^{II} reduction (Fox & Walsh 1982, Miller *et al.* 1986, Walsh *et al.* 1988a). MerA is a homodimeric enzyme in its active form and it contains two functional sites at which the reduction reaction occurs. Each active site consists of a pair of redox-active cysteine residues (Cys207, Cys212; Tn501 transposon numbering), an NADPH-binding site and a bound FAD cofactor flanked between the two cysteines and a molecule of NADPH. This catalytic core represented by a combination of the cysteine pair, NADPH and FAD makes MerA similar in structure, and to some extent in function, to glutathione reductase and lipoamide dehydrogenase, which are both members of the flavin disulfide oxidoreductase family (Schiering *et al.* 1991). However, MerA is also characterized by the presence of several additional cysteine residues in comparison with other members of the flavin disulfide oxidoreductase family. MerA has a second critical pair of cysteine residues (Cys13, Cys16) located in its N-terminal domain. This N-terminal domain (residues 1-69) is a structurally and functionally homologous to MerP, which, as discussed above, plays a key role in sequestering Hg^{II} in the periplasmic space (Ledwidge *et al.* 2005). In addition, there is a third crucial pair of cysteine residues (Cys628, Cys629) located near the C-terminus of the protein (Moore *et al.* 1992, Ledwidge *et al.* 2010). This third pair of cysteine residues is oriented so that they are facing the redox-active cysteine residues in the adjacent subunit of the MerA dimer. The close proximity of the C-terminal cysteine pair to the active site cysteine pair of the alternate subunit is essential for several functions in the mercury-resistant pathway including Hg^{II} trapping, transfer and binding to the active site. These additional structural features, which are absent in other members of flavin disulfide oxidoreductase family, allows Hg^{II} to be scavenged and reduced by MerA and this prevents the Hg^{II} from binding to other thiol-containing proteins in the organism. Furthermore, these additional cysteine residues enable MerA to reduce Hg^{II} and the subsequent Hg^{0} product does not inhibit its activity, whereas binding of

Hg^{II} to other flavin disulfide oxidoreductases inhibits their enzymatic activity (Picaud & Desbois 2006).

MerA is able to acquire Hg^{II} through two different mechanisms. In the presence of extraneous thiolate ligands in the cytosol, such as glutathione (GSH), the Hg-thiolate ligand complex functions as a substrate for MerA where the two C-terminal cysteine residues function to displace Hg^{II} from the Hg-thiolate ligand complex and acquire it (Ledwidge *et al.* 2005). The more dominant mechanism takes place in either the absence or depletion of cytosolic extraneous thiolate ligands, which occurs under oxidative stress or following exposure to electrophilic agents such as Hg^{II} (Lund *et al.* 1993). In this mechanism, it has been postulated that there is a direct transfer of Hg^{II} bound to MerT on the inner membrane to the cysteine pair in the N-terminal domain of MerA (NMerA), which subsequently transfers Hg^{II} to the cysteine pair in catalytic core of MerA (Ledwidge *et al.* 2005). Both NMerA and MerP adopt a βαββαβ structural fold with a conserved CXXC motif and this similarity suggested a role for NMerA in acquiring Hg^{II} from MerT on the cytosolic side of the inner membrane. This transfer would thus be similar to the transfer of Hg^{II} from MerP to MerT on the periplasmic side of the inner membrane and is also supported by the fact that the mercury bound form of NMerA was found to be structurally complementary to the active site cleft of MerA in molecular docking experiments (Ledwidge *et al.* 2005). In addition, biochemical studies demonstrated that Hg-NMerA complex was able to directly transfer Hg^{II} to the cysteine residues in the catalytic core of MerA (Johs *et al.* 2011). In summary, the mechanism of Hg^{II} reduction starts with the binding of Hg^{II} to the cysteine pair near the C-terminus through a direct transfer from either an extraneous thiolate ligand complex or from NMerA. Once bound to the cysteine pair near the C-terminus, the Hg^{II} is passed to the redox-active cysteine pair in the active site. Simultaneously, an electron pair is transferred from NADPH to FAD and these two electrons pass to the redox-active site to reduce Hg^{II} to Hg^{0}, which is then released by the bacteria due to its volatility.

1.4.3.2 MerB

In addition to the *merA* gene, bacteria that display broad-spectrum resistance to mercury compounds are associated with the presence of a *merB* gene, which encodes for the

organomercurial lyase MerB. Bacteria that express both the MerA and MerB proteins have resistance to organomercurial compounds as well as inorganic mercury (Walsh *et al.* 1988b). Unlike inorganic mercury, which must be transported into the cell, organomercurial compounds enter the bacteria cytosol by direct diffusion through the cell membrane due to their hydrophobic nature. After the organomercurial compounds enter into the cytosol, they are bound with high affinity by MerB, which then cleaves the carbon-Hg bond to yield two products, a hydrocarbon moiety (methane in the case of MeHg) and Hg^{II}. The hydrocarbon moiety is released immediately after cleavage of the carbon-Hg bond, whereas the Hg^{II} stays bound to the active site until it can be directly transferred to MerA for reduction to Hg^0 as discussed above (**Figure 7**). MerB has the ability to cleave the carbon-Hg bond on a wide range of organomercurial compounds including aliphatic, aromatic and conjugated substrates. The gene coding for MerB has been identified in both gram-positive and gram-negative bacterial strains, but it occurs more commonly in gram-positive bacteria (Pitts & Summers 2002, Lello *et al.* 2010).

1.4.3.2.1 Enzymatic characterization of MerB

The first known MerB enzyme was isolated from the mercury resistant *Pseudomonas* K-62 strain and the purified enzyme was found to be active in cleaving the carbon-Hg bond of a variety of organomercurial compounds like MeHg, EtHg, PMA and PCMB (Furukawa & Tonomura 1971, Tezuka & Tonomura 1976, Tezuka & Tonomura 1978). Subsequent enzymatic studies were performed with MerB purified from an *Escherichia coli* (*E. coli*) strain carrying the IncM, R831b plasmid (Schottel 1978). The purification of MerB from native cells provided limited amounts of active enzyme so that MerB overexpression was essential to generate enough purified protein for detailed enzymatic studies. The *merB* gene from the IncM, R831b plasmid was subsequently subcloned on a T7 promoter vector for overexpression and purification in *E. coli*. Following overexpression, MerB was purified using DEAE-sepharose, Q-sepharose and a final purification by gel filtration chromatography (Ultrogel AcA44) (Begley *et al.* 1986a). The production and purification of large quantities of MerB (R831b) made it the most extensively characterized MerB variant. In kinetic studies, the enzymatic activity of MerB (R831b) was assayed either by

gas chromatographic detection of volatilized hydrocarbon (CH_4 in case of MeHg) or by detection of volatilized Hg^0, when the MerA enzyme is coupled into the reaction mixture to allow for the subsequent reduction of the Hg^{II} product. In contrast to MerA, MerB was found to purify as a monomer in solution, and there is currently no evidence for a bound cofactor. However, the initial enzymatic studies demonstrated that the activity of MerB is dependent on the presence of thiol-containing compounds in the buffer and that both the composition and concentration of the buffer thiol compound can have a tremendous affect on the catalytic activity of MerB. For example, MerB cleaves the carbon-Hg bond of EtHg 8 times faster when cysteine is added into the buffer in comparison to 2-mercaptoethanol. These studies also suggested that MerB had a strong preference for physiological thiols versus non-physiological thiols. In addition, the catalytic activity of MerB appeared to require two moles of the thiol compound for each mole of the organomercurial substrate, and it was suggested that the thiols were required to generate an organomercurial-thiolate complex which functions as the preferred substrate for MerB. It was also determined that the optimal pH for carbon-Hg bond cleavage by MerB (R831b) was above pH 9 when EtHg was the substrate and stoichiometric analysis showed that in the absence of buffer thiols, MerB binds free Hg^{II} from $HgCl_2$ in a 1:1 ratio (Begley *et al.* 1986a, Begley *et al.* 1986b). Taken together, these results support the conclusion that there is a single-binding site. Interestingly, the resulting MerB-Hg complex obtained in the presence of free Hg^{II} is catalytically inactive, but the catalytic activity is restored by the addition of an exogenous thiol, which displaces the bound Hg^{II} from the active site of MerB. In an attempt to determine the role of cysteine residues in the catalytic activity of MerB, three conserved cysteine residues were identified in all known MerB variants at the time, and they corresponded to Cys96, Cys117 and Cys159 in MerB (R831b). Subsequent studies demonstrated that mutating Cys117 to an alanine resulted in the expression of an insoluble protein, which suggested that Cys117 plays a structural role in folding of the protein as opposed to a true catalytic role. In contrast, mutating either of Cys96 or Cys159 to alanine results in a soluble protein with greatly impaired catalytic activity, and this suggested that these two cysteine residues play an essential role in the enzymatic activity associated with MerB (Griffin *et al.* 1987, Laddaga *et al.* 1987, Pitts & Summers 2002).

In more comprehensive kinetic studies, a series of organomercurial compounds was tested to examine the substrate specificity of MerB (R831b). In these studies, MerB was shown to cleave primary, secondary and tertiary alkyl compounds as well as allyl, vinyl and aryl organomercurial substrates. MeHg and EtHg were cleaved with turnover rates of 0.7 and 5.5 min^{-1} respectively, whereas phenyl mercuric acetate (PMA) had a turnover rate of 15 min^{-1} and cis-butenylmercuric chloride had the fastest turnover rate at 240 min^{-1}. In general, the turnover rates (1-240 min^{-1}) for carbon-Hg bond cleavage are slow in comparison to other known enzymatic reactions (Begley *et al.* 1986a). However, the turnover rates are still accelerated by 10^8-fold over the rates for non-enzymatic protonolysis of carbon-Hg bonds (Kreevoy 1957). For example, only 1% of MeHg is cleaved when incubated for 100 min in concentrated HCl, and this slow rate of non-enzymatic carbon-Hg bond cleavage under drastic conditions highlights the significant task that the MerB enzyme faces when attempting to cleave a carbon-Hg bond under physiologic conditions.

There are four possible mechanisms that could be invoked for cleaving a carbon-metal bond and they involve a carbocation (S_N1), a carbanion (S_E1), a homolytic radical or a concerted process (S_E2 electrophilic substitution, in which reactive intermediates are not involved) (**Figure 8**).

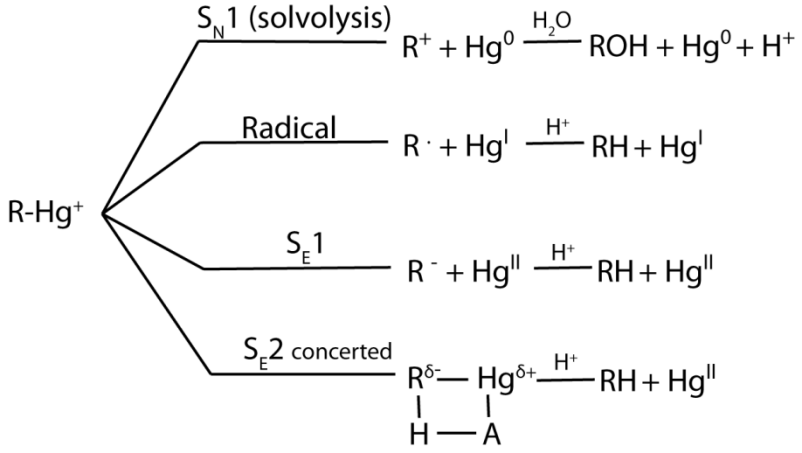

Figure 8: Possible mechanistic routes for cleaving a carbon-Hg bond. A corresponds to the species that protonates the hydrocarbon moiety.

The carbocation (S_N1, solvolysis reaction) pathway was eliminated due to the fact that a hydrocarbon product is formed after the carbon-Hg bond cleavage as opposed to an alcohol product. The S_E1 mechanism also appeared to be unlikely since an intermediate carbanion has not been detected following carbon-Hg bond cleavage even after examining a wide range of organomercurial substrates (Begley *et al.* 1986b, Moore *et al.* 1990). Homolytic cleavage has been excluded because Hg^{II} is produced rather than Hg^{I}. Based on studies suggesting the role of the two catalytic cysteine residues and an S_E2 mechanism, a model for the catalytic mechanism of MerB was proposed by the Walsh group (Walsh *et al.* 1988b). In their model (**Figure 9**), a thiolated organomercurial compound binds to the sulfhydryl groups from two cysteine residues to form the MerB-substrate complex. The binding to the two sulfur atoms polarizes the carbon-Hg bond so that the mercury and carbon atoms will gain partial positive and partial negative charges, respectively. At this point, the carbon atom is now activated for protonolysis and the proton can be donated by either the solvent or by another amino acid residue located in the vicinity of the active site.

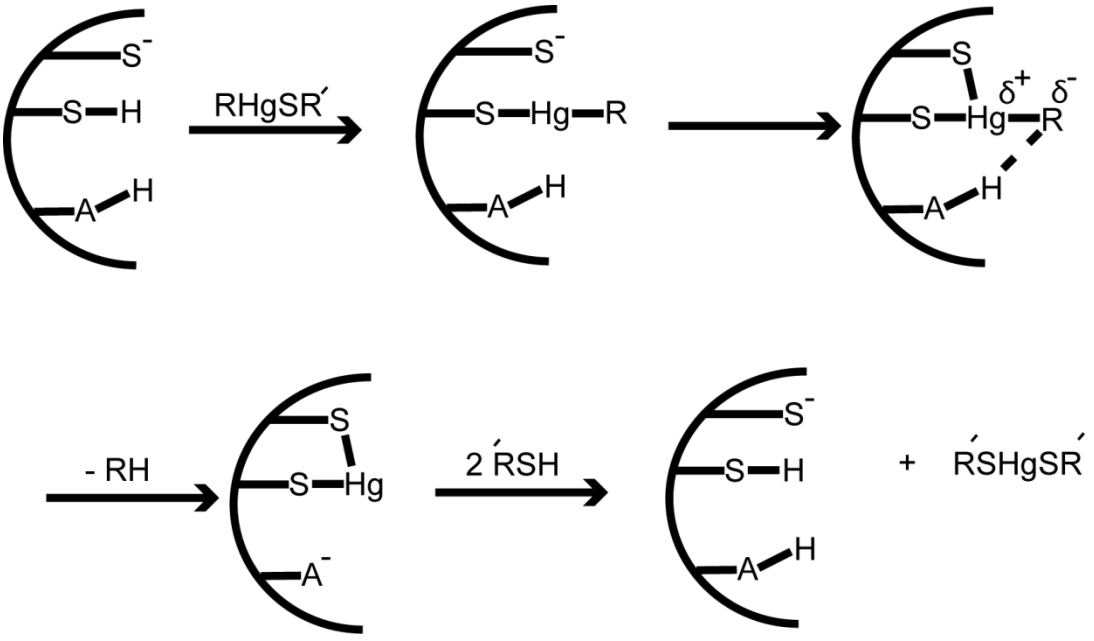

Figure 9: Walsh proposal for mechanism of cleaving carbon-Hg bond by MerB through S_E2 mechanism. A is the amino acid residue that donates a proton to the leaving hydrocarbon moiety. Adapted from (Walsh *et al.* 1988b).

Protonolysis leads to cleavage of the carbon-Hg bond and the formation of two products, the hydrocarbon (RH) and an atom of Hg^{II} that stays bound in the active site of MerB. The bound Hg^{II} atom is then removed by exogenous thiols in the cells, such as cysteine or glutathione, after which the enzyme is ready for the next catalytic cycle. The exogenous thiols are important for both the initial delivery of the organomercurial compounds to the active site as well as for extracting the Hg^{II} product from the active site. In this mechanism, carbon-Hg bond cleavage requires three nucleophilic groups with one of them acting as the proton donor and this is consistent with an earlier study demonstrating that non-enzymatic degradation of organomercurial compounds is enhanced 1000-fold in the presence of bis-dithiol compounds in comparison with mono-thiol compounds (Gopinath & Bruice 1987). In addition, these studies also demonstrated that a carboxylic acid species was able to function as a proton donor in non-enzymatic carbon-Hg bond cleavage with bis-dithiol compounds. Taken together, these results supported the importance of two cysteine residues (Cys96 and Cys159) in the mechanistic model and suggested that a carboxylic acid residue in MerB might function as the proton donor. However, a subsequent study proposed that only the cysteine residues (Cys96 and Cys159) were required for carbon-Hg bond cleavage, and in this model one of the cysteine residues also functions as the proton donor.

1.4.3.2.2 NMR solution structure of MerB

In an attempt to better understand the structure and catalytic mechanism, the three-dimensional structure of MerB (R831b) was solved in solution by NMR spectroscopy (Di Lello *et al.* 2004a, Di Lello *et al.* 2004b). The NMR solution structure of MerB contains three anti-parallel β-sheets and six α-helices (**Figure 10A**) and at the time the structure represented a novel fold since there were no structural homologs in the Protein Data Base (PDB). The NMR structure of MerB consists of two distinct regions, an N-terminal domain and a core region that contains the active site. The N-terminal domain displays an αααββ topology, with three α-helices (α1 residues 26-32, α2 residues 39-46 and α3 residues 50-58) followed by a β-sheet (β-sheet A) consisting of two short twisted anti-parallel β-strands (β1 residues 65-66 and β2 residues 70-71). The larger core region contains two perpendicular β-sheets (β-sheets B and C), with β-sheet B consisting of 5 anti-parallel β-strands (β3

residues 83-87, β4 residues 90-94, β5 residues 111-116, β6 residues 123-128 and β7 residues 133-137). As part of the core region, β-sheet B is packed against an α-helix (α4 residues 103-108). Similarly, β-sheet C consists of 3 anti-parallel β-strands (β8 residues 142-145, β9 residues 163-165, β10 residues 185-188), which are packed against an α-helix (α5 residues 168-176). The last part of the core region includes a final α-helix, α6, between residues 189-204 (Di Lello *et al.* 2004b).

Due to a limited number of NMR restraints, the N-terminal domain of MerB (residues 26-71) is less well defined in comparison with the core region and it was not possible to determine the positions of residues 1-25 due to fast exchange of the amide proton signals for the residues in this region. This helps to explain the higher root mean square deviation (rmsd) of the 20 lowest energy structures for the N-terminal domain with respect to the core region of MerB. The core region is well-defined by the NMR data with the exception of a long loop between residues 146-161. As was the case for the N-terminal domain, this loop is less precisely defined due to a limited number of NMR restraints. This is attributed to the dynamic nature of these residues, which leads to a faster exchange rate for several of the amide proton signals in this region (**Figure 10**). The structure did provide a good description of the location of the three highly conserved cysteine residues (Cys96, Cys117 and Cys159) and an idea of their importance for catalytic activity of MerB. Cys117 is part of the hydrophobic core of the core region of the protein and mutating this residue would most likely disrupt proper folding of MerB. In contrast, Cys96 and Cys159 are located near each other in three-dimensional state and this suggests that they are part of the active site of MerB. In support of this, their amide chemical shifts are significantly altered in the presence of organomercurial substrate (Benison *et al.* 2004, Di Lello *et al.* 2004b).

The NMR structure of MerB provided an initial idea of the location of the active site based on the location of Cys96 and Cys159. However, it was not possible to define the proton donor required for the carbon-Hg bond cleavage from this structure. In addition, no structural or dynamic information could be obtained for residues 1-25 of MerB under the NMR experimental conditions. Based on the primary sequence, the first 25 residues are predicted to form an α helix, but as mentioned above it was impossible to characterize these

residues due to rapid amide proton exchange at pH 7.5, which caused almost complete elimination of signals associated with these residues in the NMR spectra. Alternatively, a rapid conformational exchange involving this region may lead to line broadening and loss of signals in the NMR spectra.

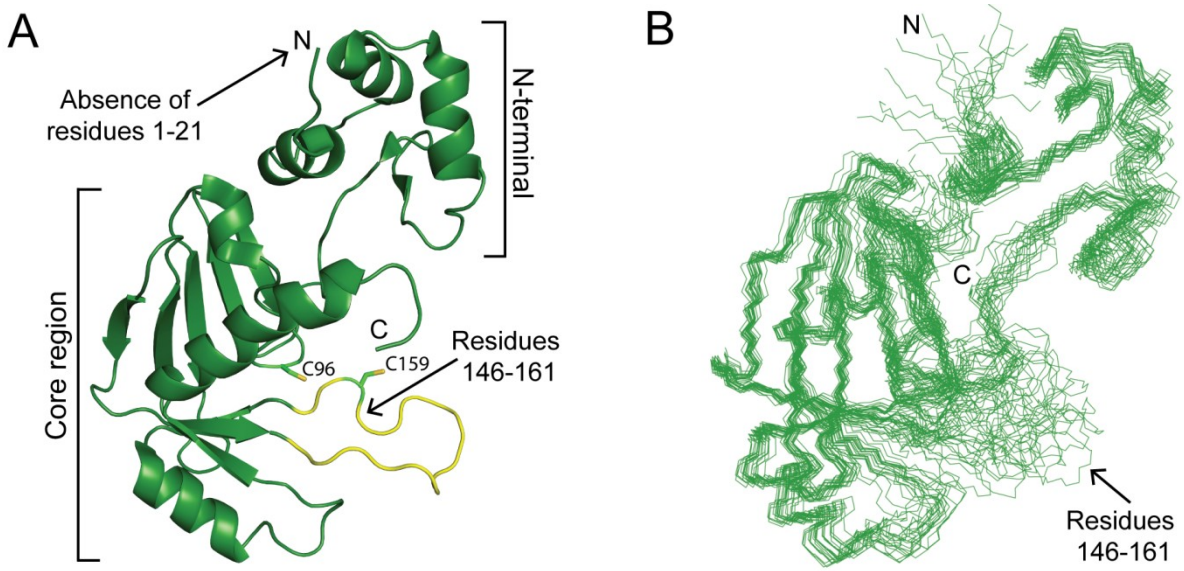

Figure 10: NMR structure of MerB (A) Ribbon model of the average NMR structures of MerB showing the N-terminal domain and the core region. The flexible loop between residues 146-161 (yellow) and the first 21 residues missing from the N-terminal are highlighted with an arrow for clarity. (B) Overlay of the 20 lowest energy NMR structures of MerB. This figure was reproduced from (Lello *et al.* 2010) and prepared using Pymol.

1.4.3.2.3 X-ray crystal structure of MerB

Due to the absence of the amide signals for the first 21 amino acids as well as for several residues in the large loop between residues 146-161, our group decided to pursue studies to determine the crystal structure of MerB in hopes of obtaining a more complete structural picture of this unique enzyme. To obtain a high-resolution crystal structure of MerB, crystallization trials were initiated and MerB crystals that diffracted to 1.76 Å were obtained (**Figure 11 A**) (Lafrance-Vanasse *et al.* 2009). Although MerB exists as a monomer in solution, two identical MerB molecules were present in the form of a homodimer in the asymmetric unit of the crystal with a monoclinic $P2_1$ space group. The

two subunits (subunit A and subunit B) are related to each other by two-fold non-crystallographic symmetry and the overall topologies of the crystal structure and the solution structure are very similar. However, there are three important differences when comparing the X-ray crystal structure with the NMR solution structure. First, the loop

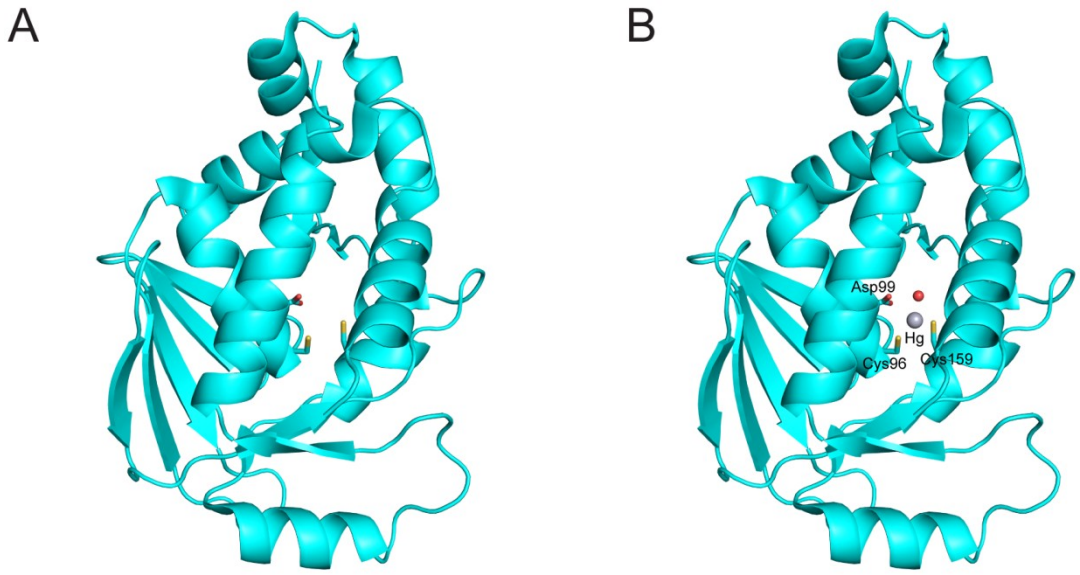

Figure 11: X-ray crystal structure of MerB and MerB-Hg complex.

A) The X-ray crystal structure of MerB. B) The X-ray crystal structure of MerB-Hg complex showing the bound mercuric atom (gray) in the center of the catalytic triad consisting of Cys96, Cys159 and Asp99. The sulfur atoms of cysteine are displayed in yellow, whereas the oxygen atoms of aspartic acid and water are displayed in red.

between residues 146-161, which is poorly defined in the NMR structure, forms an α-helix in the crystal structure (**Figure 12**). Second, the first 25 residues, which appear to be disordered under the NMR experimental conditions, form an α-helix between residues 3-14 in the crystal structure. Interestingly, this α-helix between residues 3-14 is packed against the α-helix formed between residues 146-161 in the core region through a series of hydrophobic contacts. This interaction between these two helices brings the N-terminal domain in close contact with the core region of MerB. The third significant difference is that the crystal structure presents a compact closed conformation of MerB whereas the

solution structure appears to represent a more open conformation of MerB (**Figure 12**). This difference between the solution and crystal structures strongly suggests that MerB is undergoing significant dynamic movements in solution with the N-terminal domain opening and closing over the active site, which maybe important for either its catalytic activity or substrate specificity. In the solution structure, the first 25 residues and residues 146-161 are highly dynamic and this establishes an open confirmation of MerB until ligand binding occurs. Following ligand binding, the interaction between the N-terminal domain and residues 146-161 is stabilized in order to allow carbon-Hg bond cleavage to occur (Lafrance-Vanasse *et al.* 2009, Lello *et al.* 2010).

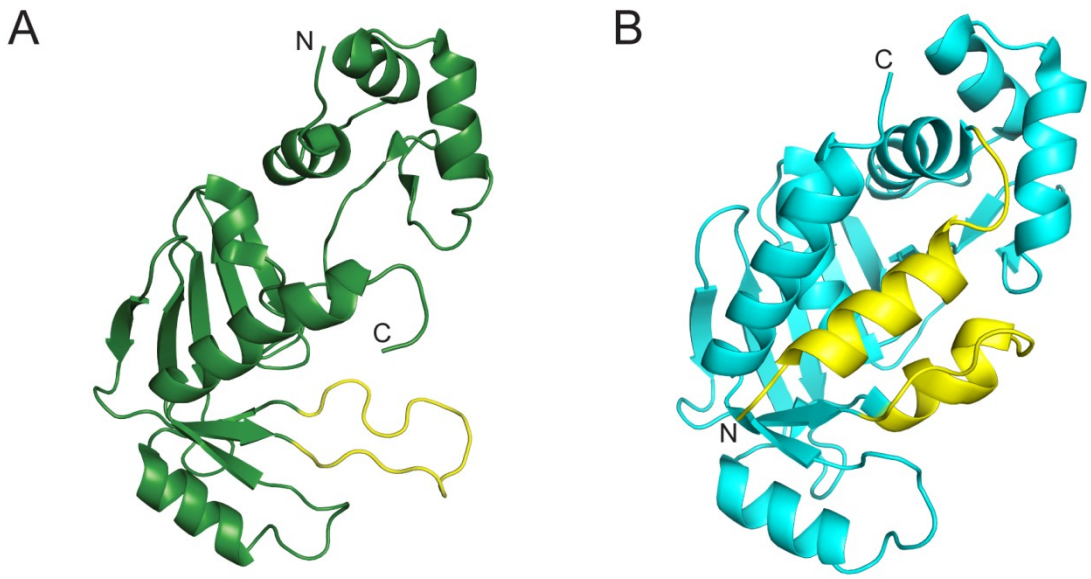

Figure 12: Comparison of the NMR and crystal structures of MerB.

In the NMR structure (A), the flexible loop between residues 146-161 is highlighted in yellow. In the NMR structure, the N-terminal begins at residue 22 since no structural information was obtained in the NMR experiments for residues 1-21. In the crystal structure (B), residues 1-21 are displayed in yellow and there is an α-helix between residues 3-14 that was not observed in the NMR structure.

There is an additional α-helix between residues 146-161 and these residues are also displayed in yellow. N and C refer to the N- and C-terminus respectively. The figure was prepared by Pymol software using the deposited crystal (PDB code: 3F0O) and NMR structure (PDB code: 1S6L)

The hypothesis that catalytic activity is linked to a dynamic conformational change in MerB is supported by Heteronuclear Single Quantum Coherence (HSQC) NMR experiments on a MerB-Hg-DTT complex. DTT is a racemic compound that forms a stable complex with mercury-bound MerB and $^{1}H–^{15}N$ HSQC experiments were used to map the binding pocket for DTT on MerB. The racemic DTT give rise to two signals for a select set of amino acid residues from MerB in $^{1}H–^{15}N$ HSQC spectra due to the formation of two different diastereomeric forms, and the residues that are associated with the two signals are located in the vicinity of the bound DTT molecule. The presence of the two forms of the MerB-Hg-DTT complex was confirmed by the absence of the duplicate signals when the racemic DTT is replaced with optically active L-DTT. Mapping the amino acid residues that form two signals in the presence of racemic DTT on the NMR solution structure suggested an extremely large binding site for DTT, which was inconsistent with the small size of the DTT molecule. However, mapping the same residues onto the crystal structure defines a much smaller binding site that is more consistent with the size of the DTT molecule (Benison *et al.* 2004) (**Figure 13**). This result supports the notion that in solution the N-terminal domain transiently associates with the core region and the MerB structure is exchanging between the open and closed conformation with the closed confirmation being a low energy form trapped in the X-ray crystal structure.

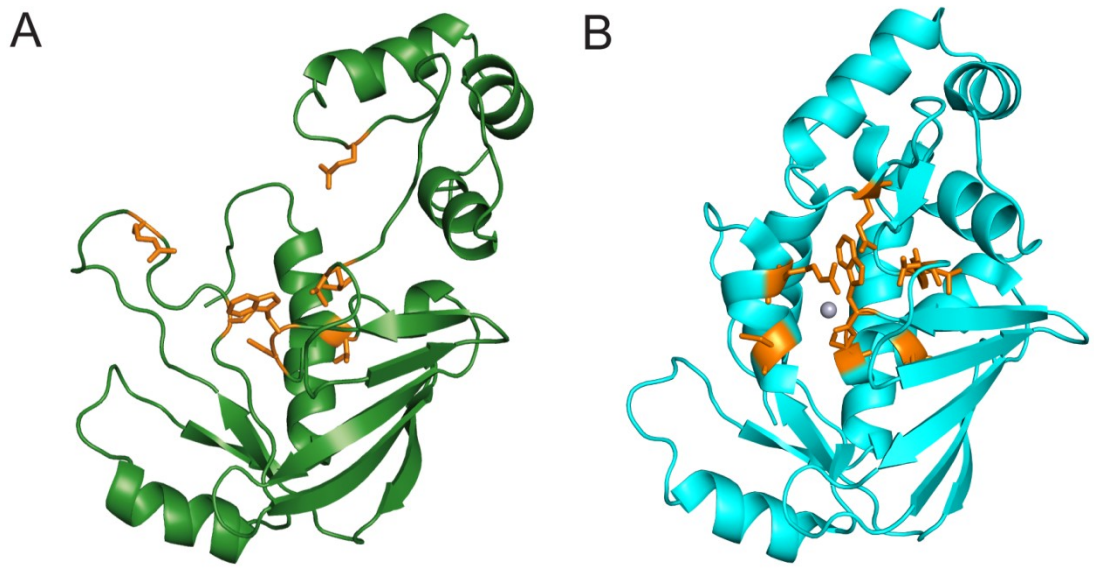

Figure 13: DTT-affected residues in MerB-Hg-DTT complex.

A) The residues that generate two signals in the 2D ^{1}H-^{15}N HSQC spectrum of MerB-Hg-DTT complex when using racemic DTT are highlighted on the NMR structure in orange. B) The same residues highlighted in orange on the crystal structure of the MerB-Hg complex. The figure in panel A was adapted from (Benison *et al.* 2004).

1.4.3.2.4 X-ray crystal structure of the Hg-MerB complex

Since previous studies demonstrated that free Hg^{II} binds at a 1:1 ratio and inhibits the enzymatic activity of MerB, our group attempted to determine the structure of a MerB-Hg complex by soaking our apo-MerB crystals in a solution of $HgCl_2$. After soaking in $HgCl_2$, the structure of the resultant MerB-Hg crystal is almost identical to the structure of the apo-MerB with the exception of a bound mercury atom present in the active site (Lafrance-Vanasse *et al.* 2009) (**Fig 11 B**). The mercury atom in the MerB-Hg complex is bound in a planar-trigonal conformation to sulfur atoms of Cys96 and Cys159 as well as to an oxygen atom of a water molecule. The distance between the mercury atom and the sulfur atoms of Cys96 and Cys159 are 2.3 Å and 2.4 Å, respectively, whereas the oxygen from the bound water is 2.6 Å away (**Figure 14**). In addition, there is a fourth coordination between the bound mercury atom and an oxygen atom from the carboxylate of Asp99 at a distance of 2.9 Å. The distances between the side chains of Cys96, Asp99 and Cys159 in the free and

Hg^{II}-bound MerB structures are almost identical. The oxygen atom of Asp99 is 3.6 Å and 4.3 Å from the sulfur atoms of Cys96 and Cys159, respectively. The close proximity of Asp99 to the bound mercury and the sulfhydryl group of Cys96 suggests that it might play a key role as the proton donor during carbon-Hg bond cleavage. All three residues (Cys96, Cys159 and Asp99) are located inside a hydrophobic pocket, which serves to accommodate the hydrophobic organomercurial substrates. However, the active site in the crystal structure is buried and not solvent accessible. The sulfhydryl groups of Cys96 and Cys159 as well as the carboxylate group of Asp99 are buried as a result of hydrophobic contact between the α-helix between residues 3-14 at the N-terminal end of the protein and the helix between residues 148-161 in the core region. The accessibility of organomercurials to the buried active site can be explained by two possible mechanisms. The first mechanism requires the movement of the N-terminal α-helix out of the active site. This mechanism is supported by the fact that this α-helix is dynamic in solution based on the NMR experiments. The second mechanism requires that the organomercurial substrate is able to induce a conformational change in the loop involving residues 148-154. The dynamic nature of residues 148-154 is consistent with their high B-factor and weak electron density map in the crystal structure. This is further supported by the fact that the apo-MerB crystals are catalytically active and soaking them with a solution of an organomercurial compounds (MeHg or PHMBA) results in the formation of a MerB-Hg complex. This would not be possible unless there is some conformational dynamics occurring between the N-terminal domain and the region containing residues 148-154 (Lafrance-Vanasse *et al.* 2009, Lello *et al.* 2010).

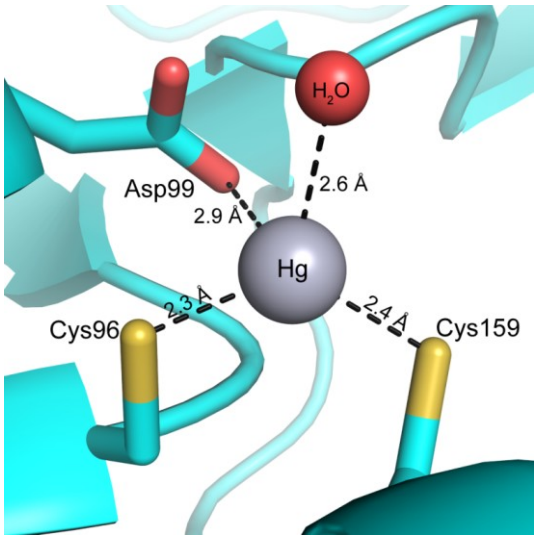

Figure 14: The MerB active site. The active site of the MerB-Hg complex shows Cys96 and Cys159 binding to the Hg^{II} atom along with one water molecule. Asp99 also is in proximity to Cys96 and the bound Hg^{II}. The backbone of the MerB-Hg complex is displayed as a ribbon (cyan), and the side chains of the three active site residues (Cys96, Asp99, and Cys159) are displayed as sticks with the sulfur atoms (yellow) of Cys96 and Cys159 and the oxygen atom (red) of Asp99. Hg^{II} is a sphere of gray color. A molecule of bound water (red sphere) is also present.

1.4.3.2.5 The Key catalytic residues are conserved in most MerB variants.

In order to help verify that Cys96, Asp99 and Cys159 are in fact the key catalytic residues in MerB as proposed based on the crystal structure of Hg-bound MerB, a Blast analysis was performed with the MerB (R831b) sequence (Lello *et al.* 2010). The Blast analysis revealed the presence of 65 known variants of MerB ranging between 210-220 amino acid residues in length. ClustalW alignment of these 65 organomercurial lyase sequences showed that they all contain cysteines in the positions corresponding to Cys96 and Cys159 in the MerB (R831b) sequence. In addition, the residue in the position corresponding to Asp99 in the MerB (R831b) sequence is also conserved in 61 out of the 65 organomercurial lyase variants. However, the four remaining organomercurial lyase variants contain a serine residue in the position corresponding to Asp99. These four MerB variants exist in *Bacillus Cereus, Bacillus megaterium, Clostridium butyricum* and *Bacillus*

sp. (strain RC607) and they share 100% sequence identity with each other, but only 22% sequence identity with MerB (R831b). These four sequences are all considered as MerB2 proteins because the *mer* operon from which they are expressed encodes for two distinct organomercurial lyases and the serine variants are the second of the two MerB sequences in the operon (Pitts & Summers 2002, Lello *et al.* 2010). Interestingly, the first MerB sequence (known as MerB1) encoded by these operons contains an aspartic acid residue in the position corresponding to Asp99 in all four cases. Thus, the four *mer* operons that encode for the serine-containing MerB2 protein, all express a MerB1 protein that contains the three proposed catalytic residues (Cys96, Asp99 and Cys159) (Huang *et al.* 1999, Chien *et al.* 2010). The exact role for the MerB2 protein with a serine residue in its active site is currently unknown, but it has been shown that these serine variants may have a modified substrate preference. In particular, it appears they prefer PCMB (*p*-chloro mercuric benzene) as a substrate over MeHg (Wang *et al.* 1989, Chien *et al.* 2010). However, these serine-containing variants all have lower activity in comparison to MerB variants with aspartic acid. Thus, it appears that Cys96, Asp99 and Cys159 are the key residues required for maximal efficiency of carbon-Hg bond cleavage by organomercurial lyases.

1.4.3.2.6 Proposed catalytic mechanism of MerB based on X-ray structure

Several possible catalytic mechanisms for MerB have been suggested both before and after determination of the NMR and crystal structures. These mechanisms are based on biochemical, kinetics and computational studies as well as our structural studies (Begley *et al.* 1986b, Moore *et al.* 1990, Pitts & Summers 2002, Miller 2007, Lafrance-Vanasse *et al.* 2009, Parks *et al.* 2009). In addition, non-enzymatic (chemical) cleavage of carbon-Hg bonds using mercury-thiolated complexes has been examined and these models help in better understanding the catalytic mechanism for cleaving carbon-Hg bonds by MerB (Gopinath & Bruice 1987, Wilhelm *et al.* 2004, Ni *et al.* 2006, Melnick & Parkin 2007). Due to the high resolution and accurate definition of the core catalytic residues, the MerB crystal structure was used as the basis for validating and updating the proposed catalytic mechanism. Based on the crystal structure, we proposed that the organomercurial substrate binds first to an exogenous thiol in the cytosol (**Figure 15**). Due to its proximity, Asp99

maintains the sulfhydryl group of Cys96 in the deprotonated state and Cys96 initiates the first nucleophilic attack on the mercury atom of the organomercurial substrate. Once bound to the sulfur atom of C96, there is an almost simultaneous nucleophilic attack by the sulfur atom of Cys159 on the mercury atom and this results in the displacement of the bound exogenous thiol. The bound organomercurial substrate is now polarized with a partial positive charge on the mercury atom and a partial negative charge on the carbon atom. The carbon-Hg bond is activated and ready for protonolysis by Asp99, which donates the proton to the hydrocarbon product and the mercury atom remains bound in the active site (**Figure 15**) (Lafrance-Vanasse *et al.* 2009, Lello *et al.* 2010).

This proposed mechanism is supported by previous studies examining non-enzymatic cleavage of carbon-Hg bonds, where it was clearly demonstrated that organomercurial compounds ligated with at least two thiol groups are readily activated for protonolysis in the presence of an acidic proton donor (Melnick & Parkin 2007, Melnick *et al.* 2009). In these studies, synthetic R-Hg-$(thiolate)_n$ complexes (where n represents the number of thiol groups ligating the organomercurial including mono-, di- and tri-thiolate) were prepared to provide different coordinating numbers to the organomercurial compounds. It was found that mono-thiolated (n=1) organomercurial compounds display almost no appreciable cleavage, whereas the di- and tri-thiolated complexes are readily susceptible to carbon-Hg cleavage at room temperature upon addition of thiophenol, which functioned as the proton donor (Melnick & Parkin 2007, Melnick *et al.* 2009). This model provided supporting evidence for the role of Cys96 and Cys159 in binding to mercury atom and in activating carbon-Hg bond for protonolysis and for the acidic sulfhydryl group from thiophenol in donating the proton. The proton donor residue in MerB was later identified as Asp99 based on the X-ray crystal structure. To validate the role of Asp99 as a proton donor, a computational study of the carbon-Hg cleavage by MerB based on the crystal structure was performed. This study suggested that it was also possible that the thiol group of Cys159 could initiate the attack on the organomercurial as well as Cys96, but they confirmed that Asp99 was the most likely proton donor (Parks *et al.* 2009).

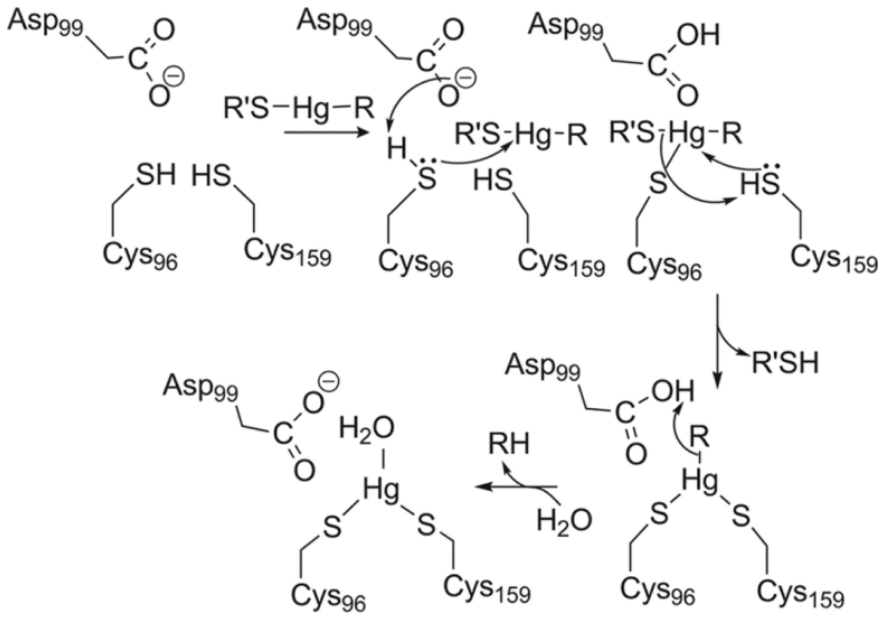

Figure 15: The mechanism of carbon-Hg bond cleavage by MerB.

In this mechanism, Asp99 acts as a general acid-base catalyst. First, Asp99 activates Cys96 through proton abstraction and Cys96 attacks the organomercurial substrate followed by a subsequent attack by Cys159. Then, Asp99 donates a proton to the carbanion (CH_3-) for protonolysis of the carbon-Hg bond. The mechanism is proposed based on the structure of MerB-Hg complex along with previous kinetic and mutagenesis studies. The figure was adapted from (Lafrance-Vanasse *et al.* 2009).

1.4.3.2.7 MerB is structurally similar to NosL

As mentioned earlier, the NMR structure of MerB revealed that it represented a novel protein fold at the time, since no structural homolog was identified in the PDB (Di Lello *et al.* 2004b). Shortly afterwards, it was determined that the copper-binding protein NosL displayed structural homology with the core region of MerB (**Figure 16**) (Taubner *et al.* 2006). NosL is one of the proteins encoded by the nitrous oxide reductase (NOS) gene cluster. NosL is a 193 residue inner-membrane binding protein. Although the exact biological function of NosL has not been precisely defined, it is generally thought to act as a metallochaperone due to its copper-binding properties (McGuirl *et al.* 2001).

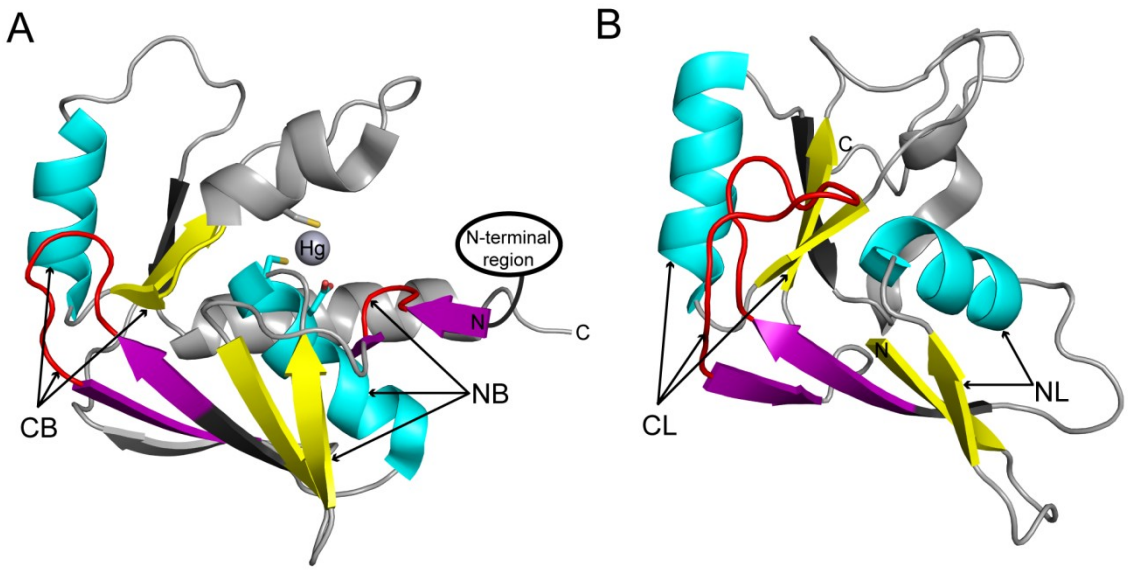

Figure 16: Folding similarity between core regions of MerB and NosL supports their evolutionary link. A) The structure of MerB core region (residues 71-212, PDB code; 3F0P) showing the fusion of two treble-clef motifs, NB and CB. B) The structure of NosL core region (residues 53-178, PDB code; 2HPU) showing the fusion of two treble-clef motifs, NL and CL. With the exception of NL, each treble-clef motif consists of a β-hairpin (yellow), an α-helix (cyan), a knuckle (red) and a β-hairpin containing the knuckle (violet). The conserved β-strand outside of the treble-clef is shown in black. All other insertions are represented in gray. The N- and C-terminal ends are labeled N and C, respectively. The N-terminal region of MerB was removed for clarity. The figure was adapted from (Kaur & Subramanian 2014)

The structure of NosL and the identity of its copper-binding site were partially determined using NMR spectroscopy and EXAFS (extended X ray absorption fine structure) experiments, respectively. For the NMR studies, the membrane-binding region (residues 1-52) was removed to enhance the solubility of the protein in solution, and the structural information was determined only for the core region of the protein between residues 53-178. This region of NosL adopts two perpendicular β-sheets and each of the β-sheets is packed against an α-helix and this topology is very similar to the core region of MerB. In addition, EXAFS studies suggested binding of Cu^{I} to NosL occurs through one nitrogen and two sulfur atoms. Due to the fact that it is highly conserved in all known variants of NosL, it was postulated that Met127 (*Achromobacter cycloclastes* numbering) donates one

of the sulfur atoms for Cu^{I} coordination, but the precise identity of the other amino acids required for metal binding is currently unknown. Interestingly, Met127 is located in a loop that can be superimposed upon the loop of MerB containing Cys159 when aligning the core region from both proteins. Although NosL and MerB (R831b) have different biological function and low sequence identity (~20%), NosL is the only structural homolog to MerB with an rmsd of 3.0 Å about the backbone and their structural and functional (metal binding) similarities suggested a possible evolutionary link between MerB and NosL (Taubner *et al.* 2006).

To determine if there was in fact an evolutionary link between the NosL proteins and the MerB proteins, a recent bioinformatics study was performed and it was found that the core regions of NosL and MerB are both composed of two TRASH-like treble-clef zinc-finger domains (Kaur & Subramanian 2014). Treble-clef zinc finger domains are typically composed of a zinc knuckle, a β-hairpin and an α-helix. These same elements could be identified in the N-terminal side (referred as NB) of the MerB core region where residues 74-75 represent the knuckle, residues 83-94 form the β-hairpin and residues 96-108 form the α-helix. In a similar manner, the second treble-clef zinc-finger domain is present in the C-terminal side of the MerB core region between residues 114-176 (CB). Likewise, two treble-clef zinc-finger domains also exist in NosL near the N and C-terminus of the core region and they are referred to as NL and CL, respectively. Both NB and CB of MerB superimpose with rmsd of 1.7 Å and NL and CL of NosL superimpose with an rmsd of 1.2 Å. Furthermore, the treble-clef zinc-finger domains of MerB and NosL have an rmsd of 1.7 Å when comparing NB of MerB and NL of NosL and an rmsd of 1.8 Å between CB of MerB and CL of NosL. As previously mentioned, the entire core region of MerB and NosL align with an rmsd of 3 Å. These results indicate that the core regions of MerB and NosL appear to have evolved from the fusion of two treble-clef zinc-finger domains. The fact that proteins containing treble-clef zinc-finger domains are often involved in metal trafficking further supports an evolutionary link between MerB and NosL (Kaur & Subramanian 2014).

1.4.3.2.8 Direct transfer of Hg^{II} product from MerB to MerA

As discussed earlier, Hg^{II} is directly transferred from MerP to MerT and from MerT to the N-terminal domain of MerA (NMerA) through a series of cysteine residues when mercury-resistant bacteria are exposed to ionic mercury. Similarly, NMerA directly delivers the Hg^{II} to two cysteine residues in the catalytic site of MerA for the final reduction to elemental mercury (**Figure 7**) (Ledwidge *et al.* 2005). Direct transfer of the toxic Hg^{II} through protein-protein interactions involving two proteins or through domain-domain interactions involving the same protein without release into the cell has a distinct physiological advantage, as this protects other cellular components from the detrimental implications of the thiophilic Hg^{II}. Although the Hg^{II} product generated after carbon-Hg cleavage by MerB is slightly less toxic than the organomercurial substrate, Hg^{II} still represents a considerable risk if it is allowed to diffuse in the cytosol, where it would quickly bind to cysteine residues of proteins. Thus, it would be of physiological benefit to the cell if the Hg^{II} product from the MerB cleavage reaction were passed directly from MerB to MerA for the final detoxification step. To test the hypothesis that Hg^{II} passes directly from MerB to MerA, our group examined the transport of Hg^{II} from the stable MerB/Hg/DTT ternary complex to MerA (Benison *et al.* 2004). The experiment provided evidence that the Hg^{II} bound in the MerB/Hg/DTT ternary complex is indeed transferred directly to MerA as opposed to being freely released. To identify the pairs of cysteines of MerA that participate in this direct transfer of the Hg^{II} from MerB to MerA, another experiment was conducted using a MerB-Hg complex in the presence of either the NMerA domain or the MerA core domain to test which domain most efficiently extracted the Hg^{II} bound to MerB (Hong *et al.* 2010). The transfer was monitored using fluorescence quenching experiments with MerB. Typically, MerB gives a fluorescent emission peak at 340 nm when it is excited at 295 nm due to the presence of three tryptophan residues. However, Hg^{II} binding to MerB quenches the intensity of the fluorescence signal due to the near proximity of Trp95 in the active site of MerB to the Hg^{II} binding site. The fluorescence intensity is restored when the Hg^{II} is released from the MerB active site, and this property was used to monitor removal of Hg^{II} by NMerA and the core domain of MerA. It was determined that NMerA was more efficient than the core domain at removing

Hg^{II} from MerB and this suggested that Cys13 and Cys16 are the residues in MerA that are responsible for the transfer of Hg^{II} from MerB and delivering it to MerA for reduction to Hg^{0}.

1.5 Organotin compounds are substrates and inhibitors of MerB

The catalytic activity of MerB towards organomercurial compounds has attracted attention for possibly using its unique properties in bioremediation applications for cleaning up mercury-contaminated sites. Indeed, using a bioreactor with mercury resistant bacteria or producing transgenic plants expressing either MerA and/or MerB are examples of using such techniques as a form of green technology. However, organomercurial compounds represent only a small fraction of the organometalic compounds contaminating the environment. For example, other organometals that pose similar threats to the environment include organotin and organolead compounds. Organotin compounds were commonly used as bactericides, fungicides and pesticides. In particular, tributyltin (TBT) and triphenyltin (TPT) were extensively employed as anti-fouling paints in the shipbuilding industry and this contributed directly to contaminating the marine environment especially in harbor areas (**Figure 17**) (Olushola Sunday *et al.* 2012, Dubalska *et al.* 2013). In the marine environment, organotin contamination has been directly linked to growth abnormalities in several small marine creatures including oysters and mussels. Like organomercurial compounds, organotin compounds have the capacity to bioaccumulate and their concentrations increase in higher organisms as they pass through the food chain (Dubalska *et al.* 2013). For humans, the two most important routes of exposure are either through consuming organotin-contaminated seafood or via direct inhalation in the work environment. The toxicity of organotin compounds varies based on the composition and number of organic groups bound to the Sn atom, and a higher number of substitutions of a particular group is generally more toxic than a lower substituted one. For example, R_3SnX is more toxic than R_2SnX_2, where X is the counter ion and R is the organic substituent.

The toxic effect of organotin compounds is in part associated with their direct impact on mitochondrial function. TBT was found to inhibit Mg-ATPase activity in mussel

mitochondria (Pagliarani *et al.* 2008). Similarly, trimethyltin and triethyltin have been shown to inhibit mitochondrial oxidative phosphorylation, whereas other diorganotin were found to inhibit α-keto acid oxidase and consequently stop mitochondrial respiration (Nesci *et al.* 2011). The toxic effects and wide-spread contamination of organotin compounds led several research groups to investigate whether or not microorganisms have developed a natural organotin-resistant system similar to the one for organomercurial resistance. Although select bacterial and fungal strains show a degree of resistance to organotin compounds, a specific organotin-detoxification system has not yet been identified. Since organotin and organomercurial compounds share similar chemical properties such as hydrophobicity and thiophilicity, it was hypothesized that organotin compounds could potentially be substrates for MerB. For example, organotin compounds, such as diethyltin dichloride, inhibit α-ketoacid oxidases through their ability to bind to two cysteine residues present in its active site (Aldridge 1976). To characterize the interaction between MerB and organotin compounds, as well as to test whether or not MerB possesses the capacity for cleaving carbon-Sn bonds, a number of organotin compounds were tested with MerB (Walts & Walsh 1988). MerB successfully cleaved the carbon-Sn of several organotin compounds, but it displayed a rather narrow range of specificity for organotin compounds in comparison to the broad specificity observed with organomercurial compounds. MerB cleaved the carbon-Sn bond of tetravinyltin (TVT), triethylvinyltin (TEVT), tetramethyltin (TTMT) and trimethyltin fluoride (TMTF), but there was no cleavage observed with tetraethyltin (TTET), tetrabutyltin (TBT), triethyltin acetate (TETA) or tributyltin oxide (TBTO). However, a decrease in MerB catalytic activity was noted as the reaction proceeded for those substrates where cleavage was observed. This suggested that the resultant di- or mono-substituted tin products might function as inhibitors of MerB. Based on this assumption, dimethyltin dibromide (DMT) was tested as a potential MerB substrate, and, as suspected, it was found to be a potent irreversible inhibitor (Walts & Walsh 1988). The fact that several organotin compounds such as DMT are inhibitors of MerB suggests they might be useful tools for better understanding the mechanism of carbon-metal bond cleavage by MerB.

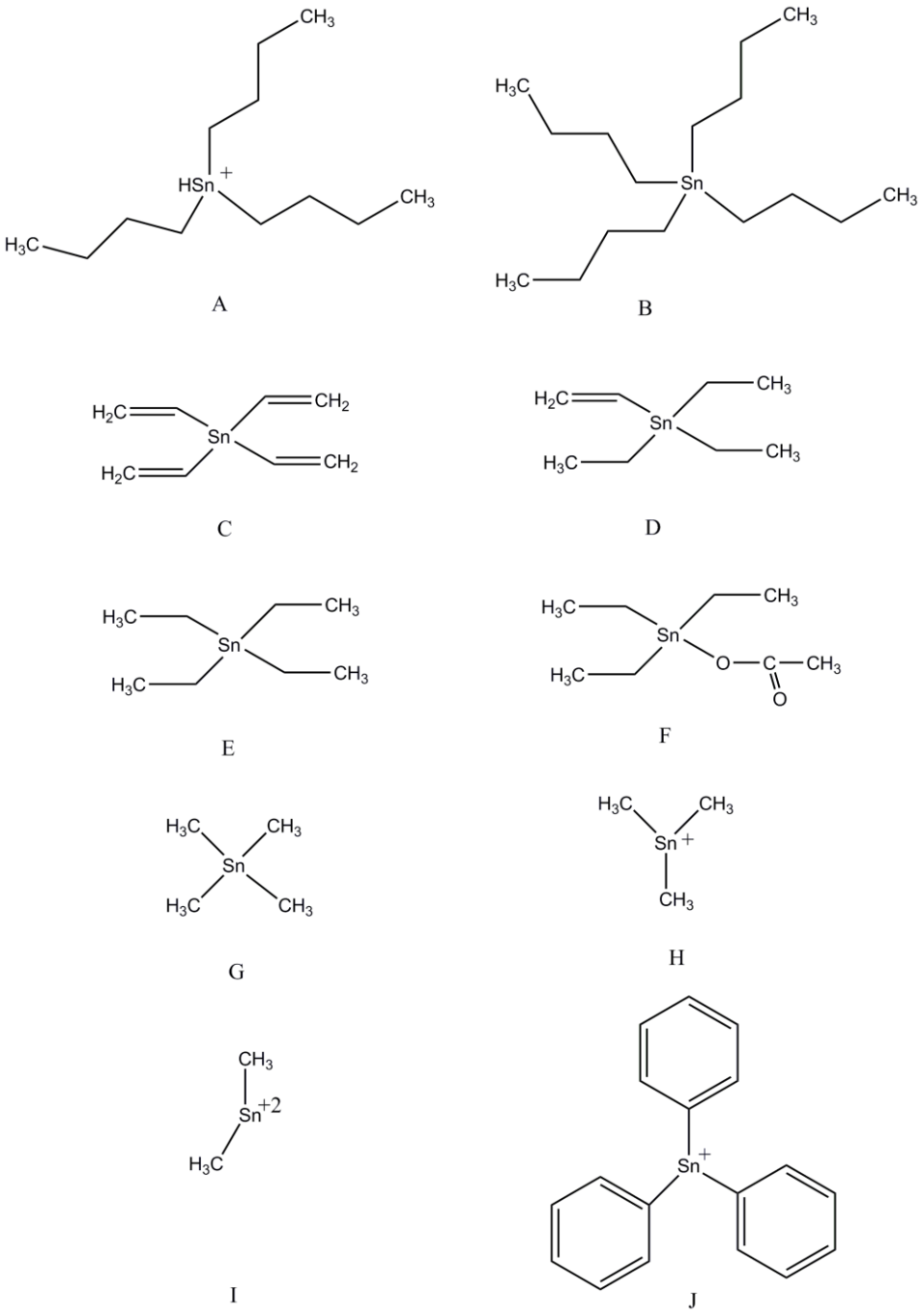

Figure 17: Structures of some organotin compounds (R_nSn^{IV}). Structures of tributyltin (TBT) (A), tetrabutyltin (TBT) (B), tetravinyltin (TVT) (C), triethylvinyltin (TEVT) (D), tetraethyltin (TTET) (E), triethyltin acetate (TETA) (F), tetramethyltin (TTMT) (G), trimethyltin fluoride (TMTF) (H), dimethyltin dibromide (DMT) (I) and triphenyltin (TPT) (J).

1.6 Organolead compounds

For decades, organolead compounds were extensively used as anti-knocking agents in combustion engines. Tetraethyl lead (TTEL) was first used as a gasoline additive in 1923 and was replaced by tetramethyl lead (TTML) starting in 1960. As a result of this extensive use of leaded gasoline, tremendous quantities of organolead compounds were released as part of automobile exhaust fumes (Mason & Benoit 2003) and this anthropogenic emission is one of the primary sources of lead contamination in our environment. Following their combustion in automobile engines, the organolead compounds remained in the vapour phase and this allowed them to distribute widely in the atmosphere. Over time, the organolead compounds were initially deposited either in soil or aquatic surfaces, and they eventually settled into sediment layers. As a result of their rather universal distribution through the atmosphere, organolead compounds can now be readily detected in roadside soils, grass, tree leaves, rain, surface water, sediments and marine animals and thus, they eventually find their way into humans (Ou *et al.* 1995). TTEL and TTML are themselves very unstable as they are rapidly converted to their respective tri-, di- and mono-alkyl lead species as well as to ionic lead following their release into the environment. However, the most persistent intermediates are the trialkylated lead species: triethyl lead (TEL) and trimethyl lead (TML) (**Figure 18**).

The degradation of TTEL and TTML in aqueous environments is attributed to chemical abiotic processes that involve a number of factors including sunlight, ozone and hydroxyl radicals (Jarvie *et al.* 1981). TTEL and TTML are degraded in a similar manner in soil, but the soil decomposition mechanisms are less precisely defined (Ou *et al.* 1995). In contrast to TTEL and TTML, TEL and TML are more stable, less volatile and more water-soluble. Thus, they have a greater capacity to dissolve in rainwater and filter into groundwater. All chemical forms of organolead compounds are toxic to some degree, and as was the case for organotin compounds, the higher substituted forms are more toxic than lower substituted ones. Therefore, the trialkyl lead compounds are more toxic than the dialkyl lead derivatives, but less toxic than the tetraalkyl derivatives. The toxicity also increases with the length of the alkyl chain so that ethyl substituted lead is more toxic than the methyl

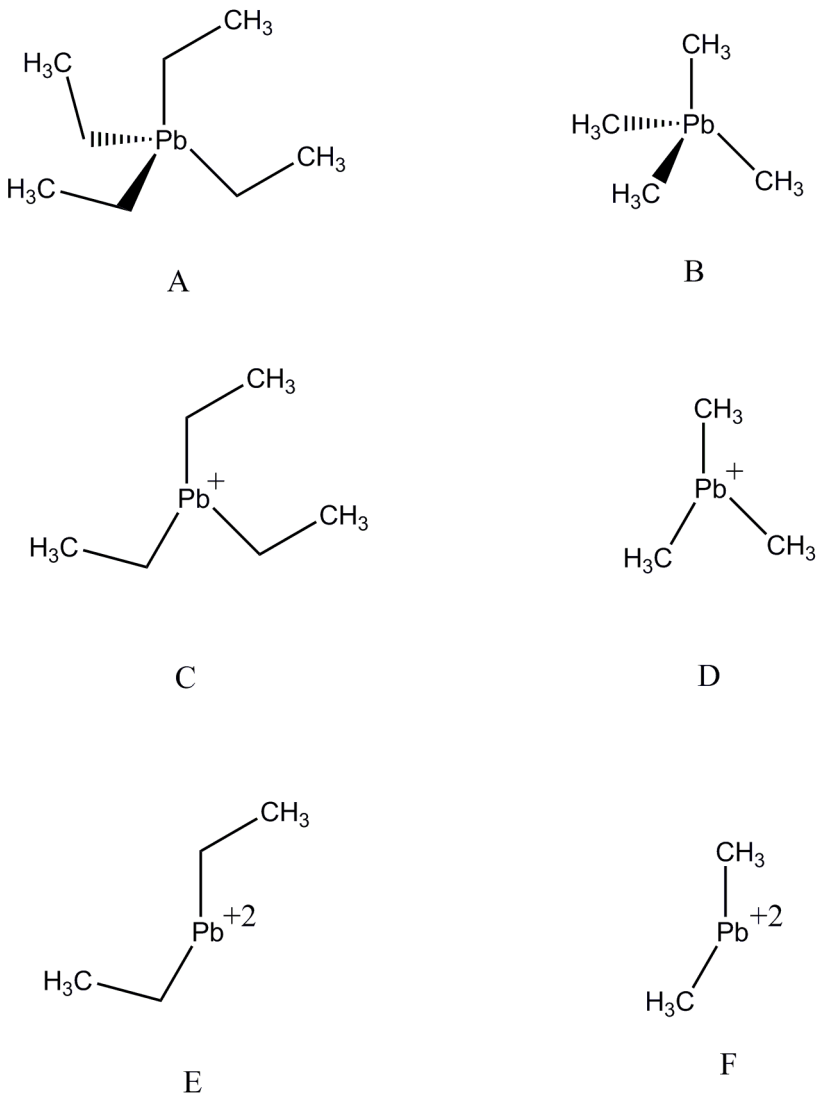

Figure 18: Structures of some organolead compounds (R_nPb^{IV}). Structures of tetraethyl lead (TTEL) (A), tetramethyl lead (TTML) (B), triethyl lead (TEL) (C), trimethyl lead (TML) (D), diethyl lead (DEL) (E) and Dimethyl lead (DML) (F).

substituted forms. Similar to both organomercurial and organotin compounds, organolead compounds show higher toxicity profile than their inorganic forms (Eisler 1988) and the stable trialkylated lead compounds are the primary toxins in most cases due to their persistence in the environment (Zachariadis & Rosenberg 2012). Although the high lipophilicity of alkylated lead compounds allows them to be easily absorbed through skin,

the most common route of exposure is through inhalation. After inhalation, TTML and TTEL rapidly concentrate in the liver, kidney as well as the nervous system since they readily cross the blood brain barrier due to their lipophilicity. The symptoms associated with exposure to high levels of organolead compounds include neurobehavioral abnormalities and impairment of memory. In addition, workers exposed occupationally to alkyllead compounds incurred elevations in their blood pressure (Sigel *et al.* 2010). The high load of organolead compounds from automobile exhaust has had an adverse effect both on the environment and human health especially for those who were subjected to organolead through their occupation. With the growing of human concern about deleterious effect of organolead compounds on human health, there was a significant decline in their use as petroleum additives. Beginning in 1980, the use of organolead additives in gasoline was prohibited in many, but not all countries. As a result, there has been a substantial decrease in lead emissions. However, there are still elevated levels of organolead compounds in soil and groundwater from decades of heavy contamination. Moreover, a recent discovery might lead to a new threat from organolead compounds. In 2009, it was discovered that methylammonium lead halides (example $CH_3NH_3PbI_3$) are remarkablely efficient compounds for use in solar cells (Zhu *et al.* 2016). Due to their high performance and low cost in combination with our great need for efficient sources of renewable energy, it is expected that organolead halide solar cells will play an important role in future generations of solar cells by replacing current silicon based solar cell (Wu *et al.* 2016). However, extreme caution is needed since this may lead to a significant quantity of organolead compounds being introduced into the environment.

As is the case for both organomercurial and organotin compounds, there have been several attempts to remediate organolead-contaminated sites using either chemical or physical remediation methods. Among the tested approaches are chemical oxidation with different reactants (hydrogen peroxide, potassium permanganate, potassium persulfate and perozone), filtration on granular activated carbon (GAC) and UV radiation. These methods were examined for *ex-situ* remediation of contaminated ground water and it was determined that a combination of GAC filtration followed by chemical oxidation with perozone was the most effective approach (Andreottola *et al.* 2008). However, this approach is only

applicable on a small scale and so far no bioremediation techniques have been developed for cleaning up organolead-contaminated sites. Since organolead compounds also have similar lipophilicity and thiophilicity to organomercurial compounds, one possibility might be to re-engineer MerB to cleave carbon-Pb bonds. Thus, we decided to test whether or not MerB has the capacity to cleave carbon-Pb bonds of organolead compounds as part of my thesis.

1.7 Overall rational of the thesis

In bacterial resistance to mercury, MerB is the key enzyme in detoxification of organomercurial compounds through its capacity to cleave carbon-Hg bonds. The biochemical basis of carbon-Hg bond cleavage has been previously investigated using a combination of biochemical, kinetic and structural studies (Lello *et al.* 2010). The kinetics studies revealed that carbon-Hg bond cleavage occurs through a concerted S_2E reaction mechanism (Miller 2007). NMR structural studies identified the catalytic core region of MerB, but failed to precisely define the proton donor involved in the catalytic reaction. In contrast, the X-ray crystal structure was able to clearly define a catalytic triad that consisted of Cys96, Cys159 and Asp99. Based on the high-resolution crystal structure of the MerB-Hg complex, a mechanism was proposed in which Asp99 deprotonates Cys96 and this initiates the binding of MerB to the organomercurial substrate (Lafrance-Vanasse *et al.* 2009). Cys159 then binds to the substrate and this leads to carbon-Hg bond cleavage, where Asp99 functions as the proton donor for the formation of the hydrocarbon product (Lafrance-Vanasse *et al.* 2009). Following the cleavage of the carbon-Hg bond, the hydrocarbon product is directly released whereas the Hg^{II} product remains bound in the active site to a sulfur atom of Cys96, a sulfur atom of Cys159 and an oxygen atom of a bound water molecule, with the closest oxygen atom of Asp99 being approximately 3 Å from the Hg^{II}. Cys96 was suggested to be the first residue to attack the substrate due to its near proximity to Asp99. A subsequent computational study based on the crystal structure suggested that either Cys96 or Cys159 could initiate the attack (Parks *et al.* 2009). However, there has been no experimental information to validate either of the two proposed mechanisms.

For my project, the goal was to better define the mechanistic details of carbon-Hg bond cleavage by MerB in order to obtain a better understanding of this unique enzyme so that it can be better exploited in either industrial applications or in remediation of mercury-contaminated sites. To accomplish this goal, I have taken two approaches to test and/or validate the two proposed mechanisms of MerB activity. The first approach was to prepare mutants of the three key catalytic residues and to test their activity for organomercurial substrates. The second approach was to test the catalytic activity of MerB for different organometalic compounds including the organotin compounds, which have been shown to function both as substrates as well as inhibitors for MerB. These two approaches were selected because they should help us define the exact role that each catalytic residue plays in carbon-Hg bond cleavage and the order in which they participate. We first tested the role of Cys96 or Cys159 by preparing two serine mutants: MerB C96S and MerB C159S. These serine mutations were chosen because serine represents the closest chemical substitution for a solvent exposed cysteine amongst the 20 amino acids. Based on our proposed mechanism, we hypothesized that if Cys96 is the first residue to bind the substrate, the MerB C96S mutant will not bind the substrate and the Hg^{II} product will not be detected in the active site of MerB crystals. In contrast, we would expect binding to the substrate through Cys96 with the MerB C159S mutant, but the reaction will not proceed to completion. To test this hypothesis, we first solved the crystal structures of both mutants and their structures were both similar to the wild-type MerB structure, as expected. Next, we soaked the MerB C96S and MerB C159S crystals in solutions containing organomercurial substrates (PCMB or EtHg). As expected, we did not detect substrate binding in the active site of the MerB C96S mutant. Unfortunately, we also failed to observe substrate binding with the MerB C159S mutant. The conclusion from these studies was that both cysteines are essential for both substrate binding and carbon-Hg bond cleavage.

Given the minimal information obtained with the C96S and C159S mutants, we decided to investigate the role of Asp99 in carbon-Hg bond cleavage by MerB. Initially, we proposed to substitute asparagine for aspartic acid since it is the closest isosteric replacement amongst the twenty amino acids. However, we then considered serine given the fact that there are four known MerB variants where Asp99 is replaced by a serine

residue (*B. megaterium* MerB2, *B. subtillis* MerB2, *Bacillus sp*. (RC607) MerB2 and *C. butyricum* MerB2). In the case of *B. megaterium* MerB2, the protein has much lower enzymatic activity and shows a preference for PCMB over either MeHg or EtHg, when compared to other MerB proteins with an aspartic acid residue at the equivalent position in their active site, including the *B. megaterium* MerB1 protein (Chien *et al.* 2010). Thus, we were interested in characterizing the role of the active-site serine residue in place of aspartic acid on MerB structure and function. To accomplish this goal, I attempted to determine the crystal structures and metal binding properties of the wild-type *B. megaterium* MerB2 protein that naturally contains a serine in the active site as well as the structure of an *E. coli* MerB protein with a serine substituted for Asp99 (MerB D99S). The results of these studies are discussed in Chapter 2 of this thesis.

As an alternative way to mechanistically probe the catalytic mechanism of MerB, I examined the structure of MerB in the presence of known inhibitors and other organometallic compounds that share similar properties to organomercurial compounds. Like organomercurials, organotin and organolead compounds are chemically stable and they are similar in terms of both hydrophobicity and thiophilicity. Previous studies have demonstrated that the organotin compound DMT inhibits the catalytic activity of MerB (Walts & Walsh 1988). Thus, we were interested in structurally investigating how DMT inhibited MerB with the hope that we would gain important insights into the catalytic mechanism of MerB. Furthermore, we were interested in examining organotin and organolead compounds as potential substrates given their chemical similarity to organomercurial compounds. This idea is supported by previous studies demonstrating that MerB could cleave certain organotin compounds albeit at a slower rate in comparison to organomercurial compounds (Walts & Walsh 1988). In particular, we were interested in assessing the role of the catalytic triad of MerB in cleaving carbon-Sn and carbon-Pb bonds. Such information will not only help in assessing the feasibility of utilizing MerB for cleaning up organomercurial contaminated site, but also other toxic organometals, which have been extensively released through anthropogenic activities. The results of these studies are discussed in Chapter 3 of this thesis.

1.8 Experimental procedures used for studying metal ion binding to protein

During the course of my Ph.D. studies, I used X-ray crystallography as the predominant technique to structurally characterize MerB, MerB2 and several mutants of MerB in either their apo or metal-bound states. In addition, I have collaborated with members of the Omichinski group, the Wilkinson group (Department of Chemistry at UdeM) and the Wilcox group (Department of Chemistry at Dartmouth College) to help define the metal-binding characteristics of these proteins. In collaboration with Dr. Kevin Wilkinson, we used Inductively Coupled Plasma Mass Spectrometry (ICP-MS) to determined that the MerB D99S mutant protein contained a bound copper after its expression and purification from bacteria. With other members of the Omichinski group, I conducted NMR spectroscopy studies to demonstrate that it was a paramagnetic copper species bound to the MerB D99S protein. I also collaborated with Dr. Dean Wilcox and his student Michael Stevenson to further demonstrate that the copper atom bound to the MerB D99S protein was paramagnetic using electron paramagnetic resonance (EPR) spectroscopy. In addition, we performed isothermal titration calorimetery (ITC) experiments with Dr. Wilcox's group to characterize the binding of organometals to MerB. Below, I provide a short description of each technique used and how they were important to my work.

1.8.1 X-Ray crystallography

X-Ray crystallography and NMR are the two most common techniques used to determine high-resolution 3D structures of proteins. In X-ray crystallography, X-ray radiation scatters after hitting the electrons from atoms present in a crystalline protein and this scattered radiation generates a diffraction pattern that is dependent on the electron density profile of the protein. This is in contrast to protein structure determination using NMR spectroscopy, which is performed with the protein in solution. In X-ray crystal structures, the exact position of metals like Hg^{II} can be easily determined, because their electron density is often several orders of magnitude higher than the electron density of the other atoms present in the protein (N, C, O and S). After determining the position of the metal, the position of coordinating residues can often be determined with very high accuracy, which is not the case in NMR spectroscopy. However, X-ray crystallography cannot be used to distinguish

the oxidation state of the bound metal. Another interesting feature is that enzymes often remain catalytically active in their crystalline state and this is the case for MerB. After soaking MerB crystal in solutions containing either EtHg or PCMB, the Hg^{II} product could be detected in the active site devoid of the hydrocarbon moiety, indicating the crystalline form of the enzyme was catalytically active. Due to the high-resolution structural details and the speed which I could perform the crystallography studies, I used this experimental technique to solve the structures of several protein-metal complexes involving MerB proteins.

1.8.2 X-ray Fluorescence spectroscopy

In addition to their high electron density, metals also have the capacity to absorb incident radiation at a select X-ray wavelength and re-emit it at a lower energy (fluorescence). So specific metals can be identified by the fact that they possess a unique absorption edge at select X-ray wavelengths (For example Hg, Cu, Pb, Sn and Zn). Thus, by scanning a crystal over a range of wavelengths, it is possible to identify the presence of a specific metal, based on this property. Furthermore, an anomalous electron density map (heavy atom density) can be calculated based on the effect of absorbed radiation at a specific wavelength and these anomalous signals can also assist in establishing a precise position of the metal in the protein crystal structure.

1.8.3 NMR and EPR spectroscopy studies with paramagnetic metals

Metals can be classified as either paramagnetic or diamagnetic depending on their magnetic properties and they behave very differently when they are examined using either NMR or EPR spectroscopy. Metals such as Cu^{II}, Ni^{II}, Co^{II}, Mn^{III}, Mn^{II}, Fe^{II} and Fe^{III} are classified as paramagnetic atoms because they have at least one unpaired electron, whereas diamagnetic metals such as Zn^{II}, Pb^{IV}, Sn^{IV}, Cd^{II}, Hg^{II} and Cu^{I} have only paired electrons. Below is a brief description of how paramagnetic metals can alter signals in NMR spectroscopy as well as a description of how EPR spectroscopy can help identify the presence of a paramagnetic metal bound to a protein.

1.8.3.1 Paramagnetic metals alter NMR specta in a characteristic manner

One important property of paramagnetic metals is that their magnetic moment is roughly three orders of magnitude larger than the magnetic moment of a proton due to the presence of an unpaired electron. The presence of a paramagnetic element bound to a protein will cause a marked effect on the magnetic properties of adjacent nuclei, especially protons. More specifically, the paramagnetic metal ion induces dramatic changes in chemical shifts of protons as well as causing a decrease in the intensity of nearby proton signals due to enhanced rates of relaxation. Importantly, these effects are related to the distance of a given proton (more pronounced closer to the metal) from the bound metal and can extend up to 30Å depending on the metal. Given that paramagnetic effects are distance dependence, it is possible to determine the distance of an affected proton from the bound metal and this information has been used for determining protein structures by NMR. Since the paramagnetic metal ion (for example Cu^{II}) decreases the intensity of nearby signals, it is important to record a reference spectrum either without the metal or with a diamagnetic metal ion substituted for the paramagnetic metal. By comparing the spectra, it is possible to accurately assess the paramagnetic effect and position the paramagnetic metal relative to nearby residues. Likewise, it is often possible to displace a paramagnetic metal with a diamagnetic metal and this will have a dramatic effect on the resulting NMR spectrum. More specifically, signals near the metal will be more intense in the presence of the diamagnetic metal than they are in the presence of the paramagnetic metal. This is one way to distinguish if the metal bound to a protein is either paramagnetic or diamagnetic.

1.8.3.2 EPR spectroscopy for identifying paramagnetic metals bound to proteins

It is also possible to directly demonstrate the presence of a paramagnetic metal bound to a protein by measuring its electron spin using EPR. Although complementary to NMR, EPR is a more sensitive technique because of the larger magnetic moment of the electron in comparison with the nuclei. The two main spectroscopic signatures to be determined for a bound metal ion in EPR experiments are spectroscopic index (g-values) and hyperfine constants (A-values). The g-value is a measure of the interaction between the applied magnetic field and the unpaired electron present in the metal. The g-value of a free electron

(g_e) is 2.0023, but the true g-value for an unpaired electron of a paramagnetic metal ion will be different from g_e due to the effect of other electrons and orbital motion. Hyperfine coupling constants are used to measure the interactions of the unpaired electron with its associated nuclei and the nuclei of directly coordinating atoms. In contrast to NMR spectroscopy, the other protein residues are not detected in EPR spectroscopy. However, EPR spectroscopy can provide detailed information on the active paramagnetic centre, which cannot be obtained from a single NMR spectroscopy experiment. In particular, the nature of the atoms attached to the metal ion can be identified (For example nitrogen and sulfur) since different atoms often give characteristic signals in the EPR spectrum.

1.8.4 Inductively Coupled Plasma Mass Spectrometry (ICP-MS) for identifying unkown metal bound to proteins

ICP-MS is very commonly used to identify the total metal content of a sample by combining high temperature plasma with mass spectral analysis. The high temperature plasma is responsible for converting all atoms in a sample into ions, so that the resulting charged ions can be separated by the mass spectrometer on the basis of their mass-to-charge ratio. In our work, ICP-MS was used to identify and quantify the metal content for several mutants of MerB as they unexpectedly displayed the presence of a bound metal following expression and purification from *E. coli*. ICP-MS was selected over other metal analysis techniques, such as atomic absorption and atomic emission spectroscopy, because of its superior sensitivity and its ability to differentiate between various isotopes for a given metal. In our studies, we compared the metal content of the mutant MerB proteins to that of wild-type MerB expressed and purified under identical conditions. In this way, we were able to determine if the mutant proteins had indeed acquired a metal since MerB itself contains no bound metals after expression and purification from *E. coli*.

1.8.5 Isothermal Titration Calorimetry (ITC) for measuring organometal binding and cleavage.

The other techniques described above have been used to provide information about the three-dimensional structure, the type of metal bound to a protein, the oxidation state of

bound metals, and the metal coordinating ligands. To obtain additional insight into the energetics of binding and cleavage of substrates by MerB, ITC studies were employed. ITC is unique in that it has the potential to provide information regarding the stoichiometry (n) of binding, the apparent dissociation constants (K_D) as well as the associated thermodynamic parameters [enthalpy (ΔH), entropy (ΔS) and free energy ($\Delta G°$)]. The method is based on measuring heat absorbed or released upon the binding of a ligand to a protein (ΔH), which is then used to calculate the K_D. This information can in turn be used to determine $\Delta G°$ (from $\Delta G° = -RTlnK$) as well as ΔS (from $\Delta G° = \Delta H - T\Delta S$). Typically, the thermodynamic parameters for a protein-ligand interaction can be determined from a single experiment. However, this is not the case when ITC studies are used to measure protein-metal interactions, as several other factors must be considered in order to derive an accurate value (Quinn *et al.* 2016). In the case of metal ions, they often have a significant affinity for buffer components and this alters the total amount of heat generated. Therefore, the ITC experiments must be corrected for any competing reactions between the buffer and the metal when reporting the parameters describing the metal-protein interaction. This can be done by using the formation constant of the metal-buffer interaction as a correction factor and these constants are available for several metals through a database maintained by the National Institute of Science and Technology (NIST). In cases were the formation enthalpies of metal-buffer interactions are not available through NIST, one must perform additional experiments to determine the metal-buffer formation enthalapy. In addition, metal-binding proteins often contain cysteine residue(s) whose thiol(s) group is (are) required for metal coordination. These thiol groups are highly susceptible to oxidation and buffer reagents are needed to keep them in the reduced state since the presence of the oxidized form could significantly alter the experimental values of the ITC experiments. Unfortunately, reducing agents typically have high affinity for metals and this must be factored into the calculations. In order to eliminate the need for reducing agents in the buffer, we dialyzed our samples into buffers devoid of reducing agents and performed ITC experiments in an oxygen free chamber (Under an Argon atmosphere). Competition between metals and displaced protons that result from the binding reaction is the final factor that must be considered in the ITC experiments. Being a Lewis acid, the proton will

compete with the protein for binding to metals when they are displaced from amino acids following metal binding and (de)protonation coupled with metal binding will contribute to the total measured enthalpy in ITC experiments. Therefore, we use three different buffers at the same pH to determine the number of displaced protons upon metal binding and this is factored into the final calculation. Given these complexities and the need for an ITC in an anaerobic environment, we collaborated with Dr. Wilcox's group to determine the interaction of MerB with the various organometal compounds using ITC.

Chapter 2: Article 1

Structural and biochemical characterization of a copper-binding mutant of the organomercurial lyase MerB: Insight into the key role of the active site aspartic acid in both Hg-carbon bond cleavage and metal-binding specificity.

Authors:

Haytham M. Wahba[1,2], Lauriane Lecoq[1], Michael Stevenson[3], Ahmed Mansour[1], Laurent Cappadocia[1], Julien Lafrance-Vanasse[1], Kevin J. Wilkinson[4], Jurgen Sygusch[1], Dean E. Wilcox[3], and James G. Omichinski[1]*

[1]Département de Biochimie et Médicine Moléculaire and [4]Chimie, Université de Montréal, Montréal, QC, Canada, [2]Faculty of Pharmacy, Beni-suef University, Beni-suef, Egypt and [3]Department of Chemistry, Dartmouth College, Hanover, NH, U.S.A.

Published in: Biochemistry 2016 January 28; *55* (7), pp 1070–1081

PDB ACCESSION CODES: 5DSF, 5C17, 5C0T, 5C0U

***Correspondence to:**

James G. Omichinski, Département de Biochimie et Médicine Moléculaire, Université de Montréal, C.P. 6128 Succursale Centre-Ville, Montréal, QC H3C 3J7 Canada.

Email: jg.omichinski@umontreal.ca; Telephone: 514-343-7341.

Detailed contribution of authors in this work:

Haytham Wahba performed the protein expression, protein purification, sample preparation for each experiment entitled, protein crystallization, X-ray data collection, solving structure and structure refinement and NMR data analysis. All figures except Figure 7 were prepared by Haytham Wahba. The overall contribution of Haytham Wahba to this work is approximately 80-90% of all generated data and he wrote the paper with help from James Omichinski. Lauriane Lecoq was responsible for the NMR data collection. Michael Stevenson and Dean E. Wilcox were responsible for EPR data collection and data analysis and preparing Figure 7. Ahmed Mansour was an intern in our lab and he helped with protein expression and purification under the supervision of Haytham Wahba. Laurent Cappadocia taught Haytham M. Wahba the principles of X-ray data collection and processing. Julien Lafrance-Vanasse provided Haytham M. Wahba with the initial training for protein purification. The ICP-MS data was collected in the laboratory of Kevin J. Wilkinson by Hadioui Madjid. The X-ray data collection at Brookhaven was collected and processed by Haytham Wahba under the supervision of Jurgen Sygusch. James G. Omichinski conceived the project, designed the study and supervised the writing of the paper.

ABSTRACT

In bacterial resistance to mercury, the organomercurial lyase (MerB) plays a key role in the detoxification pathway through its ability to cleave Hg-carbon bonds. Two cysteines (C96 and C159; *Escherichia coli* MerB numbering) and an aspartic acid (D99) have been identified as the key catalytic residues, and these three residues are conserved in all but four known MerB variants, where the aspartic acid is replaced by a serine. To understand the role of the active site serine, we characterized the structure and metal-binding properties of an *E. coli* MerB mutant with a serine substituted for D99 (MerB D99S) as well as one of the native MerB variants containing a serine residue in the active site (*Bacillus megaterium* MerB2). Surprisingly, the MerB D99S protein co-purified with a bound metal that was determined to be Cu(II) from UV-vis absorption, ICP-MS, NMR and EPR studies. X-ray structural studies revealed that the Cu(II) is bound to the active site cysteine residues of MerB D99S, but that it is displaced following the addition of either an organomercurial substrate or ionic mercury product. In contrast, the *B. megaterium* MerB2 protein does not co-purify with copper, but the structure of the *B. megaterium* MerB2-Hg complex is highly similar to the structure of the MerB D99S-Hg complexes. These results demonstrate that the active site aspartic acid is crucial for both the enzymatic activity and metal-binding specificity of MerB proteins and suggest a possible functional relationship between MerB and its only known structural homolog, the copper-binding protein NosL.

INTRODUCTION

Mercury contamination is a critical environmental problem throughout the world, and particularly in waterways where the highly toxic methylmercury (MeHg) concentrates in sediments[1]. Mercury can enter the environment either through natural sources (volcanoes, forest fires, oceanic emissions) or human action (nuclear fuel production, combustion of fossil fuels, pesticide application, and gold mining)[2]. After being introduced into the environment, mercury compounds undergo a complex biogeochemical cycle where they are interconverted between inorganic [Hg(0), Hg(I), Hg(II)], and organic forms, the most abundant of which is MeHg[1, 3, 4 1, 3-5]. The dangers associated with mercury compounds are largely linked to their high affinity for thiol groups present in cellular proteins[6]. Ionic Hg(II) is one of the most toxic metals to humans and exposure to Hg(II) has been associated with neurological, renal and immunological toxicities[7]. Organomercurials, such as MeHg, are approximately two orders of magnitude more toxic than Hg(II) due to their hydrophobic character, which allows them to efficiently permeate cellular membranes and bioaccumulate in the food chain[1, 7]. High levels of MeHg have been found in several species of freshwater fish in different areas around the world, and human consumption of seafood contaminated with MeHg represents a serious health hazard leading to toxic exposure such as the tragedy at Minamata, Japan[8, 9]. The main target for MeHg toxicity in humans is generally considered to be the nervous system[1, 7].

Over fifty years ago, research groups noticed that select strains of bacteria had the capacity to grow in environments contaminated with high concentrations of either Hg(II) or MeHg [10, 11]. Subsequent analysis of these organisms revealed that they were able to survive in mercury-contaminated environments as a result of acquiring a transferable genetic element called the *mer* operon[12-15]. Although its composition in different bacterial strains can vary, the operon usually codes for proteins involved in mercury transport (MerA, MerP, MerT), mercury metabolism (MerA, MerB) and operon regulation (MerR)[10, 16]. Expression of these mercury resistance proteins occurs in response to the presence of Hg(II) in the bacteria and is regulated by the *MerR* gene[17]. Three proteins are required to transport Hg(II)

from the periplasm of the cell to the cytosol. First, MerP scavenges the periplasm for free Hg(II) and binds it through two cysteine residues[18]. The mercury is then transferred to MerT, a cysteine-rich transmembrane protein that transports the mercury to the cytosol by directly shuttling it to cysteine residues on the cytosolic mercuric ion reductase MerA[19, 20]. In contrast, the hydrophobic organomercurials are able to pass directly though the membrane into the cytosol where they bind to the organomercurial lyase MerB.

Once either the ionic mercury or organomercurial compounds enter the cytoplasm of the bacteria, the two enzymes (MerA and MerB) of the *mer* system efficiently convert them to the less toxic and volatile elemental mercury that is expired by the bacteria[21-24]. For Hg(II), following its transfer from MerT to MerA, it is reduced by MerA to elemental mercury[23, 24]. In the case of organomercurials, MerB efficiently binds the compounds in the cytosol and catalyzes the protonolysis of the Hg-carbon bond resulting in a reduced carbon compound that is released and a bound Hg(II) that is shuttled via cysteine residues from MerB to MerA for subsequent reduction to elemental mercury[21, 22,25-27].

Given its unique ability to cleave Hg-carbon bonds, there has been considerable interest in exploiting the enzymatic activity of MerB for industrial applications or remediation efforts to clean up organomercurial contamination[28-30]. As a result, structural, chemical, biochemical and computational studies have been performed in an attempt to characterize the atomic level details of Hg-carbon bond cleavage by MerB. The NMR and X-ray structures of *Escherichia coli (E. coli)* MerB revealed that it adopts a unique fold consisting of a core domain and a flexible N-terminal domain that covers the active site[31, 32]. Consistent with the unique enzymatic activity of MerB, the only known structural homolog is NosL, a putative copper-chaperone protein involved in a nitrogen metabolism pathway in bacteria [33]. The active site of MerB is located within the core domain and consists of a catalytic triad of two cysteines (C96 and C159; numbering of the *E. coli* MerB sequence) and one aspartic acid (D99)[33]. Based on its three-dimensional structure and several studies with small-molecule analogs that mimic the active site of MerB[34-38], we proposed that Hg-carbon bond cleavage begins with the binding of the organomercurial compound by an

exogenous thiol to generate the substrate[32]. Next, the substrate binds to C96 of MerB, which is located in close proximity to D99 in an α-helix. The subsequent binding of a second thiolate from the second cysteine (C159) in the active site displaces the exogenous thiol and activates the Hg-carbon bond. The activated carbon is then protonated by D99 with the release of the hydrocarbon product. The mercuric ion product remains tightly bound to C96, C159, D99 and a water molecule until it is directly transferred to MerA through a shuttling mechanism for subsequent reduction to elemental mercury. Similar mechanisms have been proposed based on the crystal structure and computational studies [39, 40], but they all involve C96, C159 and D99 within the active site.

The key catalytic roles for C96, C159 and D99 are supported by the fact that the two cysteine residues are conserved in all known variants of MerB and the aspartic acid is conserved in all but four of the known variants [*Bacillus megaterium* MerB2*, Bacillus subtillis* MerB2, *Bacillus sp.* (RC607*)* MerB2, *Clostridium butyricum* MerB2], in which the D99 is replaced by a serine residue [41]. Although these four serine-containing MerB variants are derived from different organisms, they have 100% amino acid sequence identity so they are in fact identical proteins. Interestingly, the presence of the serine in the active site appears to alter both the cleavage activity and the relative substrate specificity of these variant proteins. In the case of *B. mergaterium*, its MerB2 protein with a serine in the active site has much lower activity and shows a preference for p-chloromercuribenzoate (PCMB) over either methylmercury or ethymercury, when compared to other MerB proteins with an aspartic acid residue at the equivalent position in their active site, including the *Bacillus megaterium* MerB1 protein[42]. Of note, the four organisms that express a MerB2 protein with a serine in the active site also express a second MerB1 protein that contains an aspartic acid in the active site. This suggests that these proteins with a serine in the active site may have slightly different function in the mercury resistance of the organisms that also have a MerB protein with an aspartic acid in the active site.

Given that the MerB variants with a serine in the active site have substantially lower catalytic activity and different substrate specificity relative to MerB variants with an

aspartic acid in the active site[42], we were interested in characterizing the role of the active site serine residue on MerB structure and function. To accomplish this goal, we determined the structure and metal-binding properties of the wild-type *B. megaterium* MerB2 protein that naturally contains a serine in the active site and an *E. coli* MerB mutant protein with a serine substituted for D99 (MerB D99S). Our results indicate that the aspartic acid in the active site of MerB plays a key role in both metal-binding specificity and Hg-carbon bond cleavage, thereby enabling MerB to efficiently cleave organomercurial substrates and retain the Hg(II) for transfer to MerA for reduction to elemental mercury.

EXPERIMENTAL PROCEDURES (Materials and Methods)

Construction of protein expression vector

The expression vectors for wild-type *E. coli* MerB as well as the C96S and C159S mutants have been described previously [31,32]. The D99S (MerB D99S) and D99N (MerB D99N) mutants of MerB were generated by site directed mutagenesis starting from the cDNAs encoding wild-type MerB in the pET21b expression vector (Novagen). The sequence encoding for the the *B. megaterium* MerB2 protein (Uniprot code Q9WWL2_BACSR) was ordered as oligonucleotides (Bio Basic INC) with flanking BamHI and EcoRI restriction enzymes sites, 5' phosphorylated, annealed and cloned as a BamHI-EcoRI fragment into the pET21b expression vector. All constructs were verified by DNA sequencing.

Expression and purification of enzymes

MerB and mutants: The wild-type MerB protein and mutant proteins (C96S, C159S, D99S and D99N) were expressed in *E. coli* host strain BL21 (DE3) (Novagen) and purified as previously described for the wild-type MerB[31, 43]. During the purification, all buffers contained 7.5 mM DTT and 1 mm EDTA. Prior to crystallization, the proteins were further purified by an additional gel filtration step over a Superose-12 (GE Healthcare) column using a buffer consisting of 10 mM sodium phosphate, pH 7.5, 1 mM EDTA, 10 mM sodium chloride and 7.5 mM DTT (Buffer A). All proteins were concentrated to 10 mg/mL using an Amicon ultrafiltration device with a 3 kDa MW cutoff (Millipore). For the ^{15}N-

labeled proteins, the cells were grown in minimal media with ^{15}N-labeled ammonium chloride as the only nitrogen source.

MerB2: The *B. megaterium* MerB2 protein was expressed in *E. coli* host strain BL21 (DE3). The cells were initially grown for 8 h in 100 mL Luria Bertani (LB) broth in the presence of ampicillin (100 μg/mL) at 37 °C and this culture was used for inoculation of 8 L of LB, with ampicillin and IPTG (20 μM). The resulting culture was grown overnight (16 h) at 30 °C. The cells were harvested and suspended in 50 mM sodium phosphate buffer, pH 7.3, with 1 mM EDTA and 7.5 mM DTT (Buffer B). The suspended cells were lysed using a French press and centrifuged at 105,000 x g for 30 min at 4 °C. The resulting supernatant was applied to an SP-Sepharose Fast Flow (GE Healthcare) column (200 mL) equilibrated with Buffer B. The *B. megaterium* MerB2 protein was eluted using a 0-1 M NaCl gradient over 1.8 L. The fractions containing MerB2 were pooled and dialyzed overnight against Buffer B. The pooled fractions were then applied to an SP-Sepharose High performance (GE Healthcare) column (50 mL) equilibrated with buffer A. The *B. megaterium* MerB2 protein was eluted using a gradient of 0-1 M NaCl over 0.5 L. Fractions containing the *B. megaterium* MerB2 were pooled and dialyzed overnight in Buffer A for purification by gel filtration using a Superose-12 column equilibrated with Buffer A.

UV-visible spectroscopy

UV-visible spectra of MerB, MerB mutants and MerB2 after the initial purification were collected on a Cary50 UV-vis spectrophotometer. The spectra were recorded between 200 and 800 nm with a 0.5 mM solution of protein in 10 mM sodium phosphate, pH 7.5, 1 mM EDTA, 10 mM sodium chloride and 7.5 mM DTT. For the experiments examining Hg(II) displacement of copper from MerB D99S, 1.2 equivalents of either either $HgCl_2$ (Aldrich) or *p*-chloromercuribenzoate (PCMB; Aldrich) were added 16 h prior to recording the spectra. For the experiments with diethylenetriaminepenta-acetic acid (DPTA), the sample was dialyzed for 16 h against a solution of 10 mM sodium phosphate, pH 7.5, 10 mM DPTA, 10 mM sodium chloride and 7.5 mM DTT prior to recording the spectra.

ICP-MS measurements

Inductively coupled plasma mass spectrometry (ICP-MS, PerkinElmer NexION 300x) was used to analyze metal bound to *E. coli* MerB, the *B. megaterium* MerB2, *E. coli* MerB D99S, *E. coli* MerB D99S-Hg complex, *E. coli* MerB D99N, *E. coli* MerB D99N-Hg complex, *E. coli* MerB C96S and *E. coli* MerB C159S. Following their initial purification, the samples were dialyzed into 10 mM sodium phosphate, pH 7.5, 1 mM EDTA, 10 mM sodium chloride and 7.5 mM DTT. ICP-MS analysis was performed using 5 μM of protein dissolved in 1 % ultrapure HNO_3. Samples were quantitatively analyzed for Mn, Co, Ni, Cu, Zn, As, Cd, Sn, Pb and Fe. Indium was used as an internal standard. The NIST 1640a certified reference material (Inorganic Ventures) used for quality control indicated recoveries between 95.3-103.7%. MerB D99S-Hg complex and MerB D99N-Hg complex were prepared by incubating for 1 day with 1.2 equivalents of $HgCl_2$ prior to dialysis against 1 L of Buffer A.

Crystallization Conditions

MerB D99S*:* Crystals of MerB D99S were grown by the vapor diffusion method at 23 °C using either a 1:1 or 1:2 mixtures of protein solution (10 mg/mL) and precipitant buffer, respectively. The precipitant buffer was 23 % polyethylene glycol 2000 MME in 0.2 M sodium acetate pH 5.5 with 0.2 M potassium bromide. Before flash freezing, the same precipitant was used except 25 % polyethylene glycol 2000 MME was used as a cryo-protectant.

MerB D99S-Hg: To obtain the MerB D99S-Hg complex, crystals were soaked in a solution containing 25 % polyethylene glycol 2000 MME in 0.2 M sodium acetate pH 5.5 with 0.2 M potassium bromide with either 1 mM $HgCl_2$ or 1 mM PCMB for a period of 10 min.

MerB2-Hg complex: Crystals of the MerB2-Hg complex were grown by the vapor diffusion method at 23 °C using a 2:1 mixture of protein solution (5 mg/mL protein with a

1:1 ratio of $HgCl_2$) and precipitant buffer, respectively. The precipitant buffer was 1.8 M ammonium citrate tribasic pH 7.0. Before flash freezing, 10% glycerol was added as a cryo-protectant.

X-Ray data collection, processing and structure determination

Diffraction data were collected from single crystals using an ADSC Quantum 315 charge-coupled device at beam line X29 of the National Synchrotron Light Source (NSLS I) at Brookhaven National Laboratory (BNL, USA), using a Pilatus 6M PAD detector at beamline 12-2 at the Stanford Synchrotron Radiation Lightsource (SSRL, USA) or using a Rayonix MX300 detector at beamline 08ID-1 at the Canadian Light Source (CLS; Canada). All data sets were processed with HKL2000 and the results are summarized in **Table 1**. The X-ray absorption edge of Cu was detected at the X29 beamline and measured with a fluorescence detector.

MerB D99S: The initial phases for determining the MerB D99S structures were obtained by molecular replacement using the structure of wild-type MerB (PDB 3F0O) as a search template [32]. Phases were improved by iterative cycles of model building with Coot[44] and refinement was performed with PHENIX[45]. Test data sets were randomly selected from the observed reflections prior to refinement. Statistics for the final models obtained with PHENIX[45] and Molprobity[46] are shown in **Table 1**. The structure coordinates (PDB Codes **5C0T, 5C0U, 5DSF**) and structure factors have been deposited in the RCSB Protein Data Bank. The figures were visualized using PYMOL.

MerB2: Given the low sequence identity of MerB2 (only 22%), attempts to determine the phases by molecular replacement using Phaser[47] with MerB as a search model failed. As a result, molecular replacement and single anomalous dispersion (MR-SAD) were used to calculate the structure. First, Chainsaw from the CCP4 package was used to modify the structure of wild-type MerB (PDB 3F0O) by substituting the amino acids according to the MerB2 sequence[48]. This generated a modified search model. MR calculations were performed with Phaser[47] using the modified search model. A partial structure with the

mercury position was obtained. SAD phase calculations were then performed with PHENIX. Phases were improved by iterative cycles of model building with Coot[44] and refinement was performed with Phenix[45]. Statistics for the final models obtained with PHENIX[45] and Molprobity[46] are shown in **Table 1**. The structure coordinates (PDB Code 5C17) and structure factors have been deposited in the RCSB Protein Data Bank. The figures were visualized using PYMOL.

NMR spectroscopy

For the NMR studies, purified ^{15}N-labeled MerB D99S and ^{15}N-labeled MerB D99N were concentrated to 0.5 mM by centrifugation using an Amicon ultrafiltration device with a 3 kDa MW cutoff and exchanged into an NMR buffer consisting of 10 mM sodium phosphate pH 7.5, 10 mM NaCl, 1 mM EDTA and 7.5 mM DTT in 10% D_2O/90%H_2O (v/v). 2D ^{1}H-^{15}N HSQC (Heteronuclear Single Quantum Correlation) spectra were recorded on a 600 MHz Varian Inova spectrometer at 300 K. Following the collection of the ^{1}H-^{15}N HSQC spectra of the free form of the proteins, 1.2 equivalents of either PCMB or $HgCl_2$ was added to the sample 30 min prior to collection of an additional ^{1}H-^{15}N HSQC spectra.

EPR spectroscopy

EPR spectra were obtained with a Bruker EMX 300 X-band EPR spectrometer on frozen aqueous solutions in quartz EPR tubes immersed in a liquid nitrogen (77 K) dewar. The spectra consist of four signal-averaged scans obtained with the following parameters: 9.68 GHz microwave frequency, 6.42 mW microwave power, 100 KHz modulation frequency, 3.0 G modulation and 40.96 ms time constant. Spectra were simulated with EasySpin[49], allowing for both *g* strain and *A* strain in the simulation.

RESULTS

The MerB D99S mutant binds copper

Four of the known variants of MerB contain a serine as opposed to an aspartic acid (D99, *E. coli* numbering) in the active site [41] (**see Figure S1 in Supplemental**

Information), and this change alters both the enzymatic activity and the relative substrate specificity for these variants[42]. In an attempt to structurally characterize the basis for these observed differences with the MerB serine variants, we initially prepared a protein where serine was substituted for aspartic acid in the *E. coli* MerB (MerB D99S). Comparison of this model protein with our previously determined crystal structures of the wild-type *E. coli* MerB in the free and mercury-bound state would allow us to determine whether or not the serine substitution results in any major structural differences. Following expression and purification, the MerB D99S protein solution had a distinct pink color that is not observed following purification of the wild-type MerB. The pink color suggests that the MerB D99S protein binds a metal during its expression in *E. coli* cells and that this metal remains bound to the protein throughout the entire purification process, despite the constant presence of 1 mM EDTA and 7.5 mM DTT in all the purification buffer solutions. As an initial test for the presence of a bound metal, the MerB D99S protein solution was evaluated by UV-visible absorption spectroscopy. The UV-visible spectrum shows absorption maxima at 389 and 492 nm that are not present in the spectra of the wild-type MerB (**Figure 1**). Addition of a slight molar excess of either $HgCl_2$ or PCMB to the MerB D99S solution resulted in a loss of the pink color as well as disappearance of the 389 and 492 nm absorption maxima in the UV-visible spectrum (**Figure 1**). These results demonstrate that despite binding a metal during purification, the MerB D99S mutant is still able to interact with both organomercurial substrates and the ionic mercury product.

In an attempt to identify the metal bound to MerB D99S, ICP-MS analysis was performed on the protein solution following purification and this indicated the presence of copper at a ratio of 0.33 moles of copper per mole of protein (**Table 2**). The copper remains bound to the protein despite the presence of both DTT (7.5 mM) and EDTA (1.0 mM) in all purification buffers and attempts to remove the copper with the chelating agent DPTA (5 mM) were unsuccessful (**see Figure S2 in Supplemental Information**). This indicates that MerB D99S has an appreciable affinity for copper. In addition, the copper-binding capacity appears specific to this particular active site mutant of MerB, since copper does not bind to either the C96S or C159S MerB mutants during their expression and purification using

identical procedures (**Table 2 and see Figure S2 in Supplemental Information**). Furthermore, the addition of cupric chloride to a solution of wild-type MerB, either in the presence or absence of DTT, failed to generate a MerB-Cu complex (**Figure 1**).

Copper binds to the active site of MerB D99S in a similar manner as mercury

To define the copper-binding site in MerB D99S at the atomic level, we attempted to determine its high-resolution structure by X-ray crystallography and crystals of MerB D99S that diffracted at 1.87 Å resolution were obtained (**Table 1**). These crystals have the same space group ($P2_1$) and same number of proteins in the asymmetric unit (2) as the crystals of wild-type MerB[32]. The crystal structure of MerB D99S is very similar to that of wild-type MerB, and the two structures align with a root mean square deviation (r.m.s.d.) of 0.16 Å about the C_α positions (**Figure 2A**). The only major difference is that the MerB D99S crystals have electron density, along with an anomalous peak, centered between C96, C159 and S99 that is not observed for the wild-type MerB crystals (PDB code 3F0O). This is due to a copper ion bound in the active site (**Figure 2B**) as established by X-ray fluorescence detection around the copper K-absorption edge (**see Figure S3 in Supplemental Information**). The copper binds to the sulfurs of C96 (2.2 Å) and C159 (2.2 Å) and is near an oxygen of S99 (2.9 Å) and an oxygen from a bound water molecule (3.0 Å) (**Figure 3A and Figure S4 in supplemental information**). Interestingly, the copper binds at ~30% occupancy in virtually the same location within the active site as the Hg(II) product binds to wild-type MerB following incubation with organomercurial substrate, which is bound to the sulfurs of C96 (2.3 Å) and C159 (2.4 Å) and near the oxygen of D99 (2.9 Å) and an oxygen from a bound water molecule 2.6 Å) (**Figure 3B**).

Since copper binds to MerB D99S in a site that is similar to that of the Hg(II) product bound to wild-type MerB, we attempted to replace the bound copper with a mercuric ion. To accomplish this, the MerB D99S crystals were soaked with either a solution of 1 mM PCMB or 1 mM $HgCl_2$ for 10 min. The resulting crystals diffract at 1.95 Å following either soaking (**Table 1**). In the structure after the soaking in the PCMB solution, the mercury binds at ~80% occupancy in a similar manner as copper to C96 (2.4 Å) and C159 (2.3 Å)

and in proximity to oxygen atoms of S99 (3.1 Å), and a bound water molecule (2.6 Å). (**Figure 3C and Figure S4 in supplemental information**). Thus, the structure of the MerB D99S-Hg complex is very similar to that of both the MerB D99S-Cu and MerB-Hg complexes.

Characterization of the structure and metal-binding properties of MerB2

Since MerB D99S is able to sequester copper from a bacterial growth media, we attempted to determine whether the four natural MerB variants containing a serine residue in the active site are also copper-binding proteins. Although these variant proteins are derived from different organisms, they share 100% amino acid sequence identity. Thus, they are in fact identical proteins. For our studies, we expressed and purified the *B. megaterium* MerB2 serine-containing variant. The purification procedure is essentially identical to the one used for the purification of the *E. coli* MerB and the MerB D99S mutant. Following purification, the resulting *B. megaterium* MerB2 protein solution did not display any noticeable pink color as observed with the MerB D99S mutant. To determine whether copper is bound to the protein following purification, we analyzed the *B. megaterium* MerB2 protein solution by UV-visible spectroscopy and ICP-MS. In contrast to what is observed following purification of MerB D99S, there are no absorption bands in the 375-500 nm range in the UV-visible spectrum of *B. megaterium* MerB2 (**Figure 4**). In addition, the ICP-MS results indicate there is no significant metal content in the *B. megaterium* MerB2 sample (**Table 2**). These results suggest that both the wild-type MerB and *B. megaterium* MerB2 sequences have evolved to be able to distinguish mercury from copper.

Structural comparison of the MerB-Hg, MerB2-Hg and MerB D99S-Hg complexes

Given the low sequence identity between the *B. megaterium* MerB2 protein and *E. coli* MerB (22.2 %), and the fact that the two enzymes have different catalytic activities and relative substrate specificity[42], we attempted to determine the crystal structure of the *B. megaterium* MerB2 protein for comparison with that of *E. coli* MerB protein. Attempts to crystallize the free form of *B. megaterium* MerB2 were unsuccessful despite screening a

number of different crystallization conditions. Next, we attempted to crystallize the *B. megaterium* MerB2 protein in the presence of PCMB, methylmercury, ethymercury, $HgCl_2$ and $CuCl_2$. Although we did obtain crystals that diffract to 1.25 Å resolution, we were only able to obtain them in the presence of $HgCl_2$ (**Table 1**). The structure of the *B. megaterium* MerB2-Hg complex (**Figure 5A**) is similar to our previous structure of the *E. coli.* MerB-Hg complex[32]. The two structures align with an r.m.s.d. of 2.10 Å about the backbone C_α positions (**Figure 5B**). However, the core regions (residues 75-208 of MerB; residues 77-209 of MerB2) align with an r.m.s.d of 0.89 Å, whereas the amino-terminal regions (residues 1-74 of MerB; residues 3-76 of MerB2) align with an r.m.s.d. of 3.18 (**Figure 5B**). The higher r.m.s.d value observed with the amino-terminal region indicates that it has a more significant variation in the folding pattern. However, the structural alignment shows that the two conserved catalytic cysteine residues in *B. megaterium* MerB2 (C102, C165) align almost exactly with their counterparts in *E. coli* MerB (C96, C159) and the serine residue of *B. megaterium* MerB2 (S105) occupies a position similar to that of D99 in *E. coli* MerB (**Figure 5C**). As a result, the overall dimensions of the mercury-binding site of *B. megaterium* MerB2 is highly similar to that of *E. coli* MerB, if one considers the distances between the key atoms involved in catalytic activity (**Figure 5C-D and Figure S5 in supplemental information**).

MerB D99S with bound copper is paramagnetic

Since both the ICP-MS analysis and X-ray fluorescence results indicated that copper was the metal bound to MerB D99S, we attempted to determine the oxidation state of the bound copper ion. As an initial step, we used NMR spectroscopy to determine whether the sample is diamagnetic or paramagnetic. NMR can potentially distinguish the oxidation state of the bound copper based on a quenching of the NMR signals if the bound copper is paramagnetic[50-52]. A 2D ^{1}H-^{15}N HSQC spectrum was recorded with ^{15}N-labeled MerB D99S (**Figure 6A**). This spectrum contains several signals with nearly identical chemical shifts as those seen in the 2D ^{1}H-^{15}N HSQC spectrum of ^{15}N-labeled MerB[31, 43], consistent with the very similar structures of the two proteins. However, several of the signals located in the vicinity of the MerB catalytic site based on comparison with the assigned HSQC

spectrum of MerB[31, 43] were either very weak or absent from the spectrum of MerB D99S. This suggests that the bound copper is paramagnetic, consistent with Cu(II) bound to MerB D99S.

To evaluate the role of the amino acid at the D99 position in the enzymatic activity and coordination of metal ions, we added several organomercurial substrates including PCMB to the pink ^{15}N-labeled MerB D99S that contains copper. However, we observed no changes in any of the 2D ^{1}H-^{15}N HSQC spectra after 30 min incubation with these substrates. This observation is in sharp contrast to our previous studies with wild-type *E. coli* MerB, where significant chemical shift perturbations are observed following addition of substrate due to the formation of a MerB-Hg complex[25]. This suggests that the MerB D99S has lower catalytic activity than wild-type MerB, which could be the result of either the substitution of serine for aspartic acid at residue 99 or the presence of bound copper in the active site. Next, $HgCl_2$ was added to ^{15}N-labeled MerB D99S and this results in significant changes in the 2D ^{1}H-^{15}N HSQC spectrum of MerB D99S (**Fig. 6B**) as well as a loss of the pink color. Interestingly, the resulting spectrum is very similar to the spectrum of the wild-type MerB-Hg complex. In particular, the signals that are either missing or weak in the presence of the paramagnetic copper are restored in the spectrum of MerB D99S in the presence of the non-paramagnetic mercury. As expected, those signals that appear following the addition of mercury correspond to residues that are clustered around the active site when mapped onto the structure of MerB-Hg complex (**Fig. 6C**). Thus, based on the NMR data the copper bound to MerB D99S is most likely paramagnetic Cu(II). In addition, these results indicate that the catalytic activity of MerB D99S is significantly lower than that of wild-type MerB under the NMR conditions.

The MerB D99N mutant also binds copper

The copper binding properties of the MerB D99S mutant are important for understanding the metal binding specificity of the MerB protein, since similar substitutions of serine for the two Hg-binding cysteines (MerB C96S and MerB C159S) does not result in proteins with copper binding properties. Based on the results of these serine

substitutions, it could be suggested that the residue corresponding to D99 in *E. coli* MerB is key for defining the metal-binding specificity of MerB as well as its catalytic activity. To further test the significance of the MerB amino acid at this position, we prepared a D99N mutant of *E. coli* MerB. Asparagine was chosen because it is a near-isosteric replacement for aspartic acid, making it the most structurally similar to the wild-type MerB protein. Interestingly, expression and purification of the MerB D99N protein yields a pink solution very similar to that observed following purification of the MerB D99S mutant, suggesting that the MerB D99N protein also sequesters a metal during its expression. As observed with the MerB D99S mutant, the UV-visible absorption spectrum of MerB D99N solutions displays absorption maxima at 389 and 492 nm that disappear following the addition of 1.2 equivalents of $HgCl_2$ (**see Figure S6 in Supplemental Information**). To further characterize the metal bound to MerB D99N, ICP-MS were performed with the MerB D99N solution (**Table 2**). Similar to MerB D99S, ICP-MS analysis indicates that MerB D99N binds copper and NMR studies indicate that the metal is paramagnetic, again suggesting a bound Cu(II) molecule (**see Figure S7 in Supplemental Information**).

EPR spectra indicate an unusual Cu(II) electronic structure

Quenching of the signals around the metal-binding site in the 2D ^{1}H-^{15}N HSQC spectra of ^{15}N-labeled MerB D99S and MerB D99N suggests that the bound copper is paramagnetic Cu(II) and not diamagnetic Cu(I). To gain additional information about the copper, we obtained EPR spectra of the as-isolated copper-bound forms of both MerB D99S and MerB D99N (**Figure 7**). The EPR spectra of these samples have a similar strong and rather unique set of features. Power saturation analysis indicates that, other than the sharp feature at g = 2.00, which appears to be from a small a mount of carbon-centered radical, all features in these spectra arise from the same EPR-detectable species. Simulation of these spectra with EasySpin[49] software indicates an axial Cu(II) with somewhat smaller $g_{\parallel}$ and larger $A_{\perp}$ values. The magnitudes of the $g_{\parallel}$ and $A_{\parallel}$ values are consistent with sulfur coordination[53], but the unusually large $A_{\perp}$ seems to be unique to Cu(II) bound in these protein sites.

DISCUSSION

The key amino acids required for the catalytic activity of *E. coli* MerB are two cysteines (C96 and C159) and one aspartic acid (D99), which bind organomercurial substrates for cleavage of the Hg-carbon bond and retention of the mercuric ion product. The crucial role for these three residues is supported by the fact that the two cysteines are conserved in all known MerB variants, and the aspartic acid is conserved in all but four known variants. These four variants contain a serine residue in the equivalent position as D99 of *E. coli* MerB and they are all considered members of the MerB2 family of organomercurial lyase because they are expressed from a *mer* operon that encodes for two distinct MerB proteins[16]. Here, we have investigated the role of the serine residue in the active site by comparing the structure of the native serine containing *B. megaterium* MerB2 with the structure of an *E. coli* MerB containing a serine residue substituted for D99 (MerB D99S). Surprisingly, the MerB D99S mutant co-purifies with a bound metal acquired from the bacterial expression medum. Analysis with ICP-MS and UV-vis spectroscopy indicated that the bound metal is copper. X-ray structural studies of the MerB D99S-Cu complex demonstrated that the copper ion was bound to the side-chain sulfur atoms of C96 and C159 in the active site, and that soaking the crystals with either an organomercurial or $HgCl_2$ solution displaces it. In contrast, the wild-type *B. megaterium* MerB2 protein did not co-purify with a bound metal, but the structure of the MerB2-Hg complex is virtually identical to the structure of the *E. coli* MerB-Hg complex and the MerB D99S-Hg complex. Both EPR and NMR studies of MerB D99S and a second mutant, MerB D99N, confirmed that the bound copper was Cu(II).

Our NMR results demonstrating that the MerB D99S mutant has reduced catalytic activity in comparison to the wild-type *E. coli* MerB further supports the key role of D99 in carbon-mercury bond cleavage by MerB[32]. The reduced activity of the MerB D99S protein relative to the wild-type *E. coli* MerB protein could be due to the serine substitution, the presence of the copper ion or both. Previous studies have shown that the serine containing *B. megaterium* MerB2 protein has different relative specificity for organomercurial

substrates in comparison to other MerB proteins containing an aspartic acid residue in the active site, including the *B. megaterium* MerB1 protein [42]. However, its absolute activity is significantly lower for all substrates tested relative to the aspartic acid-containing MerB proteins, including a MerB2 protein with an aspartic acid in the catalytic site[42]. Taken together with our results on the MerB D99S mutant, this suggests that the aspartic acid residue plays an important role not only in enhancing the rate of Hg-carbon bond cleavage by MerB but also in establishing the metal ion binding specificity, which is crucial for the retention of the mercuric ion product for its subsequent transfer to MerA[25-27]. Thus, the serine-containing variants of MerB may represent a less active precursor of the MerB proteins with an aspartic acid in the active site. This would be consistent with the fact that the *mer* operons expressing the serine-containing variants also express a second MerB protein with an aspartic acid in the active site. In these cases, the MerB protein with the aspartic acid in the active site probably accounts for a significant portion of the metabolic activity towards organomercurial substrates associated with these mercury-resistant strains[42].

Given MerB's unique ability to cleave Hg-carbon bonds, it is not surprising that its three-dimensional structure displays limited similarity to other known protein structures[31, 32]. In fact, the only known structural homolog of MerB is NosL[33], a copper-binding protein that is expressed from the nitrous oxide reductase (NOS) gene cluster[54, 55]. Functionally, NosL is a periplasmic membrane-bound protein that is found in most bacterial strains that reduce nitrous oxide. Although the structure of the periplasmic region of a NosL variant has been determined by NMR spectroscopy, the copper-binding residues of NosL have not yet been completely determined[33, 54]. Since mutating D99 to either serine or asparagine converts MerB to a copper-binding protein, our results point towards a possible link between the copper-binding site of NosL and the mercury-binding site of MerB. In further support of the connection between MerB and NosL proteins, it has recently been suggested that both proteins evolved through gene duplication of a treble-clef zinc-finger motif from the TRASH-like family of proteins and gene duplication of a metal-binding treble-clef sequence, which would be consistent with MerB evolving from an existing bacterial metal-binding protein[56]. The connection between MerB and copper-binding proteins is further

supported by the fact that direct transfer of the Hg(II) product from MerB to the mercuric ion reductase MerA[20, 25-27] is reminiscent of the transfer of Cu(I) between proteins in bacterial copper-trafficking systems[57-67]. In both systems, the metals are maintained in a tightly bound state to avoid possible deleterious effects that could result from their release and interaction with other cellular proteins. Thus, our results indicate that the insertion of an aspartic acid residue into the active site of MerB is crucial not only for maximal catalytic activity, but also for binding the mercury ion product for transfer to MerA.

ACKNOWLEDGEMENTS: We thank Hadioui Madjid for help with the ICP-MS data.

SUPPORTING INFORMATION: Figure S1- Sequence alignment of MerB variants highlighting serine substitution for aspartic acid; Figure S2- UV-vis spectra of MerB C96S and MerB C159S; Figure S3- The X-ray fluorescence spectra demonstrating the presence of copper in the MerB D99S structure; Figure S4- Fo-Fc omit map and anomalous difference map of the active sites of the MerB D99S-Cu and MerB D99S-Hg complexes; Figure S5- Fo-Fc omit kick map of MerB2-Hg complex active site; Figure S6- UV-vis spectra of MerB D99N; Figure S7- ^{1}H-^{15}N HSQC spectra of ^{15}N-labeled MerB D99N; Crystallographic files for the MerB D99S-Cu, MerB D99S-Hg and MerB2-Hg complexes. This information is available free of charge via the Internet at http://pubs.acs.org.

Table 1. Data collection and refinement statistics.

Data set	**MerB D99S-Cu complex**	**MerB D99S-Hg complex**	**MerB D99S-PCMB complex**	**MerB2**
PDB code	**5C0U**	**5DSF**	**5C0T**	**5C17**
Data Collection				
Beamline	12-2, SSRL	X29, NSLS	X29, NSLS	08-ID, CLS
Wavelength (Å)	1.376 Å	1.075 Å	1.075 Å	0.9794 Å
Space group	$P2_1$	$P2_1$	$P2_1$	C2
Unit-cell parameter (Å)	a=37.90, b=88.95, c=52.00	a=38.06, b=89.11, c=51.82	a=37,68, b=88.34, c=52.67	a=82.29, b=53.42, c=47.71
	α=90, β=100.64, γ=90	α=90, β=100.79, γ=90	α=90, β=100.93, γ=90	α=90, β=96.85, γ=90
Resolution (Å)	50.00-1.87 (1.93-1.87)	50.00-1.95 (2.02-1.95)	50 - 1.95 (2.02-1.95)	50.00-1.24 (1.28-1.24)
Total reflections	86825	89818	89355	220481
No. of unique reflections	25298	24392	24336	56523
Multiplicity	3.4	3.7	3.7	3.9
Completeness (%)	90.29 (80.93)	99.38 (96.97)	99.12(96.81)	96.35 (78.16)
R_{merge}	0.052 (0.13)	0.089 (0.70)	0.076(0.58)	0.076 (0.45)
I/σ(I)	19.50 (6.70)	12.45 (1.87)	12.14 (2.07)	13.34 (1.29)
Refinement Statistics				
Resolution (Å)	50.00-1.87	50.00-1.95	50.00-1.95	50.00-1.24
R_{work}/R_{free} (%)	15.90/19.90	17.20/21.50	18.00/22.00	15.40/17.40
Number of atoms				
(excluding hydrogens)				
Protein	3200	3193	3174	1680
Water	322	252	207	279
Ligands	3	3	3	21
B-factors ($Å^2$)				
Protein	26.80	35.90	32.60	15.40
Water	34.40	39.10	37.30	32.30
Ligands	27.70	31.30	34.70	24.00
Metal Occupancy	0.30	0.80	0.80	0.80
RMSDs				
Bond lengths (Å)	0.009	0.007	0.013	0.010
Bond angles (°)	1.23	1.11	1.38	1.25
Ramachandran[b]				
Favored (%)	97	97	95	97
Outliers (%)	0	0	0	0

Values in parentheses are for highest-resolution shell. $R_{sym} = \sum hkl \sum i |I_{hkl,i} - \langle Ihkl \rangle| / \sum_{hkl,i} \langle Ihkl \rangle$, where $I_{hkl,i}$ is the intensity of an individual measurement of the reflection with Miller indices *hkl* and I_{hkl} is the mean

intensity of that reflection. $R_{work} = \sum hkl <|F_o| - |F_c>| / \sum hkl |F_o|$, where $|F_o|$ is the observed structure-factor amplitude and $|F_c|$ is the calculated structure-factor amplitude. R_{free} is the R factor based on at least 500 test reflections that were excluded from the refinement. [a] Reflections with $F_o > 0$. [b] MolProbity analysis.

Table 2 ICP-MS analysis.

Purified protein at 5 μM was analyzed by ICP-MS to give the concentrations (μM) of various metals in samples containing *E. coli* MerB, *B. megaterium* MerB2, MerB D99S, MerB D99S-Hg complex, MerB D99N, MerB D99N-Hg complex, MerB C96S and MerB C159S. The measured ratio of metal to protein was provided in the table for each metal combination.

Metals		MerB	MerB2	MerB D99S	MerB D99S Hg complex	MerB D99N	MerB D99N Hg complex	MerB C96S	MerB C159S
Mn	*μM*	0.018	0.048	0.014	0.012	0.012	0.01	0.007	0.009
	ratio	0.004	0.01	0.003	0.002	0.002	0.002	0.001	0.002
Co	*μM*	0.001	0.002	0.001	0.001	0.002	0.001	0	0
	ratio	0	0	0	0	0	0	0	0
Ni	*μM*	0.013	0.034	0.013	0.011	0.012	0.009	0.006	0.006
	ratio	0.003	0.007	0.003	0.002	0.002	0.002	0.001	0.001
Cu	*μM*	0.258	0.276	1.865	0.391	1.718	0.485	0.115	0.121
	ratio	0.052	0.055	0.373	0.078	0.344	0.097	0.023	0.024
Zn	*μM*	0.118	0.283	0.119	0.077	0.104	0.098	0.048	0.041
	ratio	0.024	0.057	0.024	0.015	0.021	0.02	0.01	0.008
As	*μM*	0.075	0.162	0.114	0.085	0.106	0.095	0.043	0.045
	ratio	0.015	0.032	0.023	0.017	0.021	0.019	0.009	0.009
Sn	*μM*	0.001	0.002	0.001	0.001	0.002	0.001	0.001	0
	ratio	0	0	0	0	0	0	0	0
Pb	*μM*	0.001	0.003	0.001	0.001	0.001	0.001	0	0.001
	ratio	0	0.001	0	0	0	0	0	0
Fe	*μM*	0.124	0.291	0.096	0.087	0.122	0.082	0.048	0.05
	ratio	0.025	0.058	0.019	0.017	0.024	0.016	0.01	0.01

REFERENCES:

[1] Morel, F. M. M., Kraepiel, A. M. L., and Amyot, M. (1998) The chemical cycle and bioaccumulation of mercury, *Ann. Rev. Ecol. Evol. Syst. 29*, 543-566.

[2] Mason, R. P., Fitzgerald, W. F., and Morel, F. M. M. (1994) The biogeochemical cycling of elemental mercury- Anthropogenic influences, *Geochim. Cosmochim. Acta 58*, 3191-3198.

[3] Munthe, J. (1992) The aqueous oxidation of elemental mercury by ozone., *Atmos. Environ. Part A 26*, 1461-1468.

[4] Pleijel, K., and Munthe, J. (1995) Modelling the atmospheric mercury cycle - chemistry in fog droplets., *Atmos. Environ. 29*, 1441-1457.

[5] Keating, M. H., Mahaffey, K. R., Schoeny, R., Rice, G. E., Bullock, O. R., Ambrose, R. B., Swartout, J., and Nichols, J. W. (1997) Mercury study report to congress, pp 2:1-2:9, U.S. Environmental Protection Agency, Washington, D.C.

[6] Carty, A. J., and Malone, S. F. (1979) The chemistry of mercury in biological systems, In *The biogeochemistry of mercury in the environment* (Nriagu, J. O., Ed.), pp 433-479, Elsevier/Biomedical Press, Amsterdam.

[7] Clarkson, T. W. (1994) The toxicology of mercury and its compounds, In *Mercury Pollution Integration and Syntehesis* (Watras, C. J., and Huckabee, J. W., Eds.), pp 631-642, Lewis Publishers, Ann Arbor, MI.

[8] D'Itri, F. M. (1991) Mercury contamination: What me have learned since Minamata., *Environ. Monitor. Assess. 19*, 165-182.

[9] D'Itri, P. A., and D'Itri, F. M. (1978) Mercury contamination: a human tragedy, *Environ. Manage. 2*, 3-16.

[10] Barkay, T., Miller, S. M., and Summers, A. O. (2003) Bacterial mercury resistance from atoms to ecosystems, *FEMS Microbiol. Rev. 27*, 355-384.

[11] Richmond, M. H., and John, M. (1964) Co-transduction by Staphylicoccal phage of genes responsible for penicillinase synthesis + resistance to mercury salts, *Nature 202*, 1360-1361.

[12] Schottel, J., Mandal, A., Clark, D., Silver, S., and Hedges, R. W. (1974) Volatilisation of mercury and organomercurials determined by inducible R-factor systems in enteric bacteria, *Nature 251*, 335-337.

[13] Schottel, J. L. (1978) The mercuric and organomercurial detoxifying enzymes from a plasmid-bearing strain of Escherichia coli, *J. Biol. Chem. 253*, 4341-4349.

[14] Jackson, W. J., and Summers, A. O. (1982) Biochemical characterization of $HgCl_2$-inducible polypeptides encoded by the mer operon of plasmid R100, *J. Bacteriol. 151*, 962-970.

[15] Summers, A. O. (1986) Organization, expression, and evolution of genes for mercury resistance., *Ann. Rev. Microbiol. 40*, 607-634.

[16] Huang, C. C., Narita, M., Yamagata, T., and Endo, G. (1999) Identification of three merB genes and characterization of a broad-spectrum mercury resistance module encoded by a class II transposon of Bacillus megaterium strain MB1, *Gene 239*, 361-366.

[17] Brown, N. L., Stoyanov, J. V., Kidd, S. P., and Hobman, J. L. (2003) The MerR family of transcriptional regulators, *FEMS Microbiol. Rev. 27*, 145-163.

[18] Hamlett, N. V., Landale, E. C., Davis, B. H., and Summers, A. O. (1992) Roles of the Tn21 merT, merP, and merC gene products in mercury resistance and mercury binding, *J. Bacteriol. 174*, 6377-6385.

[19] Morby, A. P., Hobman, J. L., and Brown, N. L. (1995) The role of cyteine residues in the transport of mercuric ions by the TN501 MerT and MerP merury-resistance proteins, *Mol. Microbiol. 17*, 25-35.

[20] Schue, M., Glendinning, K. J., Hobman, J. L., and Brown, N. L. (2008) Evidence for direct interactions between the mercuric ion transporter (MerT) and mercuric reductase (MerA) from the Tn501mer operon, *Biometals. 21*, 107-116.

[21] Begley, T. P., Walts, A. E., and Walsh, C. T. (1986) Mechanistic studies of protonolytic organomercurial cleaving enzyme: bacterial organomercurial lyase, *Biochemistry 25*, 7192-7200.

[22] Begley, T. P., Walts, A. E., and Walsh, C. T. (1986) Bacterial organomercurial lyase: overproduction, isolation, and characterization, *Biochemistry 25*, 7186-7192.

[23] Fox, B., and Walsh, C. T. (1982) Mercuric reductase: Purification and characterization of a transposon-encoded flavoprotein containing and oxidation-reduction-active disulfide., *J. Biol. Chem. 257*, 2498-2503.

[24] Fox, B. S., and Walsh, C. T. (1983) Mercuric reductase: homology to glutathione reductase and lipoamide dehydrogenase: iodoacetamide alkylation and sequence of the active site peptide., *Biochemistry 22*, 4082-4088.

[25] Benison, G. C., Di Lello, P., Shokes, J. E., Cosper, N. J., Scott, R. A., Legault, P., and Omichinski, J. G. (2004) A stable mercury-containing complex of the

organomercurial lyase MerB: Catalysis, product release, and direct transfer to MerA, *Biochemistry 43*, 8333-8345.

[26] Omichinski, J. G. (2007) Biochemistry - Toward methylmercury bioremediation, *Science 317*, 205-206.

[27] Hong, B., Nauss, R., Harwood, I. M., and Miller, S. M. (2010) Direct measurement of mercury(II) removal from organomercurial lyase (MerB) by tryptophan fluorescence: NmerA domain of coevolved gamma-proteobacterial mercuric ion reductase (MerA) is more efficient than MerA catalytic core or glutathione, *Biochemistry 49*, 8187-8196.

[28] Bizily, S. P., Rugh, C. L., and Meagher, R. B. (2000) Phytodetoxification of hazardous organomercurials by genetically engineered plants, *Nature Biotechnol. 18*, 213-217.

[29] Bizily, S. P., Rugh, C. L., Summers, A. O., and Meagher, R. B. (1999) Phytoremediation of methylmercury pollution: merB expression in Arabidopsis thaliana confers resistance to organomercurials, *Proc. Natl. Acad. Sci. USA 96*, 6808-6813.

[30] Rugh, C. L., Wilde, H. D., Stack, N. M., Thompson, D. M., Summers, A. O., and Meagher, R. B. (1996) Mercuric ion reduction and resistance in transgenic Arabidopsis thaliana plants expressing a modified bacterial merA gene, *Proc Natl Acad Sci USA 93*, 3182-3187.

[31] Di Lello, P., Benison, G. C., Valafar, H., Pitts, K. E., Summers, A. O., Legault, P., and Omichinski, J. G. (2004) NMR structural studies reveal a novel protein fold for MerB, the organomercurial lyase involved in the bacterial mercury resistance system, *Biochemistry 43*, 8322-8332.

[32] Lafrance-Vanasse, J., Lefebvre, M., Di Lello, P., Sygusch, J., and Omichinski, J. G. (2009) Crystal structures of the organomercurial lyase MerB in its free and mercury-bound forms: Insights into the mechanism of methylmercury degradation, *J. Biol. Chem. 284*, 938-944.

[33] Taubner, L. M., McGuirl, M. A., Dooley, D. M., and Copie, V. (2006) Structural studies of Apo Nosl, an accessory protein of the nitrous oxide reductase system: Insights from structural homology with MerB, a mercury resistance protein, *Biochemistry 45*, 12240-12252.

[34] Melnick, J. G., and Parkin, G. (2007) Cleaving mercury-alkyl bonds: A functional model for mercury detoxification by MerB, *Science 317*, 225-227.

[35] Melnick, J. G., Yurkerwich, K., and Parkin, G. (2009) Synthesis, Structure, and Reactivity of Two-Coordinate Mercury Alkyl Compounds with Sulfur Ligands: Relevance to Mercury Detoxification, *Inorg. Chem. 48*, 6763-6772.

[36] Parkin, G. (2007) Applications of tripodal [S-3] and [Se-3] L2X donor ligands to zinc, cadmium and mercury chemistry: organometallic and bioinorganic perspectives, *New J. Chem. 31*, 1996-2014.

[37] Strasdeit, H. (2008) Mercury-alkyl bond cleavage based on organomercury lyase, A*ngew. Chem. Int. Ed. 47*, 828-830.

[38] Wilhelm, M., Deeken, S., Berssen, E., Saak, W., Lutzen, A., Koch, R., and Strasdeit, H. (2004) The first structurally authenticated organomercury(1+) thioether complexes - Mercury-carbon bond activation related to the mechanism of the bacterial enzyme organomercurial lyase, *Europ. J. Inorg. Chem.*, 2301-2312.

[39] Parks, J. M., Guo, H., Momany, C., Liang, L. Y., Miller, S. M., Summers, A. O., and Smith, J. C. (2009) Mechanism of Hg-C Protonolysis in the Organomercurial Lyase MerB, *J. Am. Chem. Soc. 131*, 13278-13285.

[40] Ni, B., Kramer, J. R., Bell, R. A., and Werstiuk, N. H. (2006) Protonolysis of the Hg-C bond of chloromethylmercury and dimethylmercury. A DFT and QTAIM study, *J. Phys. Chem. A 110*, 9451-9458.

[41] Di Lello, P., Omichinski, J. G., and Lafrance-Vanasse, J. (2011) *The organomercurial lyase MerB*, John Wiley & Sons Ltd., New York.

[42] Chien, M. F., Narita, M., Lin, K. H., Matsui, K., Huang, C. C., and Endo, G. (2010) Organomercurials removal by heterogeneous merB genes harboring bacterial strains, *J. Biosci. Bioengin. 110*, 94-98.

[43] Di Lello, P., Benison, G. C., Omichinski, J. G., and Legault, P. (2004) Letter to the Editor: H-1, N-15, and C-13 resonance assignment of the 23 kDa organomercurial lyase MerB in its free and mercury-bound forms, *J Biomol. NMR 29*, 457-458.

[44] Emsley, P., and Cowtan, K. (2004) Coot: model-building tools for molecular graphics, *Acta Crystallogr. Section D: Biol. Crystallogr. 60*, 2126-2132.

[45] Adams, P. D., Afonine, P. V., Bunkoczi, G., Chen, V. B., Davis, I. W., Echols, N., Headd, J. J., Hung, L.-W., Kapral, G. J., Grosse-Kunstleve, R. W., McCoy, A. J., Moriarty, N. W., Oeffner, R., Read, R. J., Richardson, D. C., Richardson, J. S., Terwilliger, T. C., and Zwart, P. H. (2010) PHENIX: a comprehensive Python-based system for macromolecular structure solution, *Acta Crystallogr. Section D: Biol. Crystallogr. 66*, 213-221.

[46] Chen, V. B., Arendall, W. B., III, Headd, J. J., Keedy, D. A., Immormino, R. M., Kapral, G. J., Murray, L. W., Richardson, J. S., and Richardson, D. C. (2010) MolProbity: all-atom structure validation for macromolecular crystallography, *Acta Crystallogr. Section D: Biol. Crystallogr. 66*, 12-21.

[47] McCoy, A. J., Grosse-Kunstleve, R. W., Adams, P. D., Winn, M. D., Storoni, L. C., and Read, R. J. (2007) Phaser crystallographic software, *J. Appl. Crystallogr. 40*, 658-674.

[48] Winn, M. D., Ballard, C. C., Cowtan, K. D., Dodson, E. J., Emsley, P., Evans, P. R., Keegan, R. M., Krissinel, E. B., Leslie, A. G. W., McCoy, A., McNicholas, S. J., Murshudov, G. N., Pannu, N. S., Potterton, E. A., Powell, H. R., Read, R. J., Vagin, A., and Wilson, K. S. (2011) Overview of the CCP4 suite and current developments, *Acta Crystallogr. Section D: Biol. Crystallogr. 67*, 235-242.

[49] Stoll, S., and Schweiger, A. (2006) EasySpin, a comprehensive software package for spectral simulation and analysis in EPR, *J. Magn. Reson. 178*, 42-55.

[50] Bertini, I., Luchinat, C., Parigi, G., and Pierattelli, R. (2005) NMR spectroscopy of paramagnetic metalloproteins, *Chembiochem 6*, 1536-1549.

[51] Bertini, I., Luchinat, C., Parigi, G., and Pierattelli, R. (2008) Perspectives in paramagnetic NMR of metalloproteins, *Dalton Trans.*, 3782-3790.

[52] Bertini, I., and Pierattelli, R. (2004) Copper(II) proteins are amenable for NMR investigations, *Pure Appl. Chem. 76*, 321-333.

[53] Peisach, J., and Blumberg, W. E. (1974) Structural implications derived from the analysis of electron paramagnetic resonance spectra of natural and artificial copper proteins, *Arch. Biochem. Biophys. 165*, 691-708.

[54] McGuirl, M. A., Bollinger, J. A., Cosper, N., Scott, R. A., and Dooley, D. M. (2001) Expression, purification, and characterization of NosL, a novel Cu(II) protein of the nitrous oxide reductase (nos) gene cluster, *J. Biol. Inorg. Chem. 6*, 189-195.

[55] McGuirl, M. A., Nelson, L. K., Bollinger, J. A., Chan, Y. K., and Dooley, D. M. (1998) The nos (nitrous oxide reductase) gene cluster from the soil bacterium Achromobacter cycloclastes: Cloning, sequence analysis, and expression, *J. Inorg. Biochem. 70*, 155-169.

[56] Kaur, G., and Subramanian, S. (2014) Repurposing TRASH: Emergence of the enzyme organomercurial lyase from a non-catalytic zinc finger scaffold, *J. Struct. Biol. 188*, 16-21.

[57] Boal, A. K., and Rosenzweig, A. C. (2009) Structural Biology of Copper Trafficking, *Chem. Rev. 109*, 4760-4779.

[58] Blundell, K. L. I. M., Hough, M. A., Vijgenboom, E., and Worrall, J. A. R. (2014) Structural and mechanistic insights into an extracytoplasmic copper trafficking pathway in Streptomyces lividans, *Biochem. J. 459*, 525-538.

[59] Blundell, K. L. I. M., Wilson, M. T., Svistunenko, D. A., Vijgenboom, E., and Worrall, J. A. R. (2013) Morphological development and cytochrome c oxidase activity in Streptomyces lividans are dependent on the action of a copper bound Sco protein, *Open Biol. 3*. 120163.

[60] Blundell, K. L. I. M., Wilson, M. T., Vijgenboom, E., and Worrall, J. A. R. (2013) The role of the Cys-X-X-X-Cys motif on the kinetics of cupric ion loading to the Streptomyces lividans Sco protein, *Dalton Trans. 42*, 10608-10616.

[61] Wernimont, A. K., Huffman, D. L., Lamb, A. L., O'Halloran, T. V., and Rosenzweig, A. C. (2000) Structural basis for copper transfer by the metallochaperone for the Menkes/Wilson disease proteins, *Nat. Struct. Biol. 7*, 766-771.

[62] Wernimont, A. K., Yatsunyk, L. A., and Rosenzweig, A. C. (2004) Binding of copper(I) by the Wilson disease protein and its copper chaperone, *J. Biol. Chem. 279*, 12269-12276.

[63] Chacon, K. N., and Blackburn, N. J. (2012) Stable Cu(II) and Cu(I) Mononuclear Intermediates in the Assembly of the CuA Center of Thermus thermophilus Cytochrome Oxidase, *J. Am. Chem. Soc. 134*, 16401-16412.

[64] Robinson, N. J., and Winge, D. R. (2010) Copper Metallochaperones, In *Ann. Rev. Biochem.,* (Kornberg, R. D., Raetz, C. R. H., Rothman, J. E., and Thorner, J. W., Eds.), Vol 79, pp 537-562. Annual Reviews, Palo Alto, CA.

[65] Rubino, J. T., and Franz, K. J. (2012) Coordination chemistry of copper proteins: How nature handles a toxic cargo for essential function, *J. Inorg. Biochem. 107*, 129-143.

[66] Siluvai, G. S., Mayfield, M., Nilges, M. J., George, S. D., and Blackburn, N. J. (2010) Anatomy of a Red Copper Center: Spectroscopic Identification and Reactivity of the Copper Centers of Bacillus subtilis Sco and Its Cys-to-Ala Variants, *J. Am. Chem. Soc. 132*, 5215-5226.

[67] Horng, Y. C., Leary, S. C., Cobine, P. A., Young, F. B. J., George, G. N., Shoubridge, E. A., and Winge, D. R. (2005) Human Sco1 and Sco2 function as copper-binding proteins, *J. Biol. Chem. 280*, 34113-34122.

Figures

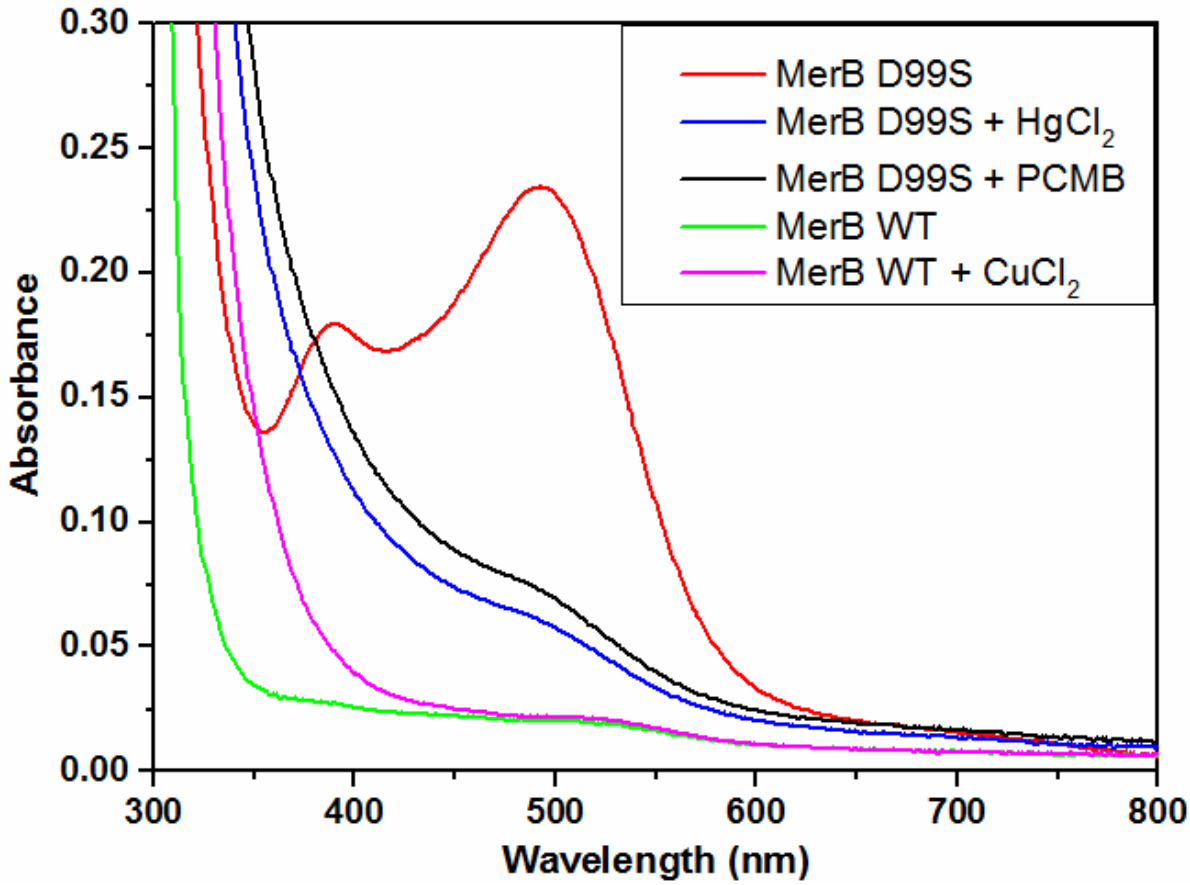

Figure 1. Comparison of the UV-visible absorption spectra of *E. coli* MerB and MerB D99S. UV-vis spectra were recorded on 0.5 mM solutions of *E. coli* MerB (green), MerB D99S (red), MerB D99S after the addition of $HgCl_2$ (blue), MerB D99S after the addition of PCMB (black) and *E. coli* MerB after the addition of $CuCl_2$ (pink).

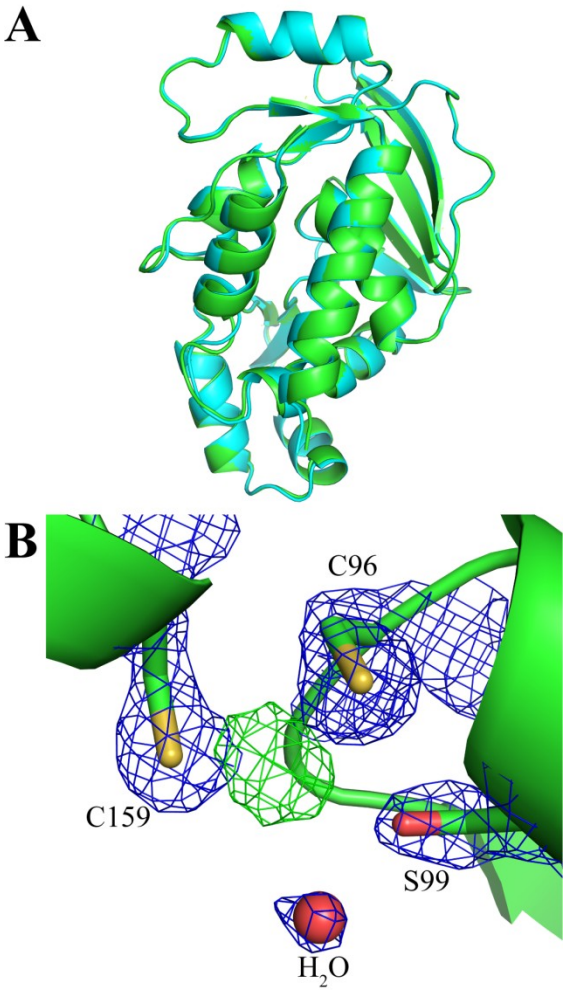

Figure 2. **Crystal structure of MerB D99S. A)** Overlay of the structure of MerB D99S (green) and the structure of *E. coli* MerB (aqua; PDB entry 3F0O). The two structures were aligned about the backbone C_α atoms. **B**) Close-up of the active site of MerB D99S indicating the presence of the copper atom. The backbone of MerB D99S is displayed in ribbon form (green) and the side chains of the three active site residues (C96, S99 and C159) are displayed in stick form with the sulfur atoms (yellow) of C96 and C159 and the oxygen atom (red) of S99. A molecule of bound water (red sphere) is also present. The 2Fo-Fc map (blue mesh) contoured at 1.5σ shows density for C96, S99, C159 and a water molecule. The Fo-Fc simulated annealing omit map contoured at 3σ shows the positive density (green mesh) of the copper ion in the active site.

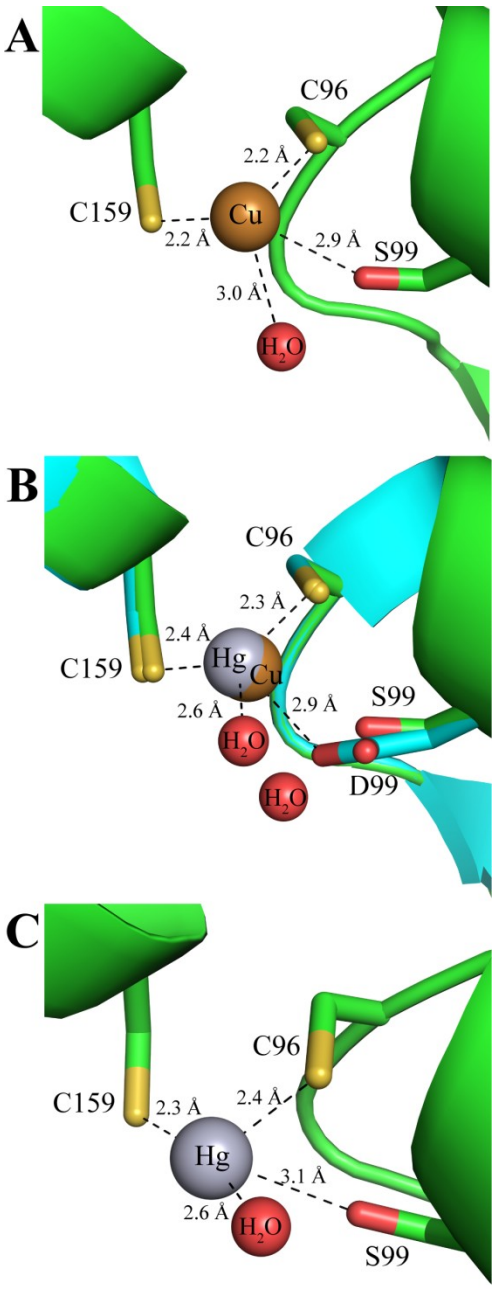

Figure 3. Copper binds to the active site of MerB D99S. **A**) Metrics of the MerB D99S-copper complex, the copper ion (copper sphere) is bound to the sulfur of C96 (2.2 Å), the sulfur of C159 (2.2 Å) and is in proximity to the oxygen of S99 (2.9 Å) and an oxygen of a bound water (red sphere) molecule (3.0 Å). The backbone of MerB D99S is displayed in ribbon form (green) and the side chains of the three active site residues are displayed in

stick form with the sulfur atoms (yellow) of C96 and C159 and the oxygen atom (red) of S99. **B**) Overlay of the active site of the MerB D99S-copper complex with the active site of the MerB-Hg complex (PDB entry 3F0P). The backbone of MerB D99S (green) and MerB (aqua) are displayed in ribbon form and the side chains of the three active site residues are displayed in stick form with the sulfur atoms (yellow) of C96 and C159 and the oxygen atoms (red) of either S99 or D99. The copper (copper), mercury (silver) and bound water molecules (red) are displayed as spheres. **C**) Close-up of the active site of the MerB D99S-Hg complex with the mercury displayed as a sphere (silver) and other representations as described in panel **A**. The mercury ion (silver sphere) is bound to the sulfur of C96 (2.4 Å), the sulfur of C159 (2.3 Å), the oxygen of S99 (3.1 Å) and oxygen from a bound water molecule (2.6 Å). In the panels, the copper (copper), mercury (silver) and bound water molecules (red) are displayed as spheres.

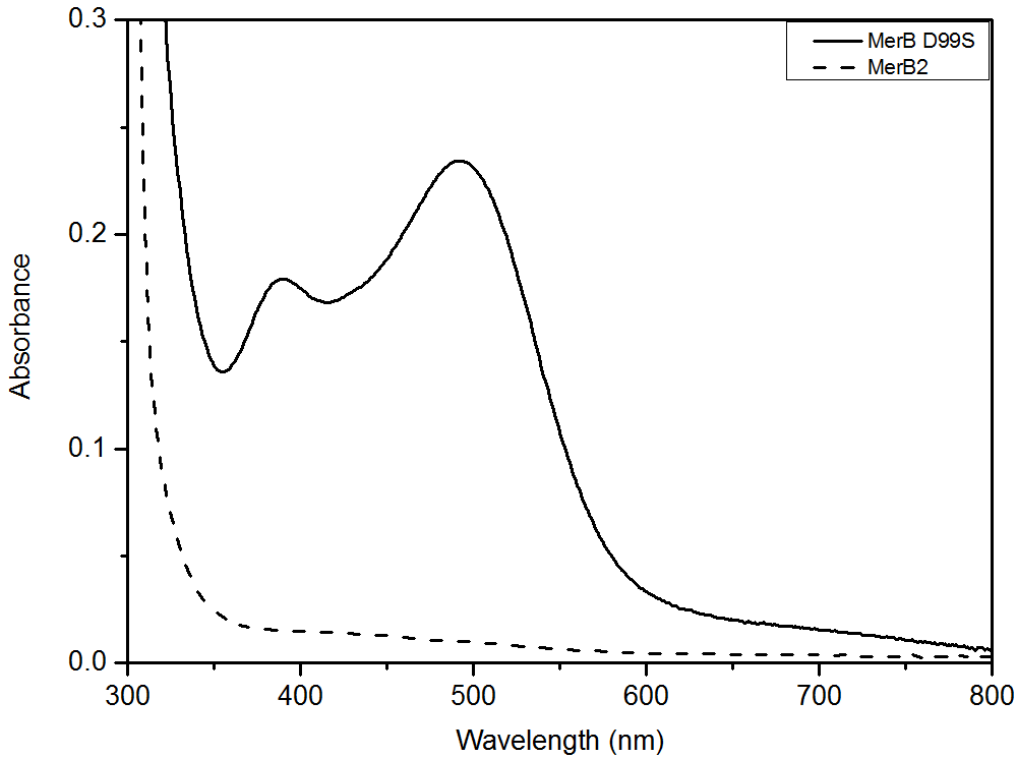

Figure 4. UV-visible absorption spectra of purified MerB2 (*B. Megaterium*). UV-vis spectra taken of 0.5 mM solutions of MerB D99S (solid line) and *B. megaterium* MerB2 (dashed line) following their expression and purification from bacterial cells.

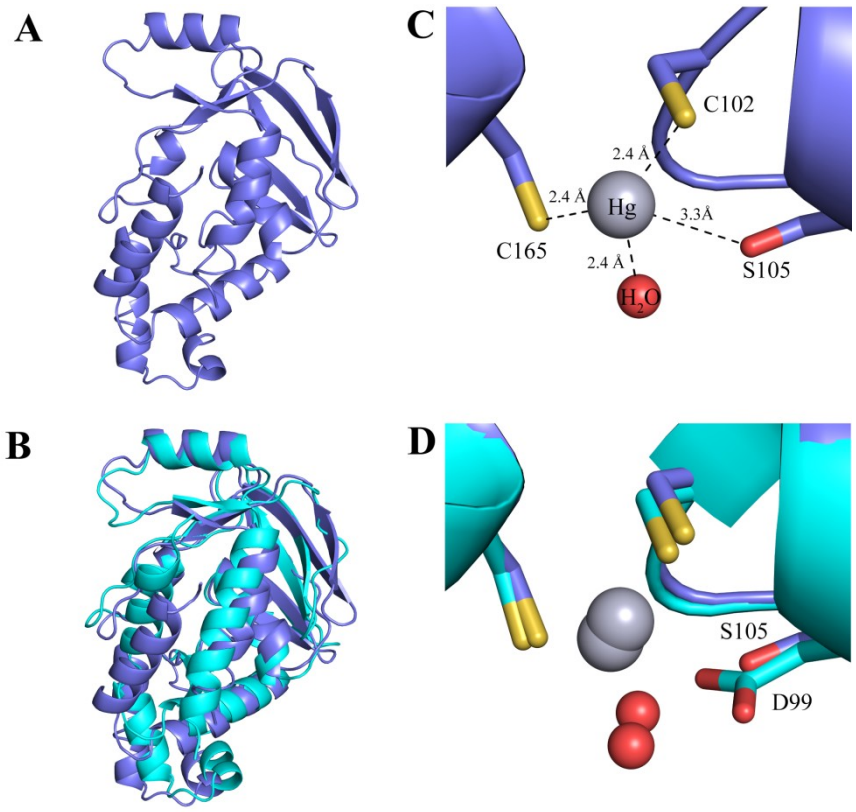

Figure 5. Crystal structure of *B. megaterium* MerB2-Hg complex. A) Ribbon diagram of the crystal structure of the *B. megaterium* MerB2-Hg complex **B)** Overlay of the structure of the *B. megaterium* MerB2-Hg complex (blue) with the structure of the *E. coli* MerB-Hg complex (aqua; PDB entry 3F0P). The two structures were aligned about the backbone C_α positions. **C**) Close-up of the active site of the *B. megaterium* MerB2-Hg complex with the backbone displayed in ribbon form (blue) and the side chains of the three active site residues displayed in stick form with the sulfur atoms (yellow) of C102 and C165 and the oxygen atom (red) of S105, and the mercury (silver) and a bound water molecule (red) represented as spheres. In the complex, the mercury is bound to the sulfur of C102 (2.4 Å) and the sulfur of C165 (2.4 Å) as well as being in proximity to the oxygen of S105 (3.3 Å) and the oxygen from a bound water molecule (2.4 Å). **D**) Overlay of active site of the *B. megaterium* MerB2-Hg complex with the active site of the *E. coli* MerB-Hg complex. The backbone of *B. megaterium* MerB2 (blue) and *E. coli* MerB (aqua) are displayed in ribbon form, whereas all other representations are as described in panel **C**.

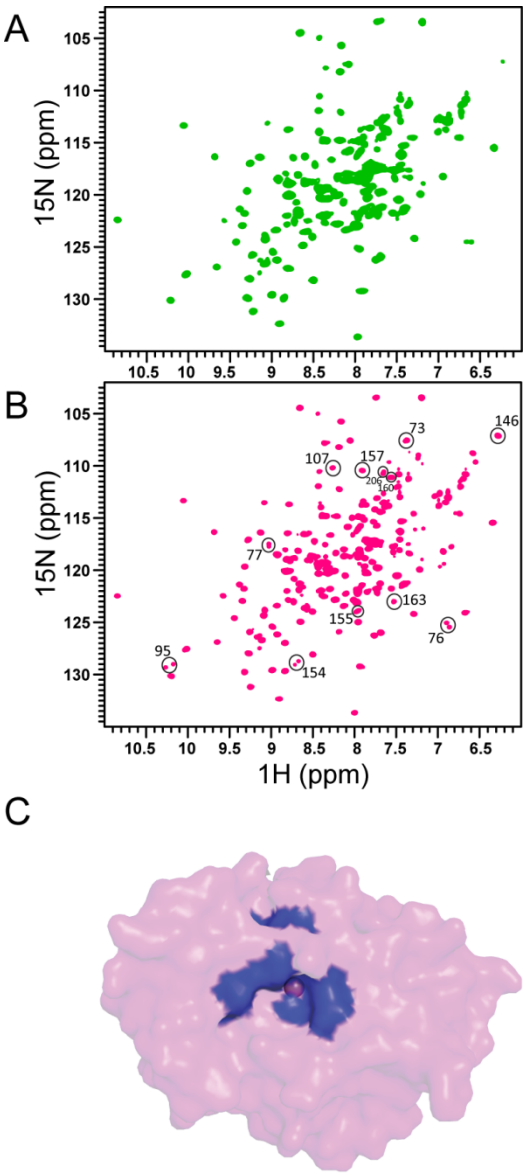

Figure 6. NMR spectra of MerB D99S. Comparison of the 2D ^{1}H-^{15}N HSQC spectra of ^{15}N-labeled MerB D99S after purification (**A**), and in the presence of 1.2 equivalents of $HgCl_2$ (**B**). The NH backbone signals that appear in the 2D ^{1}H-^{15}N HSQC spectra following addition of $HgCl_2$ are highlighted (**B)** with circles. **C**) Surface representation of the structure of *E. coli* MerB (shaded pink) in which the residues corresponding to the NH backbone signals that appear in the ^{1}H-^{15}N HSQC spectra following addition of $HgCl_2$ are highlighted (blue).

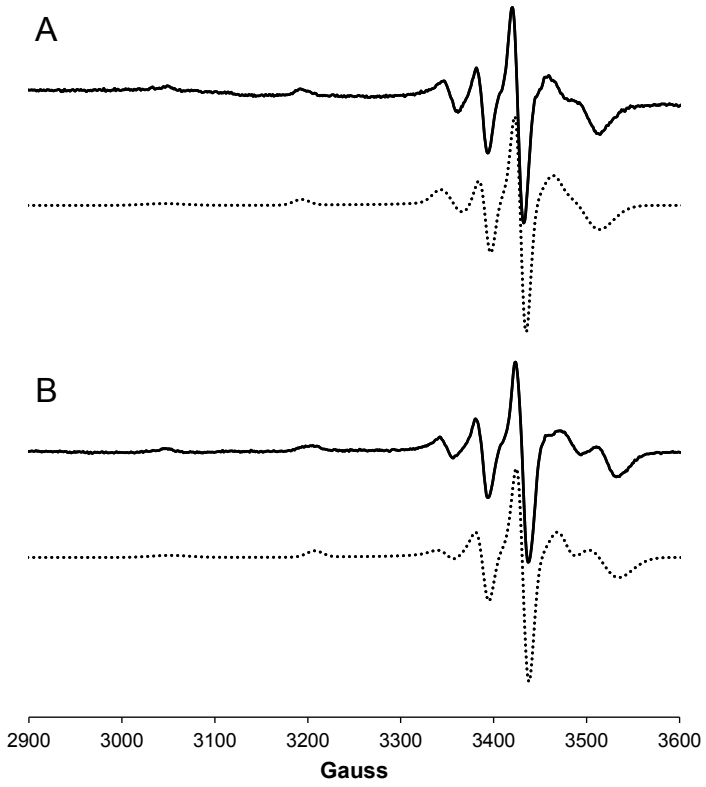

Figure 7. EPR spectra of MerB D99S and MerB D99N. Experimental (*solid line*) and simulated (*dotted line*) 77 K EPR spectra of as-isolated samples of MerB D99S (**A**) and MerB D99N (**B**) in 10 mM sodium phosphate buffer, pH 7.5, with 10 mM NaCl, 1 mM EDTA and 7.5 mM DTT; simulation parameters: (**A**) $g_{\parallel} = 2.117$, $A_{\parallel} = 144 \times 10^{-4}$ cm^{-1}, $g_{\perp} = 2.024$, $A_{\perp} = 32.4 \times 10^{-4}$ cm^{-1}; (**B**) $g_{\parallel} = 2.107$, $A_{\parallel} = 151 \times 10^{-4}$ cm^{-1}, $g_{\perp} = 2.026$, $A_{\perp} = 36.0 \times 10^{-4}$ cm^{-1}.

SUPPORTING INFORMATION

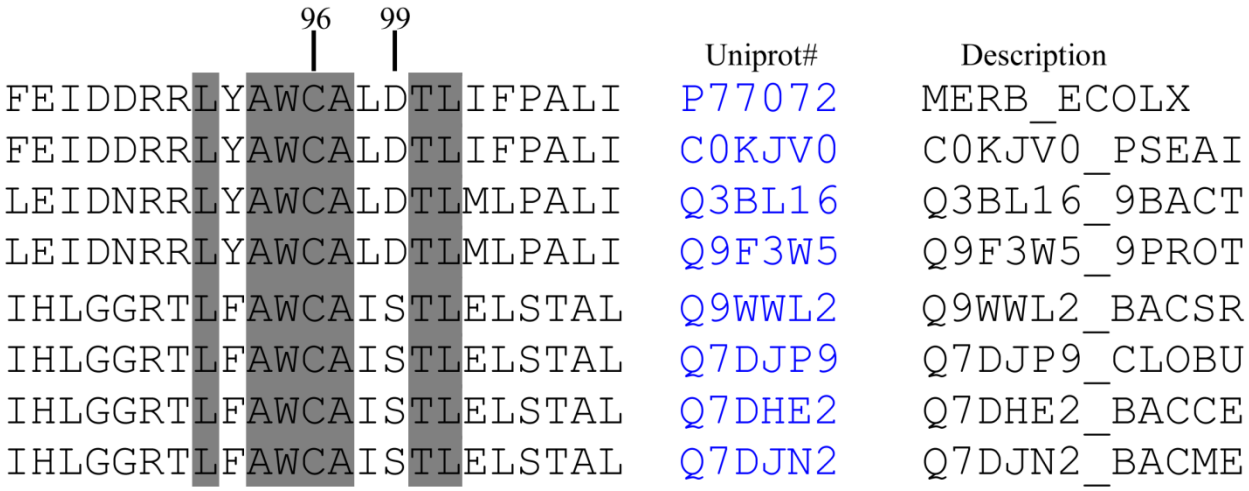

Figure S1. Sequence alignment of MerB. Eight representative MerB sequences were taken from the ClustalW alignment and the alignment highlights the conservation within residues 85-107 of *E. coli* MerB including C96 and D99. The two residues are conserved in all known MerB sequences with an exception of four variants that contain a serine instead of an aspartic acid residue in the equivalent of the D99 position in *E. coli* MerB.

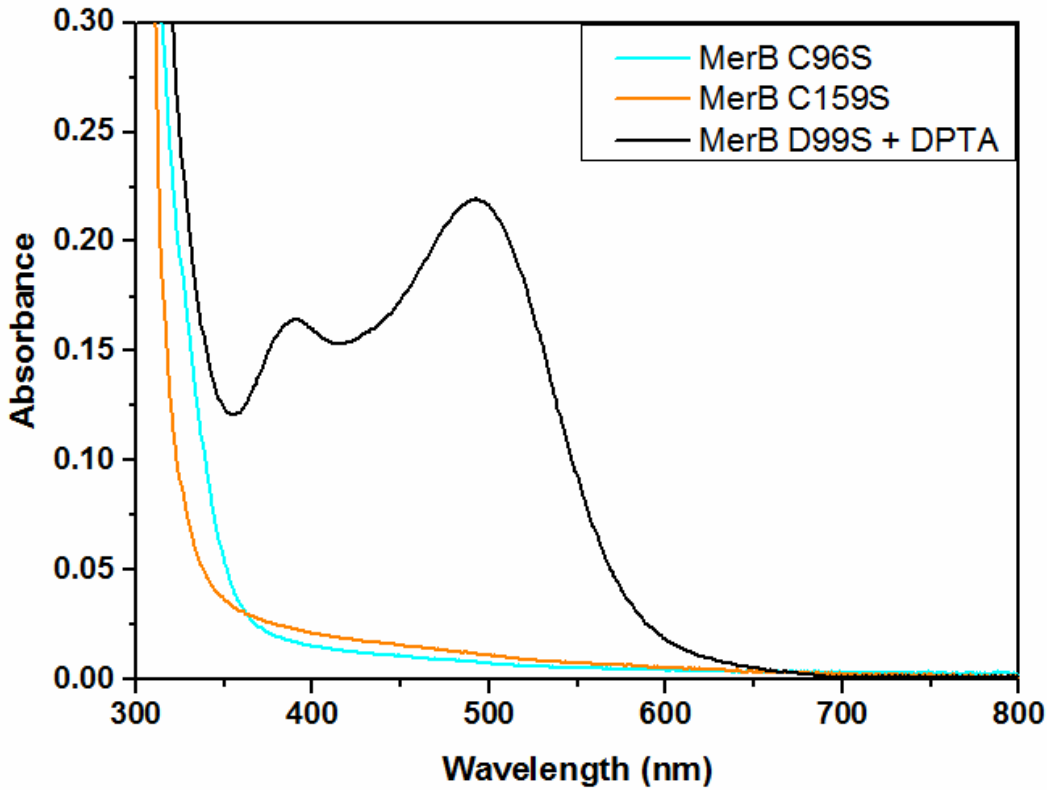

Figure S2. UV-visible absorption spectra of *E. coli* MerB mutants. The UV-vis spectra were taken with 0.5 mM solutions of MerB C96S (cyan), MerB C159S (orange) and MerB D99S after treatment with 5mM DTPA (black).

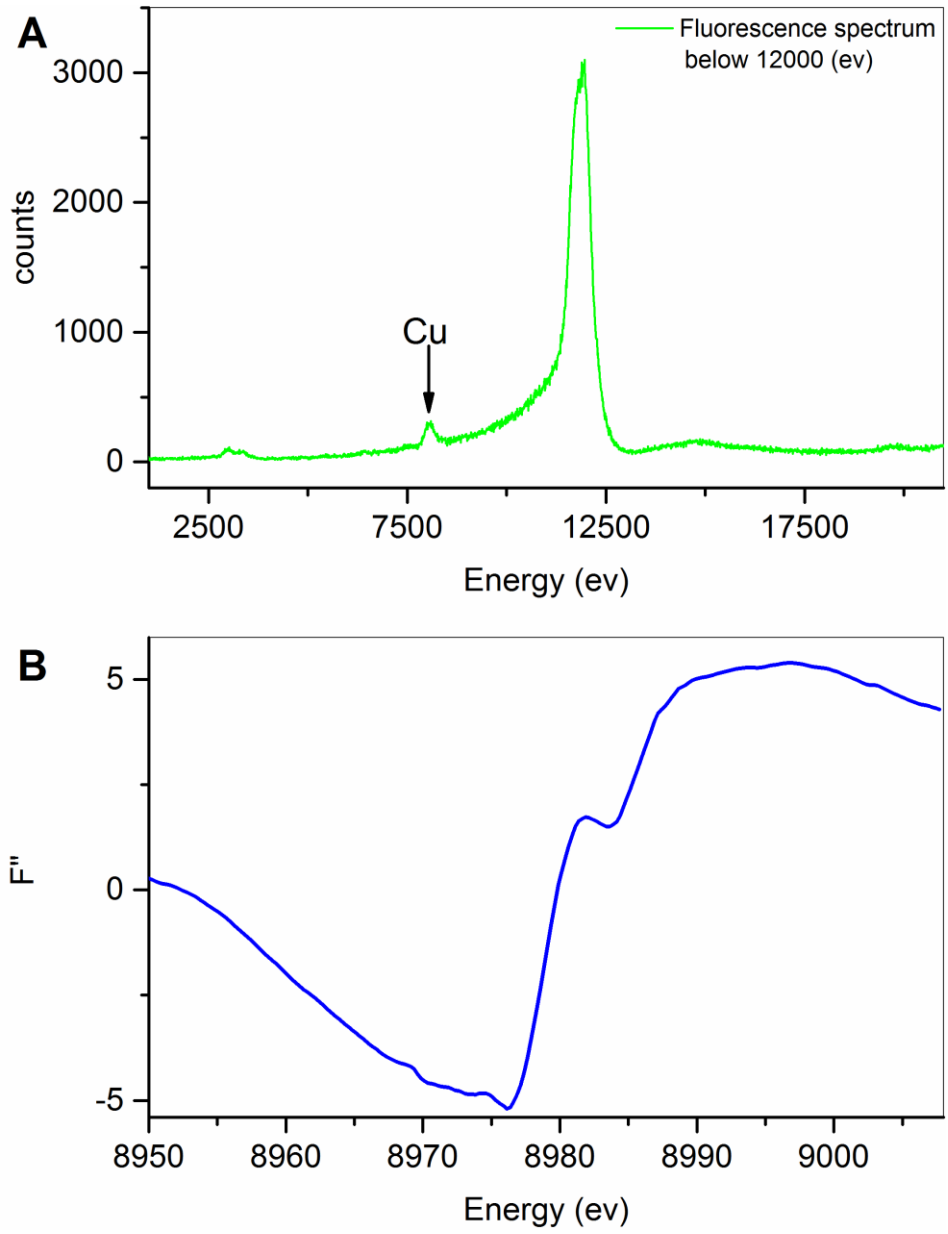

Figure S3. Copper is bound in crystals of MerB D99S. A) The fluorescence spectrum below 12000 (ev) shows the presence of copper in crystals of MerB D99S. B) The X-ray fluorescense spectrum is showing the edge for copper.

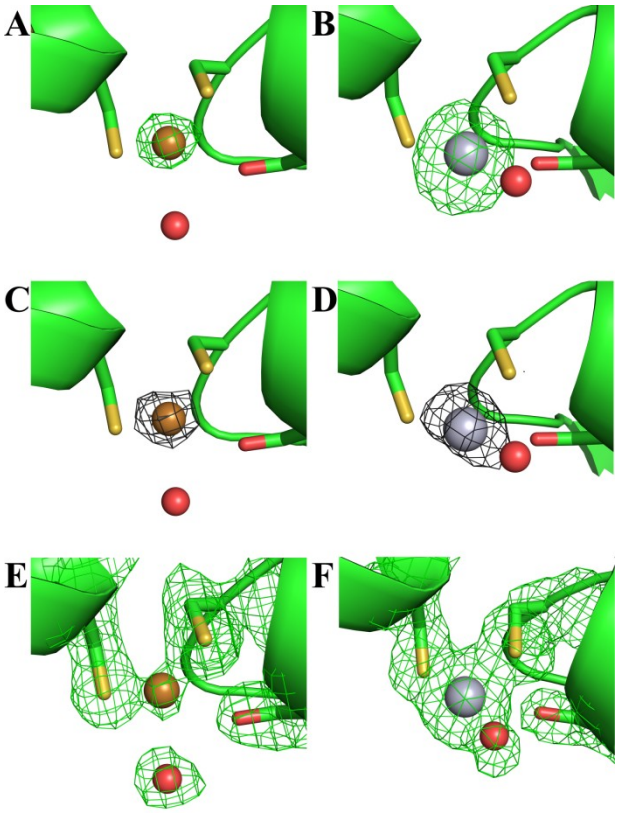

Figure S4. Comparison of the active site of the MerB D99S-Cu and MerB D99S-Hg complexes. A close-up of the Fo-Fc simulated annealing omit map of the active site displaying the positive density for the Cu and Hg ions in the MerB D99S-Cu complex (**A**) and the MerB D99S-Hg complex (**B**). The positive electron density (green mesh) in **A** and **B** is contoured at 3σ. In **C** and **D**, a close-up of the anomalous difference map (dark grey mesh) of the active site contoured at 3σ showing the anomalous peak for the Cu and Hg ions in the MerB D99S-Cu complex (**C**) and MerB D99S-Hg complex (**D**). The anomalous peak height for copper is 7.1 (data collected at Cu edge, wavelength 1.37Å) and 16 for mercury (data collected at 1.07Å). In **E** and **F**, close up of the Fo-Fc kick omit map (green mesh) of the active site of the MerB D99S-Cu complex (**E**) and the MerB D99S-Hg complex (**F**) contoured at 2σ. The occupancies of C96, S99 and C159 as well as that of the ions and bound water molecules were set to zero prior to calculating the Fo-Fc map. Phenix map was used to generate the kick omit map calculation. The backbone of MerB D99S is displayed in ribbon form (green) and the side chains of the three active site residues are

displayed in stick form with the sulfur atoms (yellow) of C96 and C159 and the oxygen atom (red) of S99. The copper (copper) and mercury (grey) ions are represented as spheres. A molecule of bound water (red sphere) is also present.

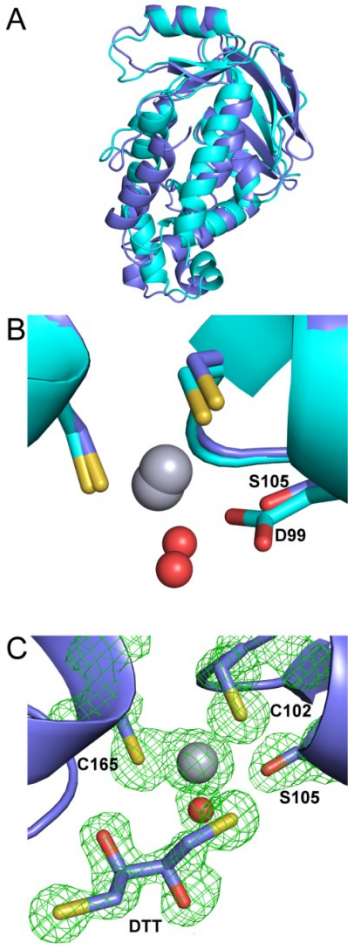

Figure S5. Structure of *B. megaterium* MerB2-Hg complex. A) Overlay of the structure of the *B. megaterium* MerB2-Hg complex (blue) with the structure of the *E. coli* MerB-Hg complex (aqua; PDB entry 3F0P). **B**) Overlay of active site of the *B. megaterium* MerB2-Hg complex with the active site of the MerB-Hg complex. The backbone of *B. megaterium* MerB2 (blue) and *E. coli* MerB (aqua) are displayed in ribbon form, and the side chains of the three active site residues are displayed in stick form with the sulfur atoms (yellow) of C102 and C165 and the oxygen atom (red) of S105. The mercury (grey) ion and the bound water (red) molecule are represented as spheres. **C)** Close up of the Fo-Fc kick omit map (green mesh) of the active site of the *B. megaterium* MerB2-Hg complex contoured at 3 σ.

The occupancies of C102, S105 and C165 as well as that of the Hg ion and the bound water molecules were set to zero prior to calculating the Fo-Fc map. The backbone of *B. megaterium* MerB2, the key elements of the active site are as described in panel **B**. In addition, there is a DTT from the protein solvent displayed in stick form (violet) with the two sulfur atoms in yellow and two oxygen atoms in red.

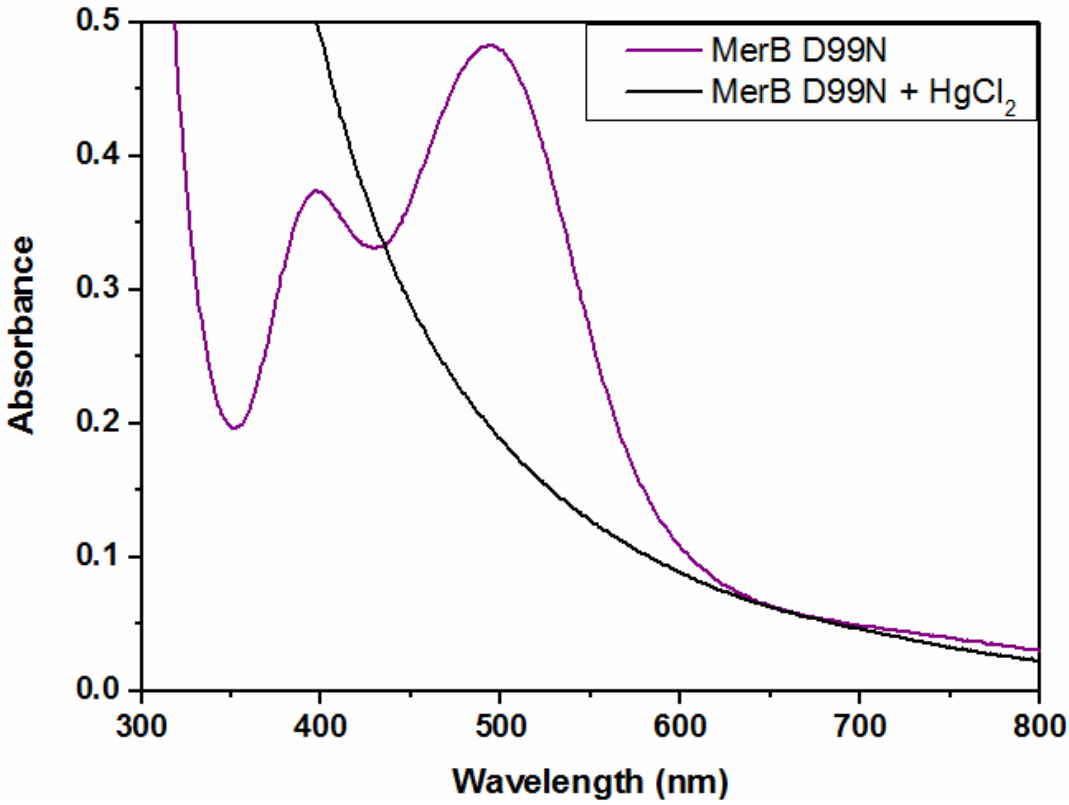

Figure S6. UV-visible absorption spectra of MerB D99N variant. UV-vis spectra were taken with 0.5 mM solutions of MerB D99N (violet) and MerB D99N following addition of $HgCl_2$ (black).

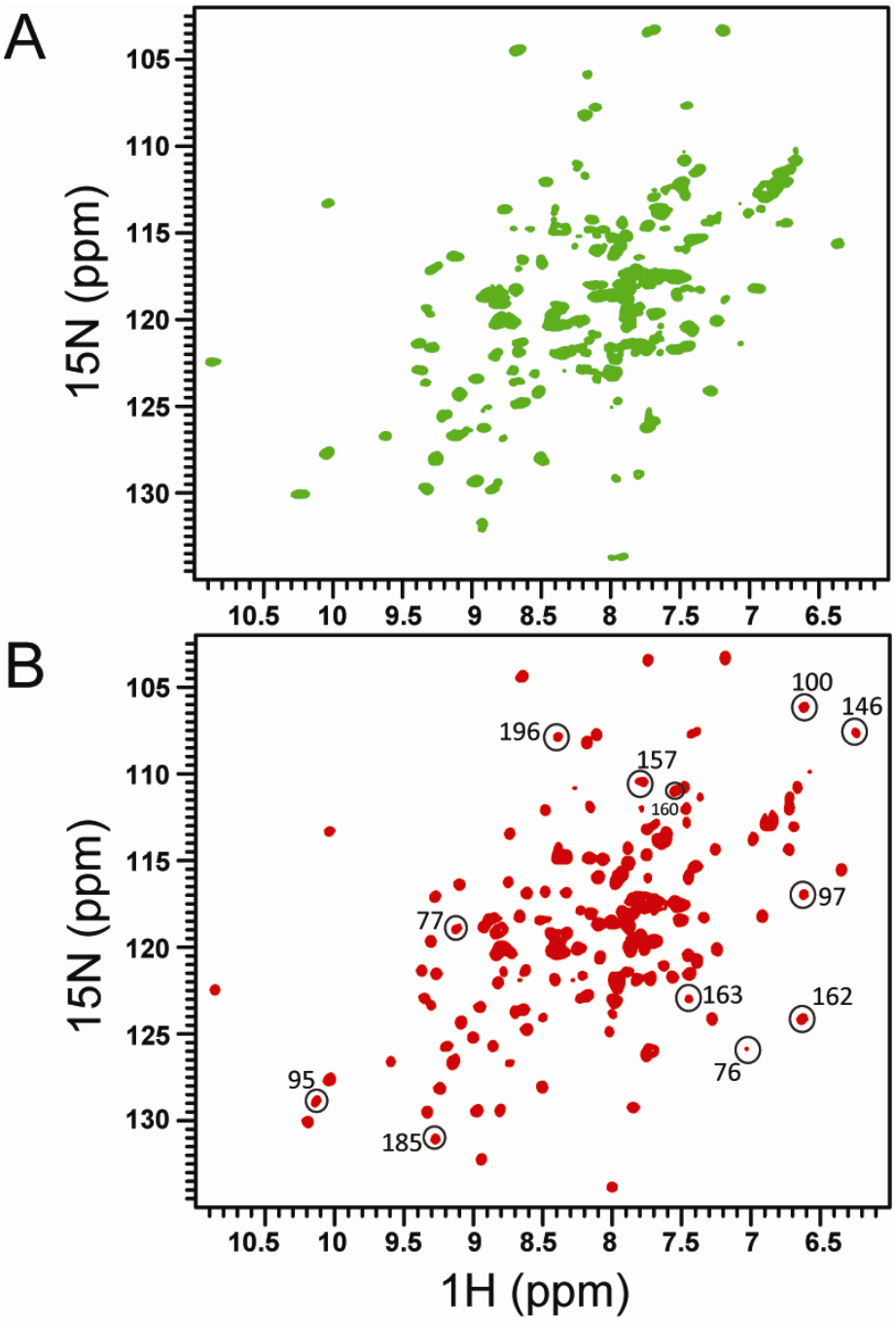

Figure S7 NMR spectra of MerB D99N. Comparison of the 2D ^{1}H-^{15}N HSQC spectra of ^{15}N-labeled MerB D99N after purification (**A**), and in the presence of 1.2 equivalents of $HgCl_2$ (**B**). The NH backbone signals that appear in the 2D ^{1}H-^{15}N HSQC spectra following addition of $HgCl_2$ are highlighted (**B)** with circles.

Chapter 3: Article 2

Structural and biochemical characterization of organotin and organolead compounds with the organomercurial lyase MerB provide important insights into its unique mechanism of carbon-metal bond cleavage.

*Haytham M. Wahba[1,2], Michael Stevenson[3], Ahmed Mansour[1], Jurgen Sygusch[1], Dean E. Wilcox[3], and James G. Omichinski[1]**

[1]Département de Biochimie et Médicine Moléculaire, Université de Montréal, Montréal, QC, Canada, [2]Faculty of Pharmacy, Beni-suef University, Beni-suef, Egypt and [3]Department of Chemistry, Dartmouth College, Hanover, NH, U.S.A.

***Correspondence:**
James G. Omichinski, Département de Biochimie et Médicine Moléculaire, Université de Montréal, C.P. 6128 Succursale Centre-Ville, Montréal, QC H3C 3J7 Canada.
Email: jg.omichinski@umontreal.ca; Telephone: 514-343-7341.

PDB ACCESSION CODES: Pending

FUNDING INFORMATION: This work was supported by grants from the Natural Sciences and Engineering Research Council of Canada (NSERC) to J.G.O and J.S. as well as from the National Science Foundation to D.E.W (CHE-1308598). H.W. was supported by a grant from the Ministry of Higher Education and Scientific Research in Egypt (Cultural Affairs and Missions Sector). Research was carried out in part at the National Synchrotron Light Source, Brookhaven National Laboratory, which is supported by the United States Department of Energy, Division of Materials Sciences and Division of Chemical Sciences under contract DE-AC02-98CH10886 and the Canadian Light Source (CLS), which is supported by NSERC, the National Research Council Canada, the Canadian Institutes of Health Research, the Province of Saskatchewan, Western Economic Diversification Canada, and the University of Saskatchewan.

Detailed contribution of authors in this work:

Haytham Wahba performed the protein expression, protein purification, sample preparation for each experiment entitled, protein crystallization, X-ray data collection, solving structure and structure refinement and fluorescence quenching data collection and analysis. All figures were prepared by Haytham Wahba. The overall contribution of Haytham Wahba to this work is approximately 90% of all generated data and he wrote the paper with help from James Omichinski. Michael Stevenson and Dean E. Wilcox were responsible for ITC data collection and data analysis and preparing Table 3. Ahmed Mansour was an intern in our lab and he helped with protein expression and purification under the supervision of Haytham Wahba. The X-ray data collection were collected and processed by Haytham Wahba under the supervision of Jurgen Sygusch. James G. Omichinski conceived the project, designed the study and supervised the writing of the paper.

ABSTRACT

The organomercurial lyase (MerB) has the unique ability to cleave carbon-Hg bonds and structural studies indicate that three residues in the active site (C96, D99 and C159 in *E. coli* MerB) play an important role in the carbon-Hg bond cleavage. However, the precise role of these active site residues in the catalytic process has not been well defined. To better define the mechanism of carbon-metal bond cleavage, we have structurally and biophysically characterized the interaction of MerB with a series of organotin and organolead compounds. Studies with two known inhibitors of MerB, dimethyltin (DMT) and triethyltin (TET), indicate that they inhibit by different mechanisms. In both cases the initial binding is to D99, but DMT also has the capacity to bind to C96, which induces a conformation change in the active site. In contrast, diethyltin (DET) is a substrate for MerB and the Sn^{IV} product remains bound in the active site in a similar manner to Hg^{II} following cleavage of organomercurial compounds. The results with the organolead compounds are similar in that trimethyllead (TML) is not cleaved and binds only to D99 whereas diethylead (DEL) is a substrate and the Pb^{IV} product remains bound in the active site. These results demonstrate that the initial binding of organometals to MerB occurs at D99 followed by subsequent binding to C96 and C159. In addition, the results suggest that MerB could be utilized for developing bioremediation application for DET, DEL and organomercurials, but that certain organolead and organotin could present an obstacle to remediation efforts by inhibiting MerB.

INTRODUCTION

Several strains of Gram-negative and Gram-positive bacteria have been isolated from mercury-contaminated sites because they possess the unique ability to grow is the presence of toxic concentrations of both inorganic mercury (Hg^{II}) and organomercurial compounds[1]. Their resistance to mercury-containing compounds is attributed to the presence of a set of genes located on a transferable genetic component known as the *mer* operon[2-4]. Although the exact composition of proteins produced from the *mer* operon varies between the different strains of resistant bacteria, the most common form of the operon encodes for proteins that function to detoxify both organomercurial compounds and ionic Hg^{II} by converting them to the less toxic elemental mercury (Hg^0)[5, 6]. The metabolic conversion of organomercurial compounds to Hg^0 requires two key enzymes encoded for by the *mer* operon[7-10]. The first enzyme is the organomercurial lyase MerB, which cleaves the carbon-Hg bond of organomercurial compounds to produce two products, a hydrocarbon moiety and Hg^{II} [7, 8, 11-13]. The second enzyme is the ionic mercuric reductase MerA that functions by reducing Hg^{II} to Hg^0, which is readily expired by the bacteria due to is volatility[9, 10].

When bacteria express both MerA and MerB, their mercury resistance is referred to as broad spectrum since they have the capacity to detoxify both Hg^{II} and organomercurial compounds[6]. Following exposure to ionic Hg^{II}, the toxic metal is initially bound to two cysteine residues present in the periplasmic protein MerP, which directly transfers the Hg^{II} to the mercury-specific transporter MerT[14-16]. MerT is an inner-membrane protein that transports Hg^{II} via two cysteine residues located on the periplasmic side of the membrane to two cysteine residues located on the cytosolic side[15]. Once bound to MerT on the cytosolic

side, the Hg^{II} is then transferred directly to two cysteine residues within the amino-terminal domain of MerA (NMerA)[15, 16]. The NMerA-bound Hg^{II} is then transferred to two cysteine residues in the active site of MerA for reduction to Hg^0 in an NADPH-dependent manner[17, 18]. In contrast to ionic Hg^{II}, organomercurial compounds pass directly into the cytosol due to their hydrophobicity. Once in the cytosol, organomercurial compounds bind to MerB, which cleaves the carbon-Hg bond. Although X-ray structural studies have demonstrated that the active site of MerB consists of three key catalytic residues C96, D99 and C159 (*E.coli* MerB numbering), the exact details of carbon-Hg bond cleavage by MerB have not been fully resolved[19, 20]. However, it appears that one of the two cysteine residues initiates the reaction and D99 functions as a proton donor[19, 20]. Following cleavage of the carbon-Hg bond, the hydrocarbon moiety is immediately released, whereas the Hg^{II} product remains bound in the active site to C96, D99 and C159 until it is directly transferred to the two cysteine residues within NMerA[13]. As is the case following exposure to Hg^{II}, MerA reduces the Hg^{II} to Hg^0 as the final detoxification step of organomercurial compounds[9, 10]. These direct transfers of Hg^{II} between the proteins in the Mer system, including between MerB and MerA, prevents the thiophilic Hg^{II} from reacting with sulfhydryl groups of cellular protein and thus limits its toxicity.

The unique catalytic property of MerB towards organomercurial compounds has attracted much attention for potentially developing bioremediation applications for cleaning up mercury-contaminated sites and several systems using either bacteria or plants expressing MerB and/or MerA have been developed as a form of green technology[21-23]. Unfortunately, organomercurial compounds represent only a small fraction of the

organometallic compounds contaminating the environment. For example, other organometals pose serious threats to the environment, such as organotin and organolead compounds[24]. Organotin compounds were commonly used as bactericides, fungicides, and as stabilizers for polyvinyl chloride tubing whereas organolead compounds were extensively used as anti-knocking agents in gasoline for combustion engines[25-28]. As a result of the extensive use of tetraethyl lead (TTEL) and tetramethyl lead (TTML) as gasoline additives, tremendous quantities of organolead compounds were released in automobile exhaust fumes[29] and these emissions still remain as an important source of organolead contamination in our environment. Likewise, tributyltin (TBT) and triphenyltin (TPT) were extensively employed as anti-fouling paints in the shipbuilding industry and this contributed directly to contaminating the marine environment especially in harbor areas[25, 30].

Like organomercurial compounds, organolead and organotin compounds have the capacity to bioaccumulate and their concentrations increase in higher organisms as they pass through the food chain[25]. The toxicity of organolead and organotin compounds depends both on the composition and number of organic groups bound to the metal with higher numbers of substitutions generally being more toxic. Although TTEL and TTML are themselves unstable, they are rapidly converted to their respective tri-, di- and mono-alkyl lead species, and the most persistent forms are the trialkylated lead species: triethyl lead (TEL) and trimethyl lead (TML)[31, 32]. Following exposure, organolead compounds rapidly concentrate in the nervous system after crossing the blood brain barrier, and the symptoms associated with exposure to organolead compounds include neurobehavioral abnormalities

and impairment of memory[33, 34]. In the case of organotin compounds, the toxic effects are associated in part with their direct impact on mitochondrial function. Trimethytin (TMT) and triethyltin (TET) have been shown to inhibit mitochondrial oxidative phosphorylation, whereas other diorganotin compounds where found to inhibit α-ketoacid oxidase and consequently stop mitochondrial respiration[35]. For organolead and organotin compounds, their toxicity is often associated with their reactivity towards sulfhydryl groups on protein as well as their capacity to bioaccumulate.

The toxic effects and widespread contamination of organotin and organolead compounds led several research groups to investigate whether or not microorganisms have developed a natural resistant system similar to the Mer system used for organomercurial compounds[32, 36, 37]. Although select bacterial strains have been shown to display resistance, a specific detoxification system similar to the Mer system has not been identified for either organolead or organotin compounds. In an attempt to determine whether or not MerB possesses the capacity for cleaving carbon-Sn bonds, a number of organotin compounds were tested[38] and it was determined that MerB has the capacity to cleave the carbon-Sn of several tetra- and tri-substituted derivatives, but it displayed lower activity and a narrower range of specificity in comparison to its activity toward organomercurial compounds. Interestingly, a decrease in MerB catalytic activity was noted as the reaction proceeded for organotin compounds where carbon-Sn bond cleavage was observed. This suggested that the resultant di- or mono-substituted tin products might function as inhibitors of MerB and dimethyltin (DMT) was identified as a potent irreversible inhibitor of MerB[38].

Given their similar properties and the fact that organotin compounds function as inhibitors of MerB, this suggests that organotin and organolead compounds could function as probes for characterizing the details of carbon-metal bond cleavage by MerB. Therefore, we attempted to structurally and thermodynamically characterize the interactions of several organotin and organolead compounds with MerB using X-ray crystallography, isothermal titration calorimetry (ITC) and fluorescence spectroscopy measurements. Soaking crystals of MerB with solutions of organotin and organolead compounds demonstrated that their initial binding to MerB occurs at D99 followed by subsequent binding to C96 and C159. In addition, our results indicate that, like organotin compounds, organolead compounds appear to have the capacity to function either as substrates or inhibitors depending on the chemical composition and the number of attached alkyl groups. Taken together, the results provide detailed insights into the unique catalytic mechanism of MerB for cleaving carbon-metal bonds and an atomic-level description of its interactions with organolead and organotin compounds.

Materials and Methods

Expression vector construction, expression and purification of MerB enzyme

The *merB* gene from plasmid R831b cloned in pET21b expression vector (Novagen) was used for the expression of wild-type *E. coli* MerB. The sequences encoding the amino-terminal 69 residues of MerA (NMerA) from *Shigella flexneri* (UniProt code: p08332) was cloned into a pGEX-TEV vector. All constructs were verified by DNA sequencing.

The *E. coli* MerB was expressed and purified as previously described[19, 39]. During the purification, all buffers contained 1 mM ethylenediaminetetraacetic acid (EDTA) and 7.5 mM dithiolthreitol (DTT) to keep the cysteine residues in their reduced state. Following the purification, MerB samples are stored at – 80° C until a further usage. Prior to crystallization, the protein samples were purified over a Superose-12 (GE Healthcare) gel filtration column using a buffer consisting of 10 mM sodium phosphate, pH 7.5, 1 mM EDTA, 10 mM sodium chloride and 7.5 mM DTT (Buffer A) and concentrated to 12 mg/mL using an Amicon ultrafiltration device with a 3 kDa MW cutoff (Millipore).

The GST-NMerA fusion protein was expressed in *E. coli* host strain TOPP2 (Stratagene). The cells were grown at 37°C in Luria Broth media, and protein expression was induced for 4h at 30°C with 0.7 mM isopropyl-beta-D-thiogalactopyranoside (IPTG; Inalco). The cells were harvested by centrifugation, resuspended in lysis buffer (20 mM Tris-HCl pH 7.4, 1 M NaCl, 0.2 mM EDTA, and 1 mM DTT), lysed in a French press and centrifuged at 105, 000 x g for 1h at 4°C. The supernatant was then collected and incubated for 1h with Glutathione Sepharose 4B (GSH) resin (GE Healthcare) at 4°C. Following incubation, the resin was collected by centrifugation, washed with lysis buffer and then placed in a TEV cutting buffer (25 mM sodium phsophate, 125 mM NaCl, and 5 mM DTT). The GST-tag was cleaved by incubating the resin for two hours with 100 units of TEV protease. The NMerA protein was eluted by two washes in TEV buffer. NMerA was further purified using Q-Sepharose High Performance in 20 mM sodium phosphate buffer, pH 7.3, with 1 mM EDTA and 7.5 mM DTT (Buffer B) and a Superdex 200 10/300 columns (GE Healthcare) in Buffer A. NMerA was flash frozen and kept at -80°C until

being processed for fluorescence quenching experiment. For the fluorescence quenching experiment both MerB and NMerA were subjected to buffer exchange by passing through a Superdex 200 10/300 columns (GE Healthcare) in 50 mM Sodium phosphate buffer.

MerB Crystallization Conditions

Crystals of MerB was grown by the vapor diffusion method at 23 °C using either a 1:1 or 1:2 mixtures of protein solution (12 mg/mL) and precipitant buffer, respectively. The precipitant buffer was 22 - 24 % polyethylene glycol 2000 MME in 0.2 M sodium acetate pH 5.5 with 0.2 M potassium bromide.

Formation of metal and organometal complexes with MerB crystals:

To obtain MerB-organometal complexes, crystals of wild-type MerB were soaked for time periods ranging between 10 min and 6h in a cryoprotectant solution containing 25% polyethylene glycol 2000 MME in 0.2 M sodium acetate pH 5.5 with 0.2 M potassium bromide and 0.5 - 1 mM dimethyltin dibromide (DMT; Aldrich), diethyltin dichloride (DET; Alfa Aesar), trimethyltin chloride (TMT; Aldrich), diethyllead dibromide (DEL; Aldrich), trimethyllead bromide (TML; Aldrich) or triethyllead chloride (TEL; Crescent Chemicals). After soaking in the organometal solutions, the crystals were flash cooled in liquid nitrogen for data collection.

X-Ray data collection, processing and structure determination

Diffraction data were collected from single crystals using an ADSC Quantum 315 charge-coupled device at beam line X29 of the National Synchrotron Light Source (NSLS I) at Brookhaven National Laboratory (BNL, USA) or using a Rayonix MX300 detector at beamline 08ID-1 at the Canadian Light Source (CLS; Canada). All data sets were processed with HKL2000 or XDS and the results are summarized in **Tables 1 and 2**. The initial phases for determining the structures were of MerB following soaking with either metals or organometals were obtained by molecular replacement using the structure of wild-type MerB (PDB 3F0O) as a search template[19, 40]. Phases were improved by iterative cycles of model building with Coot and refinement was performed with PHENIX[41, 42]. Test data sets were randomly selected from the observed reflections prior to refinement. Statistics for the final models obtained with PHENIX and Molprobity are shown in **Tables 1 and 2**[43]. The structure coordinates (PDB Codes: **To be obtained**) have been deposited in the RCSB Protein Data Bank. The figures were visualized using PYMOL.

Fluorescence quenching experiments

The binding of Hg^{II}, DEL and DET to MerB was monitored by tryptophan fluorescence quenching with a Varian Cary Eclipse Fluorescence Spectrophotometer. For the fluorescence quenching experiment both MerB and NMerA were subjected to buffer exchange by passing through a Superdex 200 10/300 columns (GE Healthcare) in 50 mM Sodium phosphate buffer pH 7.4. One molar equivalent of Hg^{II}, DEL or DET was added to 3.5-5 μM of MerB at 25 C. Emission spectra between 300-400 nm were recorded before and after addition of the metal compounds. The excitation wavelength at 295 nm was used.

After formation of the organometal –MerB complexes, 20 molar equivalents of NMerA was added to remove the bound metal and the spectra was re-recorded.

Isothermal titration calorimetry (ITC) experiments

Protein aliquots were stored in a -80 C freezer until ITC preparation. All solutions were made and stored in acid-washed glass containers. Buffer solutions were made with nanopure water and chelex-treated for at least 4h before filtration to remove the chelex resin. The metal-free buffers were then placed under vacuum (~ 5 torr) with stirring for at least 2h, or until no visible air bubbles were being produced. The buffers were moved into an argon maintained anaerobic environment in a CoyLab plexiglass glove box and purged with argon through a gas diffuser for 10 min. All sample preparations were conducted in the glove box. MerB aliquots were buffer-exchanged using a PD-10 desalting column equilibrated with 40 mL of the various anaerobic buffers. The MerB protein concentration was determined using absorbance at 280 nm. ITC stock samples were prepared by dissolving the compound in buffer for each day of experiments and from these, the working ITC samples were prepared in acid-washed glass vials. All ITC measurements were carried out in triplicate using either a MicroCal PEAQ, housed in a custom plexiglass glove box, with a 285 μL sample cell, a 40 μL titration syringe, 1–2.0 μL injection volumes and 150-180 s intervals between injections or a Micro-Cal VP-ITC, housed in a custom anaerobic plexiglass glove box, with a 1.4 mL sample cell, a 300 μL titration syringe, 6–10 μL injection volumes and 300–600 s intervals between injections.

RESULTS

Dimethyltin binds to the active site of MerB

Although dimethyltin (DMT) has previously been shown to be an irreversible inhibitor of MerB, the mechanistic details of this inhibition have not been investigated at the atomic level[38]. As an initial attempt to characterize this mechanism of inhibition, crystals of MerB (*E. coli* MerB) were soaked for 10 min in a solution of 500 μM DMT and the resulting crystals diffracted to 1.6 Å resolution with the same space group ($P2_1$) and same number of proteins in the asymmetric unit (2) as crystals of free MerB (**Table 1**). The DMT soaked crystals contain a tin atom bound in a trigonal bipyramidal geometry at an occupancy rate of 0.88 in a site that is positioned 2.14 Å away from an oxygen atom of D99 of MerB (**Figure 1A**). In contrast to what is observed following the soaking of MerB crystals with either an organomercurial substrate or $HgCl_2$, the tin atom does not appear to bind to the sulfur atoms of either cysteine residue in the active site, as it is located 5.13 Å from the sulfur atom of C96 and 5.19 Å from the sulfur atom of C159 (**Figure 1A**). Since methyl groups and bound water molecules generate similar electron density patterns, we were unable to distinguish whether or not either of the methyl groups of DMT is cleaved during formation of the complex with MerB. Attempts to refine the data with either one or two methyl groups present on the tin atom did not provide the best difference maps, and this could be attributed to the possibility that these methyl groups exist in multiple conformations about the tin atom when bound to MerB. Therefore, water was used to model the other atoms in coordination with the tin atom in the refinement of the structure following soaking in a solution of DMT (**Figure 1A**).

Given the fact that it has been reported that there is a time lag in the inhibition of MerB following incubation with organotin compounds, MerB crystals were soaked for longer time periods in DMT (up to 6h) to determine if any changes occured. Following a 1h soaking in DMT, the resulting crystals diffract to 1.53 Å resolution with the same space group and two proteins in the asymmetric unit (**Table 1**). Consistent with what we observe following the 10 min soak, analysis of subunit **B** from the asymmetric unit shows a tin atom binding at an occupancy rate of 0.88 to an oxygen atom of D99 of MerB (2.22 Å) as well as no binding to the sulfur atoms of either C96 (5.31 Å) or C159 (5.23 Å). However, analysis of subunit **A** from the asymmetric unit indicates that the tin atom is bound in a significantly different fashion. In this subunit, the tin atom is binding at an occupancy rate of 0.91 in a distorted trigonal bipyramidal conformation, where it is in contact with an oxygen atom from D99 (2.40 Å) and the sulfur atom from C96 (2.56 Å), but not with the sulfur atom of C159 (5.83 Å) from MerB (**Figure 1B**). Interestingly, the binding of the tin atom to D99 and C96 in subunit **A** results in a dramatic change in the active site that leads to the disruption of a cation-π interaction between the guanido group of R155 and the aromatic ring of W95 from MerB (**Figure 1B**). This cation-π interaction is present in the crystal structures of MerB in both the free and mercury-bound state as well as in the structures after the 10 min soaking of DMT and in subunit B following the 1h soaking (**Figure 1**). The disruption of the cation-π interaction between R155 and W95 results in a conformational change in the H6 helix of MerB, which leads to the displacement of C159 away from the bound tin atom (**Figure 1**). This displacement of the sulfur atom of C159 further away from the other two active site residues (2.35 Å further from the sulfur of C96

and 2.28 Å further from the oxygen of D99) seems to help explain why DMT is an irreversible inhibitor of MerB.

Characterization of ethyl substituted organotin compounds binding to MerB

To help gain insight into whether or not the methyl groups are cleaved by MerB during the formation of the complex following soaking in DMT, we attempted to solve the structure of MerB following soaking with diethyltin (DET) and triethyltin (TET). These compounds were selected because they are commercially available, they are partially soluble in aqueous solutions and the electron density of their ethyl side chains can be distinguished more readily from a bound water molecule than methyl substituents. In addition, TET has also been reported to be an inhibitor of MerB, whereas DET is the closest available commercial analog to DMT. Following soaking in 500 μM TET for 1h, the resulting MerB crystals diffract to 1.85 Å resolution. The crystal structure shows the presence of a MerB-TET complex where the tin atom binds at an occupancy rate of 1.0 to an oxygen atom of D99 (2.45 Å) in a trigonal bipyrimidal fashion and there is clear electron density for the three ethyl groups of TET indicating that MerB does not cleave the carbon-Sn bonds. In addition, the tin atom in the MerB-TET complex does not appear to bind the sulfur atoms of either cysteine residue in the active site, as it is located 5.44 Å from the sulfur atom of C96 and 5.04 Å from the sulfur atom of C159 (**Figure 2**). Next, MerB crystals were soaked for 1 h in a solution containing 500 μM DET. Following the soak, the resulting crystals diffract to 2.00 Å resolution. The crystal structure shows that the tin atom binds at an occupancy rate of 0.83 to the oxygen atom of D99 (2.44 Å) and is in proximity to the sulfur atoms of both C159 (2.41 Å) and C96 (2.69 Å) (**Figure 3**). In addition, there is

no clear electron density for the two ethyl groups of DET complex indicating that MerB cleaves the carbon-tin bonds of DET (**Figure 3**).

MerB has the capacity to cleave carbon-Pb bonds.

The fact that organotin compounds have both been shown to act as substrates and/or inhibitors of MerB suggests that the organic forms of other post-transitional metals may also function as substrates and/or inhibitors of MerB. Although most organic forms of post-transitional metals are either unstable at room temperature or insoluble in aqueous solutions, several different organolead compounds are both stable at room temperature and soluble in aqueous solutions. In addition, organolead compounds represent an important environmental concern[44]. Tetraethylead (TTEL) and tetramethylead (TTML) were used extensively as a gasoline additive until the mid-1980s, and their degradation products (tri-, di- and mono- derivatives) are persistent environmental contaminants that have the capacity to contaminate ground water[45]. To initially test the interaction of organolead compounds with MerB, MerB crystals were soaked for 10 min with a solution containing 500 μM trimethyllead (TML). TML was chosen since it is readily soluble in aqueous solution, commercially available and a persistent degradation product of TTML. Following the short soaking time, the resulting MerB-TML crystals diffract to 1.75 Å (**Table 2**). Analysis of the crystal indicates that the lead atom binds to MerB with an occupancy rate of 0.68, but that D99 is the only residue of MerB that appears to make a direct contact with the lead atom. Following the 10 min soak in TML, the lead is positioned at a distance of 2.74 Å from an oxygen atom of D99, but it is located 5.52 Å from the sulfur atom of C96 and 5.12 Å from the sulfur atom of C159 from MerB (**Figure 4 and see Figure S1 in Supplementary**

Information). Soaking for longer time periods (up to 6h) did not induce any changes in the binding of the lead atom of TML as was seen with DMT. In contrast to what was observed following soaking in DMT, we were able to determine that the methyl groups of TML are present in the MerB-TML complex and this suggests that TML might function as a weak inhibitor of MerB like TET, which also binds to just D99.

To further investigate the interaction of organolead compounds with MerB, we examined diethylead (DEL) binding to MerB. Like TML, DEL is readily soluble in aqueous solution, commercially available and a persistent degradation product of TTEL. MerB crystals were soaked in a solution of 500 μM DEL and the resulting crystals diffract to 1.75 Å (**Table 2**). In contrast to what was observed in the MerB-TML complex, the resulting complex shows that the lead atom binds with an occupancy rate of 0.93 to the sulfur atoms of both C96 (2.63 Å) and C159 (2.62 Å) as well as to an oxygen atom of D99 (2.35 Å). Importantly, there is no electron density indicating the presence of either of the two ethyl groups. This suggests that the two ethyl groups of DEL have been cleaved leaving the ionic lead product bound to the active site of MerB and that DEL is a substrate for MerB (**Figure 4 and see Figure S1 in Supplementary Information**).

Relative binding affinities of MeHg, DMT, DET, DEL and TML for MerB

Given that the structural studies show that DMT, DET, DEL and TML all have the capacity to bind to the active site MerB, but in slightly different manners, we were interested in evaluating their relative affinity in comparison to the native substrate MeHg. In order to compare the relative affinity of DMT, DET, DEL and TML for MerB, isothermal titration calorimetry (ITC) experiments were performed under anaerobic

conditions in multiple buffers. ITC was chosen since it is conducted in solution and there is the possibility to extract the thermodynamic parameters for binding. In addition, the stoichiometry can be determined in the case of organometals binding to MerB even if there is carbon-metal bond cleavage, since the ionic metal product remains bound in the active site in the absence of NMerA. The association constant (K_a) of MeHg with MerB was determined to serve as a control for comparing the relative association constants of DMT, DET, TML and DEL. The ITC experiments demonstrate that MeHg binds to MerB with a K_a of $7 \pm 4 \times 10^{16}$ in the different buffers, when the interaction of MeHg with the buffers is accounted for in the experiments (**Table 3**). Interestingly, DET binds to MerB with an average K_a of $2 \pm 1 \times 10^{20}$ using the same buffer conditions and taking into account the interaction between DET and the buffers (**Table 3**). In the case of DMT and DEL, there is no information in the literature regarding their interactions with the different buffers and only approximate K_a values could be determined for these compounds. However, if we assume that the DEL- and DMT-buffer thermodynamics are similar to the previously determined DEL-buffer thermodynamics, then it appears that DEL has a similar affinity for MerB as DET with an $\sim K_a$ of 1×10^{20}, whereas DMT binds about one order of magnitude weaker than DET with an $\sim K_a$ of 1×10^{19} (**Table 3**). In contrast, we saw no binding of TML to MerB under the experimental conditions indicating that the buffer was able to compete and bind with a higher affinity to TML than MerB. Thus, the ITC results are consistent with the structural studies where DEL, DET and DMT bind to multiple amino acid residues in the active site of MerB, but TML binds to Asp99 only at higher concentrations like those used when soaking the crystals. In addition, the ITC results also

demonstrate that the binding of MeHg to MerB is several orders of magnitude weaker in comparison with binding to DEL, DET and DMT and this data helps to explain how DMT functions as an irreversible inhibitor of MerB.

NMerA extracts Pb^{IV} but not Sn^{IV} from MerB-Pb^{IV} and MerB-Sn^{IV} complexes

One of the important characteristics of the Mer system is the direct transfer of Hg^{II} between proteins in the system, until the final release of volatile Hg^0 out of the cell[5]. By maintaining the highly toxic Hg^{II} in a continuously bound state, this prevents it from reacting with and damaging other cellular proteins. In all cases, key cysteine residues in the proteins of the Mer system are required for the direct transfer of the Hg^{II}. For example, the membrane transporter MerT receives Hg^{II} from the periplasmic transporter MerP and transfers it to the NMerA domain, which in turn transfers it to the active site of MerA for reduction to the less toxic Hg^0 [15, 46-48]. Similarly, the Hg^{II} product following the cleavage of the carbon-Hg bond of organomercurials is transferred directly from MerB to NMerA and then to the active site of MerA. Previous studies have shown that the transfer of the Hg^{II} from the MerB to NMerA can be monitored experimentally by measuring changes in the intrinsic fluorescent properties of tryptophan residues in MerB[13]. Following the addition of Hg^{II} to MerB, the emitted fluorescence of MerB is quenched due to the binding of Hg^{II}, and this is thought to be due to the fact that Trp95 is located very close to the Hg^{II}-binding site. Subsequent addition of excess NMerA to the MerB-Hg complex partially restores the fluorescence intensity due to transfer of the bound Hg^{II} from MerB to NMerA[13].

Given that both Pb^{IV} and Sn^{IV} are able to bind MerB in a similar manner as Hg^{II} following cleavage of the carbon-metal bonds of DEL and DET, we were interested to

determine whether or not NMerA could remove either the bound Pb^{IV} or the bound Sn^{IV}. For these studies, changes in MerB fluorescence were measured to monitor the transfer of Pb^{IV} and Sn^{IV} to NMerA. The fluorescent signal of MerB was measured before and after the addition of 1 equivalent of either DEL or DET, and a significant decrease in fluorescent intensity was observed indicating that the both metals are bound in the active site of MerB in a similar manner as Hg^{II}, as expected (**Figure 5**). Following the addition of an excess molar equivalent of NMerA to the MerB-Pb^{IV} complex, a significant percentage of the fluorescence intensity of MerB was restored (~55% of the intensity loss following the addition of DEL at 344 nm; **Figure 5A**). In contrast, no significant change in the fluorescence intensity of MerB is observed following the addition of an excess molar equivalent of NMerA to the MerB-Sn^{IV} complex (**Figure 5B**). Taken together, these results suggest that NMerA is able to remove bound Pb^{IV} from the active site of MerB in a similar manner as Hg^{II}, but it is not able to remove the bound Sn^{IV}.

DISCUSSION

MerB is one of two key enzymes involved in bacterial resistance to mercury due to its unique ability to cleave the carbon-Hg bond of a wide range of organomercurial compounds including the natural environmental toxin $MeHg^{+}$[5]. Based on previous studies, several mechanisms for carbon-Hg bond cleavage have been proposed involving three highly conserved residues present in the active of MerB (C96, D99 and C159 in *E.coli* MerB)[19, 20]. However, the exact mechanism by which these three residues orchestrate catalysis has still not been clearly defined. In an attempt to more precisely define the roles

of C96, D99 and C159 in carbon-Hg bond cleavage, we have structurally and biophysically characterized the interaction of MerB with organotin and organolead compound. These compounds were chosen because they are chemically similar to organomercurials, they are known environmental toxins and organotin compounds have been shown to be both substrates and inhibitors of MerB[38]. Structural studies with DMT and TET, two previously identified organotin inhibitors of MerB, clearly demonstrate that they bind to Asp99 in the active site. In the case of DMT, binding to C96 is also observed, but only after longer (1h) soaking times of MerB crystals. Surprisingly, neither compound binds to C159 and TET does not bind to C96 even with longer soaking times (up to 6h). In contrast, DET is cleaved by MerB and the resulting Sn^{IV} product binds to C96, D99 and C159 in a similar manner as the Hg^{II} product following cleavage of organomercurial compounds. Interestingly, structural studies with organolead compounds yielded very similar results as observed with the organotin compounds. Like TMT, TML binds only to D99, whereas the carbon-Pb bonds of DEL are cleaved and the Pb^{IV} product bind to C96, D99 and C159 much like Sn^{IV} following cleavage of the carbon-Sn bonds of DET. In agreement with the structural studies, ITC studies demonstrate that DMT, DET and DEL all bind to MerB. Importantly, their association constants are significantly higher than what is observed between MeHg and MerB. In contrast, no binding is observed with TET and TML under the experimental conditions, suggesting that their binding to MerB only occurs at higher concentrations like those used in the soaking of crystals. In addition, we show that NMerA is able to remove the Pb^{IV} product from the active site of MerB following cleavage of DEL, but it is not able to remove the Sn^{IV} product following cleavage of DET.

These results clearly demonstrate that the initial binding of organotin and organolead compounds to MerB occurs at D99 followed by subsequent binding to C96 and finally to C159. These observations are surprising given all previously proposed models for the mechanism of carbon-Hg bond cleavage by MerB postulated that the sulfhydryl group of either C96 or C159 initiates the catalytic process, and the mechanistic debate has centered around which cysteine residue binds first. The residues corresponding to C96, D99 and C159 in *E. coli* MerB are conserved in all MerB proteins expressed from a wide range of bacterial strains except in four cases[20]. In these four cases, the bacterial strains express two distinct MerB proteins from their *mer* operon. The first MerB proteins (referred to as MerB1) expressed in these strains contain the three key catalytic residues corresponding to C96, D99 and C159 in *E. coli* MerB, but the second proteins (referred to as MerB2) expressed in these strains contain a serine residue in the position of the aspartic acid residue (D99) in addition to the two cysteine residues. The four MerB2 proteins containing the active site serine residue share 100% sequence identity with each other. Interestingly, the serine containing MerB2 protein from *Bacillus megaterium* is considerably less efficient at cleaving carbon-Hg bonds when compared to its MerB protein with the aspartic acid residue in the active site[49-51]. In addition, substituting serine in place of D99 in *E. coli* MerB results in a mutant protein that binds Cu^{II} when expressed in bacteria and has significantly lower catalytic activity[52]. Taken together our current results with the organotin and organolead compounds, this suggests that initial binding to D99 is crucial not only for the catalytic activity of MerB, but also for organometal selectivity.

The observation that organolead compounds serve as substrates and possibly as inhibitors for MerB depending on the number and type of substituents attached to the metal

is similar to what has been previously reported with organotin compounds[38]. TML appears to function as a weak inhibitor of MerB in a similar manner as reported for TET, since we observe that both compounds bind only to D99 in the active site in our structural studies. This mechanism of inhibition through binding to D99 appears to be different than what is observed with the irreversible inhibitor DMT. DMT initially binds to D99, but following longer soaking times, it also binds to C96. This results in a displacement of C159 away from the tin atom and this displacement triggers the loss of an important cation-π interaction between W95 and R155 in the active site. The more potent irreversible inhibition with DMT is also consistent with our ITC studies showing that DMT associates with MerB more tightly than even MeHg. The fact that both DET and DEL function as substrates suggests that these compounds have a more optimal substitution pattern in terms of number of alkyl groups as well as length of the alkyl group. In both cases, the metal ion products (Pb^{IV} or Sn^{IV}) remain in the active site of MerB bound to C96, D99 and C159 following cleavage of the carbon-metal bond in a similar fashion as Hg^{II} following cleavage of carbon-Hg bonds. Attempts to do a more thorough examination with additional organotin and organolead compounds was limited by several factors including commercial availability, low aqueous solubility of longer alky side chain (For example: dipropyl and dibutyl substituted compounds) and the destruction of crystals following even short soaks with certain organometals. However, it is clear that the number of substitutions and type of substitution attached to the metal dramatically alters the ability of MerB to bind to and cleave both organotin and organolead compounds.

Given that select organotin and organolead compounds are cleaved by MerB, this suggests that MerB has the capacity to degrade these compounds either naturally in

bacterial strains containing the *mer* operon or when MerB is employed as part of a bioremediation system. In order to efficiently degrade these compounds, bacteria must also remove the resulting metal ion product from the active site of MerB following cleavage of the carbon-metal bond. Our results indicate that NMerA has the capacity to remove Pb^{IV} in an efficient manner from MerB, but not Sn^{IV}. Despite these results, it is not known if MerA would have the capacity to reduce the Pb^{IV} once it is transferred from MerB. In addition, it is not clear if reducing the Pb^{IV} would be helpful to bacterial survival. Reducing Hg^{II} to Hg^{0} leads to a compound that is less reactive, more volatile and readily expired from the bacteria. In the case of Pb^{IV}, the initial reduction would produce Pb^{II}, which is still highly toxic. So, it might be important to reduce it further to Pb^{0}. However, Pb^{0} is not a volatile liquid like Hg^{0} and it would probably be more efficient for the bacteria to transport the Pb^{II} directly out of the cell using a metal ion transporter. In addition, organotin and organolead compounds could competitively inhibit degradation of organomercurial compounds by MerB if they are jointly present as contaminants especially since DET and DEL have higher association constants than MeHg. Taken together, these results suggest that MerB may have a potential role in the degradation of both organotin and organolead compounds. However, it will be important in future studies attempting to use the *mer* system for the bioremediation of any organometal compounds to consider the presence of other organometals present in the site to be remediated.

Table 1. Data collection and refinement statistics for organotin compounds

Data set	**MerB –DMT 10 min**	**MerB -DMT 1 hour**	**MerB - DET 1 hour**	**MerB-TET 1 hour**
PDB code	**XXXX**	**XXXX**	**XXXX**	**XXXX**
Data Collection				
Beamline	08ID-1, CLS	X25, NSLS-I	08-ID, CLS	08-ID, CLS
Wavelength (Å)	0.9795 Å	1.100 Å	0.9724 Å	0.9724 Å
Space group	$P2_1$	$P2_1$	$P2_1$	$P2_1$
Unit-cell parameter (Å)	a=38.58, b=89.23, c=54.68	a=38.05, b=88.64, c=51.49	a=37,86, b=88.80, c=55.01	a=38.57, b=88.93, c=54.57
	α=90, β=98.48, γ=90	α=90, β=100.34, γ=90	α=90, β=97.19, γ=90	α=90, β=98.27, γ=90
Resolution (Å)	50.00-1.60 (1.66-1.60)	50.00-1.53 (1.58-1.53)	50 – 2.00 (2.07-2.00)	50.00-1.85 (1.91-1.85)
Total reflections	110133	128916	60797	78057
No. of unique reflections	45930	43607	22423	30235
Multiplicity	2.4	3.0	2.7	2.6
Completeness (%)	95.94 (94.83)	86.48 (31.30)	92.00 (60.00)	97.00 (96.00)
R_{merge}	0.043 (0.45)	0.038 (0.47)	0.053 (0.38)	0.14 (0.76)
I/σ(I)	13.26 (2.50)	16.45 (1.61)	12.07 (2.25)	8.51 (1.57)
Refinement Statistics				
Resolution (Å)	50.00-1.60	50.00-1.53	50.00-2.00	50.00-1.85
R_{work}/R_{free} (%)	17.27/20.38	17.48/21.11	16.58/22.25	19.26/24.08
Number of atoms (excluding hydrogens)				
Protein	3190	3178	3181	3188
Water	455	276	151	389
Ligands	11	8	11	23
B-factors (Å^2)				
Protein	25.80	27.90	42.70	24.79
Water	37.60	33.90	41.30	32.67
Ligands	24.70	21.10	25.70	20.48
Metal Occupancy	0.88/0.83	0.88/0.91	0.83/0.91	1.00/1.00
RMSDs				
Bond lengths (Å)	0.011	0.011	0.013	0.011
Bond angles (°)	1.29	1.35	1.38	1.17
Ramachandran[b]				
Favored (%)	97	95	95	97
Outliers (%)	0.48	1.5	0	0

Values in parentheses are for highest-resolution shell. $R_{sym} = \sum hkl \sum i |I_{hkl,i} - \langle Ihkl \rangle| / \sum_{hkl,i} \langle Ihkl \rangle$, where $I_{hkl,i}$ is the intensity of an individual measurement of the reflection with Miller indices *hkl* and I_{hkl} is the mean intensity of that reflection. $R_{work} = \sum hkl \langle F_o| - |F_c \rangle / \sum hkl |F_o|$, where $|F_o|$ is the observed structure-factor amplitude and $|F_c|$ is the calculated structure-factor amplitude. R_{free} is the R factor based on at least 500 test reflections that were excluded from the refinement.

[a] Reflections with $F_o > 0$. [b] MolProbity analysis.

Table 2. Data collection and refinement statistics for TML and DEL

Data set	**MerB -TML 10 min**	**MerB - DEL 10 min**
PDB code	**XXXX**	**XXXX**
Data Collection		
Beamline	X25, NSLS-I	08-ID, CLS
Wavelength (Å)	1.100 Å	0.9724 Å
Space group	$P2_1$	$P2_1$
Unit-cell parameter (Å)	a=38.46, b=88.78, c=54.73	a=38,06, b=88.67, c=54.83
	α=90, β=97.87, γ=90	α=90, β=98.30, γ=90
Resolution (Å)	50.00-1.80 (1.86-1.80)	50 – 1.75 (2.81-1.75)
Total reflections	113549	115869
No. of unique reflections	33653	35220
Multiplicity	3.4	3.3
Completeness (%)	99.77 (99.53)	97.00 (83.00)
R_{merge}	0.052 (0.81)	0.063 (0.67)
I/σ(I)	13.57 (1.62)	12.30 (1.91)
Refinement Statistics		
Resolution (Å)	50.00-1.80	50.00-1.75
R_{work}/R_{free} (%)	17.81/21.91	17.88/20.85
Number of atoms (excluding hydrogens)		
Protein	3190	3200
Water	252	298
Ligands	16	11
B-factors (Å^2)		
Protein	37.30	31.81
Water	41.50	40.60
Ligands	45.80	22.74
Metal Occupancy	0.68/0.68	0.93/0.94
Subunit A/B		
RMSDs		
Bond lengths (Å)	0.011	0.010
Bond angles (°)	1.35	1.05
Ramachandran[b]		
Favored (%)	95	96
Outliers (%)	1.5	0.24

Values in parentheses are for highest-resolution shell. $R_{sym} = \sum hkl \sum i |I_{hkl,i} - \langle Ihkl \rangle| / \sum_{hkl,i} \langle Ihkl \rangle$, where $I_{hkl,i}$ is the intensity of an individual measurement of the reflection with Miller indices *hkl* and I_{hkl} is the mean intensity of that reflection. $R_{work} = \sum hkl \langle |F_o| - |F_c| \rangle / \sum hkl |F_o|$, where $|F_o|$ is the observed structure-factor amplitude and $|F_c|$ is the calculated structure-factor amplitude. R_{free} is the R factor based on at least 500 test reflections that were excluded from the refinement. [a] Reflections with $F_o > 0$. [b] MolProbity analysis.

Table 3: Association constant for the binding of MeHg, DEL, DMT and DET to MerB

MerB-organometal complex	K_a
MerB-MeHg	$7 \pm 4 \times 10^{16}$
MerB-DET	$2 \pm 1 \times 10^{20}$
MerB-DEL	1×10^{20}
MerB-DMT	1×10^{19}
MerB-TML	n.d*

*No heat detected

REFERENCES

[1] Miller, S. M. (1999) Bacterial detoxification of Hg(II) and organomercurials, *Essays Biochem. 34*, 17-30.

[2] Jackson, W. J., and Summers, A. O. (1982) Biochemical characterization of $HgCl_2$-inducible polypeptides encoded by the mer operon of plasmid R100, *J. Bacteriol. 151*, 962-970.

[3] Schottel, J., Mandal, A., Clark, D., Silver, S., and Hedges, R. W. (1974) Volatilisation of mercury and organomercurials determined by inducible R-factor systems in enteric bacteria, *Nature 251*, 335-337.

[4] Schottel, J. L. (1978) The mercuric and organomercurial detoxifying enzymes from a plasmid-bearing strain of Escherichia coli, *J. Biol. Chem. 253*, 4341-4349.

[5] Barkay, T., Miller, S. M., and Summers, A. O. (2003) Bacterial mercury resistance from atoms to ecosystems, *FEMS Microbiol. Rev. 27*, 355-384.

[6] Huang, C. C., Narita, M., Yamagata, T., and Endo, G. (1999) Identification of three merB genes and characterization of a broad-spectrum mercury resistance module encoded by a class II transposon of Bacillus megaterium strain MB1, *Gene 239*, 361-366.

[7] Begley, T. P., Walts, A. E., and Walsh, C. T. (1986) Bacterial organomercurial lyase: overproduction, isolation, and characterization, *Biochemistry 25*, 7186-7192.

[8] Begley, T. P., Walts, A. E., and Walsh, C. T. (1986) Mechanistic studies of a protonolytic organomercurial cleaving enzyme: bacterial organomercurial lyase, *Biochemistry 25*, 7192-7200.

[9] Fox, B., and Walsh, C. T. (1982) Mercuric reductase. Purification and characterization of a transposon-encoded flavoprotein containing an oxidation-reduction-active disulfide, *J. Biol. Chem. 257*, 2498-2503.

[10] Fox, B. S., and Walsh, C. T. (1983) Mercuric reductase: homology to glutathione reductase and lipoamide dehydrogenase. Iodoacetamide alkylation and sequence of the active site peptide, *Biochemistry 22*, 4082-4088.

[11] Omichinski, J. G. (2007) Biochemistry. Toward methylmercury bioremediation, *Science 317*, 205-206.

[12] Benison, G. C., Di Lello, P., Shokes, J. E., Cosper, N. J., Scott, R. A., Legault, P., and Omichinski, J. G. (2004) A stable mercury-containing complex of the organomercurial lyase MerB: Catalysis, product release, and direct transfer to MerA, *Biochemistry 43*, 8333-8345.

[13] Hong, B. Y., Nauss, R., Harwood, I. M., and Miller, S. M. (2010) Direct Measurement of Mercury(II) Removal from Organomercurial Lyase (MerB) by Tryptophan Fluorescence: NmerA Domain of Coevolved gamma-Proteobacterial Mercuric Ion Reductase (MerA) Is More Efficient Than MerA Catalytic Core or Glutathione, *Biochemistry 49*, 8187-8196.

[14] Hamlett, N. V., Landale, E. C., Davis, B. H., and Summers, A. O. (1992) Roles of the Tn21 merT, merP, and merC gene products in mercury resistance and mercury binding, *J. Bacteriol. 174*, 6377-6385.

[15] Morby, A. P., Hobman, J. L., and Brown, N. L. (1995) The role of cysteine residues in the transport of mercuric ions by the Tn501 MerT and MerP mercury-resistance proteins, *Mol. Microbiol. 17*, 25-35.

[16] Schue, M., Glendinning, K. J., Hobman, J. L., and Brown, N. L. (2008) Evidence for direct interactions between the mercuric ion transporter (MerT) and mercuric reductase (MerA) from the Tn501 mer operon, *Biometals 21*, 107-116.

[17] Johs, A., Harwood, I. M., Parks, J. M., Nauss, R. E., Smith, J. C., Liang, L., and Miller, S. M. (2011) Structural characterization of intramolecular Hg(2+) transfer between flexibly linked domains of mercuric ion reductase, *J. Mol. Biol. 413*, 639-656.

[18] Hong, L., Sharp, M. A., Poblete, S., Biehl, R., Zamponi, M., Szekely, N., Appavou, M. S., Winkler, R. G., Nauss, R. E., Johs, A., Parks, J. M., Yi, Z., Cheng, X., Liang, L., Ohl, M., Miller, S. M., Richter, D., Gompper, G., and Smith, J. C. (2014) Structure and dynamics of a compact state of a multidomain protein, the mercuric ion reductase, *Biophys. J. 107*, 393-400.

[19] Lafrance-Vanasse, J., Lefebvre, M., Di Lello, P., Sygusch, J., and Omichinski, J. G. (2009) Crystal structures of the organomercurial lyase merB in its free and mercury-bound forms. Insights into the mechanism of methylmercury degradation, *J. Biol. Chem. 284*, 938-944.

[20] Lello, P. D., Lafrance-Vanasse, J., and Omichinski, J. G. (2006) The Organomercurial Lyase MerB, In *Handbook of Metalloproteins*, John Wiley & Sons, Ltd.

[21] Bizily, S. P., Rugh, C. L., Summers, A. O., and Meagher, R. B. (1999) Phytoremediation of methylmercury pollution: merB expression in Arabidopsis thaliana confers resistance to organomercurials, *Proc. Natl. Acad. Sci. U. S. A. 96*, 6808-6813.

[22] Bizily, S. P., Rugh, C. L., and Meagher, R. B. (2000) Phytodetoxification of hazardous organomercurials by genetically engineered plants, *Nat. Biotechnol. 18*, 213-217.

[23] Rugh, C. L., Wilde, H. D., Stack, N. M., Thompson, D. M., Summers, A. O., and Meagher, R. B. (1996) Mercuric ion reduction and resistance in transgenic Arabidopsis thaliana plants expressing a modified bacterial merA gene, *Proc. Natl. Acad. Sci. U. S. A. 93*, 3182-3187.

[24] Sigel, A., Sigel, H., and Sigel, R. O. (2010) Organometallics in environment and toxicology, PP 1-23 , The Royal Society of Chemistry, Cambridge.

[25] Dubalska, K., Rutkowska, M., Bajger-Nowak, G., Konieczka, P., and Namieśnik, J. (2013) Organotin Compounds: Environmental Fate and Analytics, *Critical Reviews in Analytical Chemistry 43*, 35-54.

[26] Graceli, J. B., Sena, G. C., Lopes, P. F. I., Zamprogno, G. C., da Costa, M. B., Godoi, A. F. L., dos Santos, D. M., de Marchi, M. R. R., and dos Santos Fernandez, M. A. (2013) Organotins: A review of their reproductive toxicity, biochemistry, and environmental fate, *Reprod. Toxicol. 36*, 40-52.

[27] Sousa, A. C. A., Pastorinho, M. R., Takahashi, S., and Tanabe, S. (2013) History on organotin compounds, from snails to humans, *Environ. Chem. Lett. 12*, 117-137.

[28] Lobinski, R., Boutron, C. F., Candelone, J. P., Hong, S., Szpunar-Lobinska, J., and Adams, F. C. (1994) Present century snow core record of organolead pollution in greenland, *Environ. Sci. Technol. 28*, 1467-1471.

[29] Mason, R. P., and Benoit, J. M. (2003) Organomercury Compounds in the Environment, In *Organometallic Compounds in the Environment*, pp 57-99, John Wiley & Sons, Ltd.

[30] Olushola Sunday, A., Abdullahi Alafara, B., and Godwin Oladele, O. (2012) Toxicity and speciation analysis of organotin compounds, *Chemical Speciation & Bioavailability 24*, 216-226.

[31] Jarvie, A. W. P., Markall, R. N., and Potter, H. R. (1981) Decomposition of organolead compounds in aqueous systems, *Environ. Res. 25*, 241-249.

[32] Ou, L.-T., Thomas, J. E., and Jing, W. (1994) Biological and chemical degradation of tetraethyl lead in soil, *Bull. Environ. Contam. Toxicol. 52*, 238-245.

[33] Mitchell, C. S., Shear, M. S., Bolla, K. I., and Schwartz, B. S. (1996) Clinical evaluation of 58 organolead manufacturing workers, *J. Occup. Environ. Med. 38*, 372-378.

[34] Walsh, T. J., and Tilson, H. A. (1984) Neurobehavioral toxicology of the organoleads, *Neurotoxicology 5*, 67-86.

[35] Nesci, S., Ventrella, V., Trombetti, F., Pirini, M., and Pagliarani, A. (2011) Tributyltin (TBT) and mitochondrial respiration in mussel digestive gland, *Toxicol. In Vitro 25*, 951-959.

[36] Ou, L. T., Jing, W., and Thomas, J. E. (1995) Biological and chemical degradation of ionic ethyllead compounds in soil, *Environ. Toxicol. Chem. 14*, 545-551.

[37] Cruz, A., Oliveira, V., Baptista, I., Almeida, A., Cunha, A., Suzuki, S., and Mendo, S. (2012) Effect of tributyltin (TBT) in the metabolic activity of TBT-resistant and sensitive estuarine bacteria, *Environ. Toxicol. 27*, 11-17.

[38] Walts, A. E., and Walsh, C. T. (1988) Bacterial organomercurial lyase: novel enzymic protonolysis of organostannanes, *J. Am. Chem. Soc. 110*, 1950-1953.

[39] Di Lello, P., Benison, G. C., Valafar, H., Pitts, K. E., Summers, A. O., Legault, P., and Omichinski, J. G. (2004) NMR structural studies reveal a novel protein fold for MerB, the organomercurial lyase involved in the bacterial mercury resistance system, *Biochemistry 43*, 8322-8332.

[40] McCoy, A. J., Grosse-Kunstleve, R. W., Adams, P. D., Winn, M. D., Storoni, L. C., and Read, R. J. (2007) Phaser crystallographic software, *J Appl Crystallogr 40*, 658-674.

[41] Emsley, P., and Cowtan, K. (2004) Coot: model-building tools for molecular graphics, *Acta Crystallogr. D Biol. Crystallogr. 60*, 2126-2132.

[42] Adams, P. D., Afonine, P. V., Bunkoczi, G., Chen, V. B., Davis, I. W., Echols, N., Headd, J. J., Hung, L. W., Kapral, G. J., Grosse-Kunstleve, R. W., McCoy, A. J., Moriarty, N. W., Oeffner, R., Read, R. J., Richardson, D. C., Richardson, J. S., Terwilliger, T. C., and Zwart, P. H. (2010) PHENIX: a comprehensive Python-based system for macromolecular structure solution, *Acta Crystallogr. D Biol. Crystallogr. 66*, 213-221.

[43] Chen, V. B., Arendall, W. B., 3rd, Headd, J. J., Keedy, D. A., Immormino, R. M., Kapral, G. J., Murray, L. W., Richardson, J. S., and Richardson, D. C. (2010) MolProbity: all-atom structure validation for macromolecular crystallography, *Acta Crystallogr. D Biol. Crystallogr. 66*, 12-21.

[44] Eisler, R. (1988) Lead Hazards to Fish, Wildlife, and Invertebrates: A Synoptic Review, In *Contaminant Hazard Reviews*, Laurel, MD.

[45] Jarvie, A. W. P. (1988) Organoleads in the environment: A review, *Sci. Total Environ. 73*, 121-126.

[46] Qian, H., Sahlman, L., Eriksson, P. O., Hambraeus, C., Edlund, U., and Sethson, I. (1998) NMR solution structure of the oxidized form of MerP, a mercuric ion binding protein involved in bacterial mercuric ion resistance, *Biochemistry 37*, 9316-9322.

[47] Steele, R. A., and Opella, S. J. (1997) Structures of the reduced and mercury-bound forms of MerP, the periplasmic protein from the bacterial mercury detoxification system, *Biochemistry 36*, 6885-6895.

[48] Brown, N. L., Shih, Y. C., Leang, C., Glendinning, K. J., Hobman, J. L., and Wilson, J. R. (2002) Mercury transport and resistance, *Biochem. Soc. Trans. 30*, 715-718.

[49] Chien, M. F., Narita, M., Lin, K. H., Matsui, K., Huang, C. C., and Endo, G. (2010) Organomercurials removal by heterogeneous merB genes harboring bacterial strains, *Journal of bioscience and bioengineering 110*, 94-98.

[50] Gupta, A., Phung, L. T., Chakravarty, L., and Silver, S. (1999) Mercury resistance in Bacillus cereus RC607: Transcriptional organization and two new open reading frames, *J. Bacteriol. 181*, 7080-7086.

[51] Wang, Y., Moore, M., Levinson, H. S., Silver, S., Walsh, C., and Mahler, I. (1989) Nucleotide-sequence of a chromosomal mercury resistance determinant from a bacillus sp with broad-spectrum mercury resistance, *J. Bacteriol. 171*, 83-92.

[52] Wahba, H. M., Lecoq, L., Stevenson, M., Mansour, A., Cappadocia, L., Lafrance-Vanasse, J., Wilkinson, K. J., Sygusch, J., Wilcox, D. E., and Omichinski, J. G. (2016) Structural and Biochemical Characterization of a Copper-Binding Mutant of the Organomercurial Lyase MerB: Insight into the Key Role of the Active Site Aspartic Acid in Hg–Carbon Bond Cleavage and Metal Binding Specificity, *Biochemistry 55*, 1070-1081.

FIGURES:

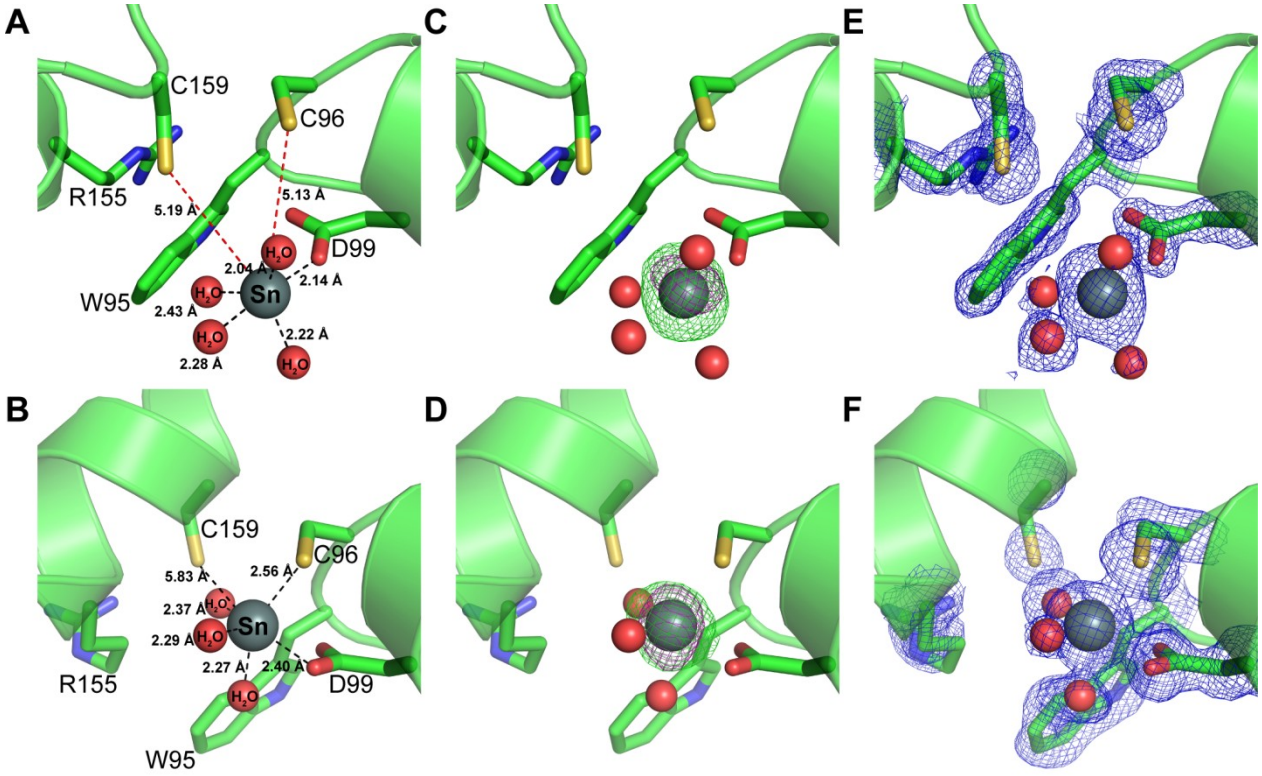

Figure 1. Comparison of the active site of the MerB-DMT complex (subunit A) after 10 min and 1 h. **A)** Metrics of the MerB-DMT complex after 10 min soaking in DMT. The Sn atom (gray sphere) is bound to an oxygen of D99 (2.14 Å) and the oxygen atoms of four bound water (red sphere) molecules (2.04, 2.43, 2.28, 2.22 Å). The Sn atom is more distant to the sulfur atoms of C96 (5.13 Å) and C159 (5.19 Å). An important cation-π interaction between W95 and R155 in the active site is also highlighted. **B)** Metrics of the MerB-DMT complex after 1 h soaking in DMT. The Sn atom (gray sphere) is bound to the sulfur of C96 (2.56 Å), an oxygen of D99 (2.40 Å) and the oxygen atoms of three bound water (red sphere) molecules (2.37, 2.29, 2.27 Å). Following the longer soak in DMT, the cation-π

interaction between W95 and R155 is no longer present. **C**-**D**) Close ups of the Fo-Fc simulated annealing omit map contoured at 3σ displaying the positive density for the Sn atom (green mesh) and anomalous difference map showing the anomalous peak for the Sn atom (pink mesh) in the MerB-DMT complex after either a 10 min soak **(C)** or a 1 h soak **(D)** in DMT. The occupancies of the Sn atoms were set to zero prior to calculating the Fo-Fc simulated annealing omit map. **E-F**) Close ups of the Fo-Fc simulated annealing omit map contoured at 2.5σ (blue mesh) for the active site residues of the MerB-DMT complex after either a 10 min soak **(E)** or 1 hour soak (**F**) in DMT. The occupancies of C96, S99 and C159 as well as that of the Sn atom and bound water molecules were set to zero prior to calculating the Fo-Fc simulated annealing omit map. Phenix map was used to generate the omit map calculation. The backbone of MerB is displayed in ribbon form (green) and the side chains of the three active site residues are displayed in stick form with the sulfur atoms (yellow) of C96 and C159 and the oxygen atoms (red) of D99.

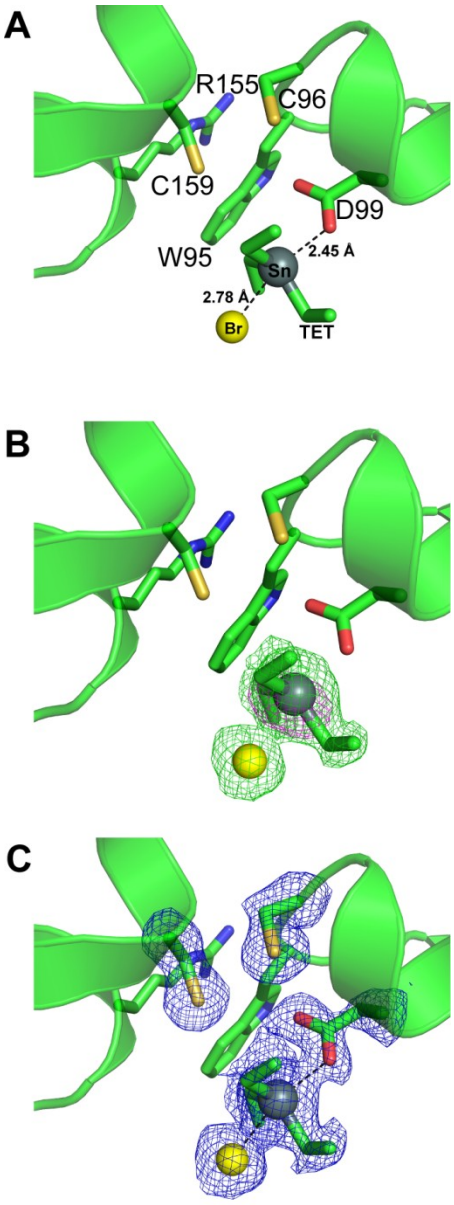

Figure 2. Binding of TET to the active site of the MerB (subunit A) after 1 h. **A)** Metrics of the MerB-DMT complex after 1h soaking in TET, the tin atom (gray sphere) is bound to an oxygen of D99 (2.45 Å) and a bromine atom (2.78 Å; yellow sphere). In this complex, the cation-π interaction is present between W95 and R155. **B)** A close-up of the Fo-Fc simulated annealing omit map displaying the positive density for the TET atom

(green mesh) and anomalous difference map showing the anomalous peak for the Sn atom (pink mesh) in the MerB-TET complex. The two maps are contoured at 3σ. The occupancy of TET was set to zero prior to calculating the Fo-Fc simulated annealing omit map. **C)** Close up of the Fo-Fc simulated annealing omit map (blue mesh; contoured at 2.5σ) of the active site residues of the MerB-TET complex. The occupancies of C96, S99, C159 and the TET molecule were set to zero prior to calculating the Fo-Fc simulated annealing omit map. The Phenix map was used to generate the omit map calculation. The backbone of MerB is displayed in ribbon form (green) and the side chains of the three active site residues are displayed in stick form with the sulfur atoms (yellow) of C96 and C159 and the oxygen atoms (red) of D99.

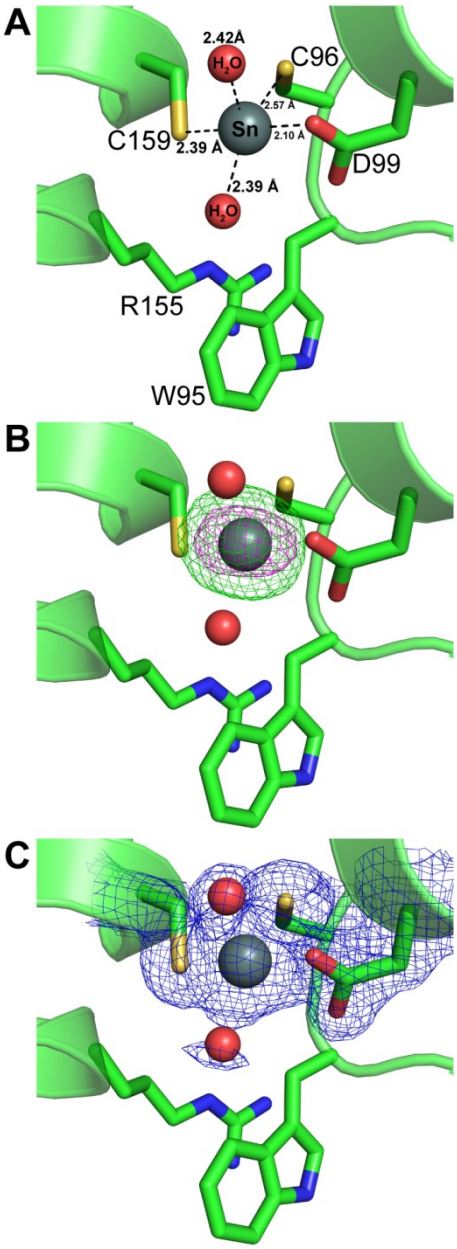

Figure 3. Binding of DET to the active site of the MerB (subunit A) after 1 h. **A)** Metrics of the MerB-DET complex after 1h soaking in TET, the tin atom (gray sphere) is bound to an oxygen of D99 (2.44 Å) and to the sulfur atoms of C96 (2.69 Å) and C159 (2.41 Å). In addition, the cation-π interaction between W95 and R155 is shown. **B)** A close-up of the Fo-Fc simulated annealing omit map displaying the positive density for the Sn^{IV}

atom (green mesh) and the anomalous difference map showing the anomalous peak for the Sn atom (pink mesh) in MerB-TET complex. The two maps are contoured at 3σ. The occupancies of Sn^{IV} was set to zero prior to calculating the Fo-Fc simulated annealing omit map. **C)** Close up of the Fo-Fc simulated annealing omit map (blue mesh; contoured at 2.5σ) of the active site residues of the MerB-DET complex. The occupancies of C96, S99, C159 and the Sn^{IV} and water molecule were set to zero prior to calculating the Fo-Fc simulated annealing omit map. The Phenix map was used to generate the omit map calculation. The backbone of MerB is displayed in ribbon form (green) and the side chains of the three active site residues are displayed in stick form with the sulfur atoms (yellow) of C96 and C159 and the oxygen atoms (red) of D99.

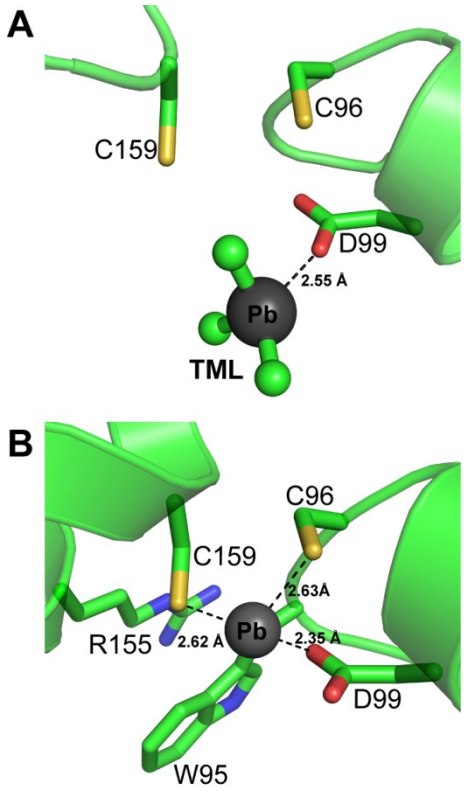

Figure 4. Binding of TML and DEL to the active site of the MerB. **A)** Metrics of the MerB-TML complex (subunit B) after 10 min soaking in TML, the Pb atom (gray sphere) is bound to an oxygen of D99 (2.55 Å). **B)** Metrics of the MerB-DEL complex (subunit A) after 10 min soaking in DEL, the Pb atom (gray sphere) is bound to an oxygen of D99 (2.35 Å) and to the sulfur atoms of C96 (2.63 Å) and C159 (2.62 Å). The backbone of MerB is displayed in ribbon form (green) and the side chains of the three active site residues are displayed in stick form with the sulfur atoms (yellow) of C96 and C159 and the oxygen atoms (red) of D99.

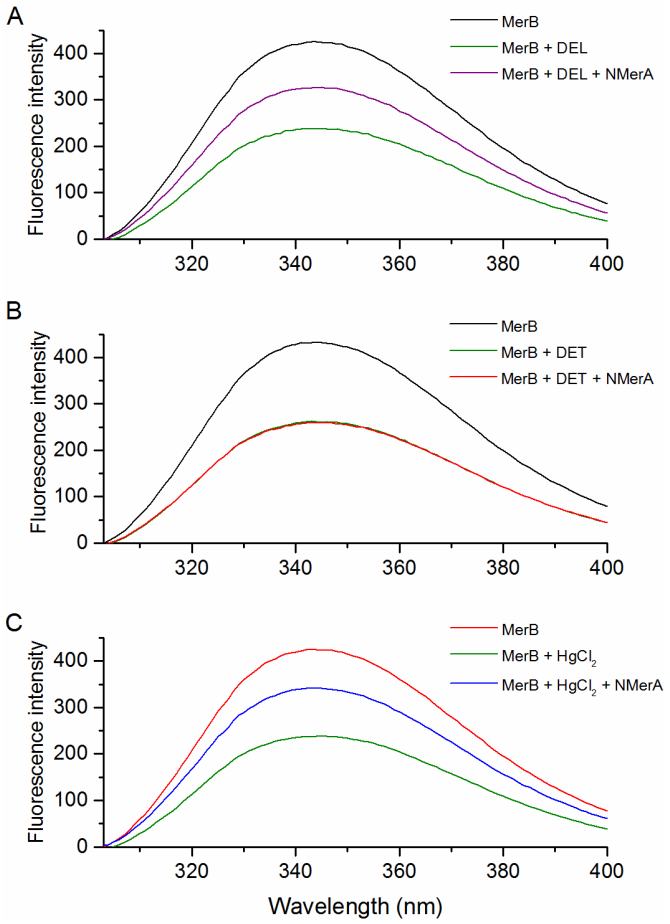

Figure 5. NMerA has the capacity to remove MerB bound lead. **A)** The intrinsic fluorescence curve of MerB (5 mM) before (Black line) and after (green line) the addition of 1 molar equivalent of DEL (green line). Following the addition of DEL, 20 molar equivalents of NMerA (purple line) were added to the MerB-Pb^{IV} complex. **B**) The intrinsic fluorescence curve of MerB (5 mM) before (Black line) and after (green line) the addition of 1 molar equivalent DEL (green line). Following the addition of DEL, 20 molar equivalents of NMerA (purple line) were added to the MerB-Sn^{IV} complex. **C**) The intrinsic fluorescence curve of MerB (5 mM) before (Black line) and after (green line) the addition of 1 molar equivalent of $HgCl_2$ (green line). Following the addition of $HgCl_2$, 20 molar equivalents of NMerA (purple line) were added.

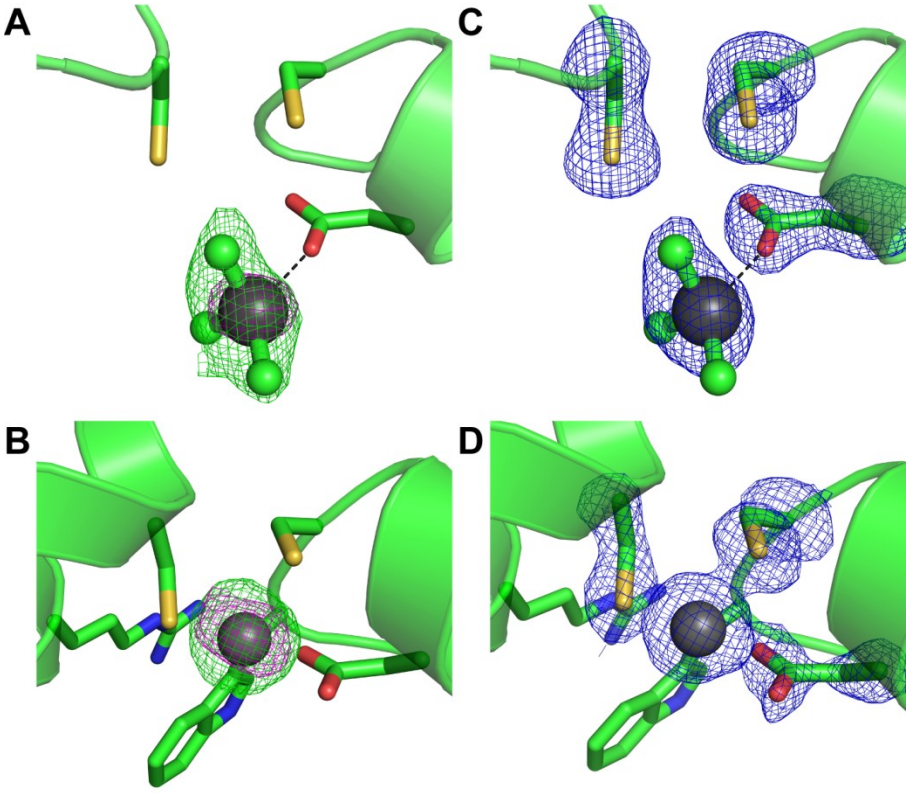

Figure S1. **Binding of TML and DEL to the active site of the MerB**. **A-B)** Close ups of the Fo-Fc simulated annealing omit map displaying the positive density for TML **(A)** and Pb from incubation with DEL **(B)** (green mesh). In addition, the anomalous difference map showing the density for the Pb atom (pink mesh) in MerB-TML complex **(A)** and the MerB-Pb complex following addition of DEL **(B)**. The maps are contoured at 3σ and the occupancies of TML molecules and Pb atom were set to zero prior to calculating the Fo-Fc simulated annealing omit map. **C-D)** Close ups of the Fo-Fc simulated annealing omit maps contoured at 2.5σ (blue mesh) of the active site residues of the MerB-TML complex **(C)** and the MerB-Pb complex after incubation with DEL (**D**). The occupancies of C96, D99, C159 and the Pb atom were set to zero prior to calculating the Fo-Fc simulated annealing omit maps. The Phenix map was used to generate the omit map calculation. The

backbone of MerB is displayed in ribbon form (green) and the side chains of the three active site residues are displayed in stick form with the sulfur atoms (yellow) of C96 and C159 and the oxygen atoms (red) of D99.

Chapter 4: Discussion

The initial mechanism of carbon-Hg bond cleavage by MerB proposed by the Walsh group in the early 1980s (**Figure 9**) suggested that there were two key cysteine residues in the active site essential for the catalytic activity (Walsh *et al.* 1988b). The initial NMR structure of MerB supported this mechanism by demonstrating that C96 and C159 where in close proximity to each other in the active site (Di Lello *et al.* 2004b). The subsequent crystal structure demonstrated that the Hg^{II} product from the cleavage reaction remains bound to C96, D99 and C159 in the active site (Lafrance-Vanasse *et al.* 2009). Based on the crystal structure of the mercury-bound MerB, our group postulated that D99 plays an important role in enhancing the rate of carbon-Hg bond cleavage by functioning as the proton donor. In addition, a catalytic mechanism was proposed, in which the initial binding event occurs at C96 followed by subsequent binding to C159 with D99 functioning as the proton donor (Lello *et al.* 2010). It was postulated that C96 was the initial attacking cysteine residue because C96 and D99 are located in a helical conformation in the crystal structure, where the sulfhydryl group of C96 is in position to be activated by the carboxylate anion of D99 due to their close proximity. Shortly afterwards, the group of Smith performed quantum mechanics calculations using the crystal structure of MerB and proposed two possible mechanisms for carbon-Hg bond cleavage, one initiated by binding to C96 and an alternative mechanism initiated by binding to C159 (**Figure 19 and 20**) (Parks *et al.* 2009). In the mechanism where C159 functions as the initial binding residue, the mechanism proceeds through an intermediate where D99 abstracts the proton from C96. The deprotonated C96 functions as the second thiol binding to $MeHg^{+}$, which results in the formation of an activated carbanion intermediate. In the second mechanism where C96 functions as the initial binding residue, a catalytic water molecule is required. In this case, C159 donates the proton to D99 in a water-assisted fashion and the deprotonated C159 functions as the second thiolate ligand to generate the activated carbanion intermediate (Parks *et al.* 2009). In both mechanisms, the reaction depends on proton transfer from D99 to the carbanion intermediate. In order to perform these calculations, the authors has to assume that the organomercurial substrate already formed the initial reaction with the

thiolate anion of either Cys159 or Cys96. However, the authors failed to explain how C159 would be deprotonated to form the thiolate anion, since at physiological pH it would be expected to be predominantly in its protonated states unless there was a significantly altered pK_a due to folding of the protein. In addition, the authors failed to consider that the carboxylate anion of D99 might initiate the reaction with the organomercurial compounds.

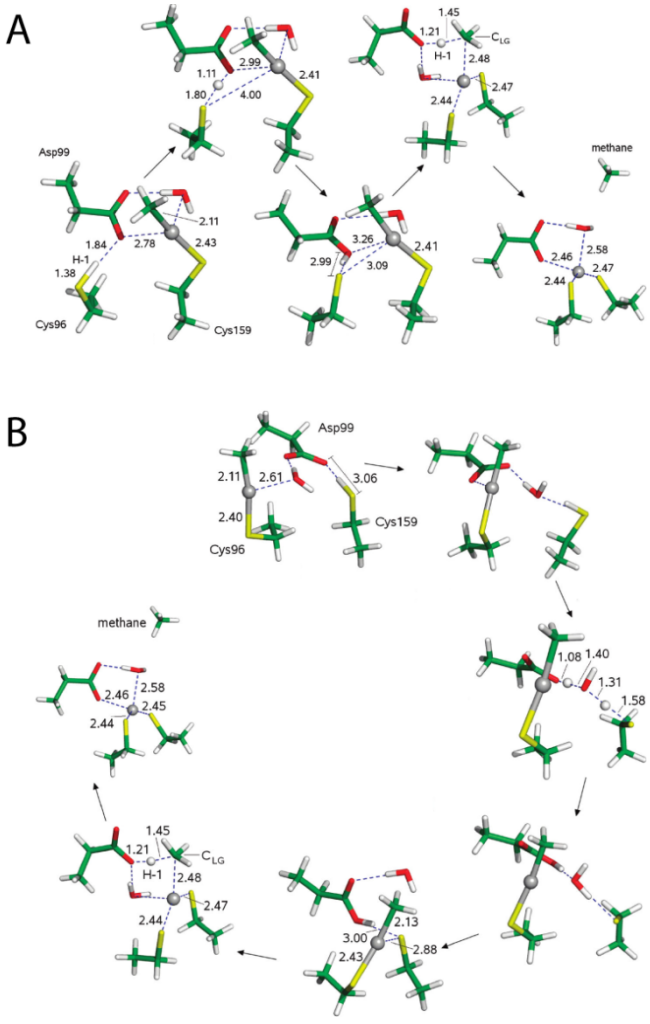

Figure 19: Proposed mechanisms of carbon-Hg bond cleavage based on computational studies. Results from computational studies (A) First mechanism in which the substrate forms the initial covalent adduct with Cys159. (B) Mechanism in which the substrate forms the initial covalent adduct with Cys96. Important distances (Å) are labeled. Colors: Hg, silver; C, green; S, yellow, O, red; H, white. Adapted from (Parks *et al.* 2009)

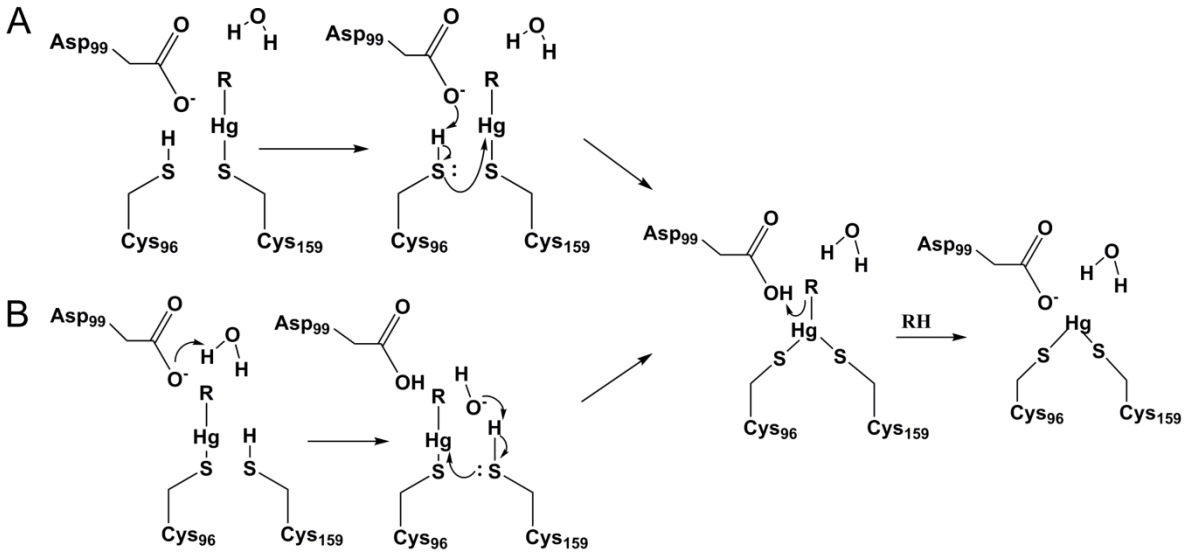

Figure 20: Schematic representation of proposed mechanisms of carbon-Hg bond cleavage by MerB based on computational studies. Schematic representation based on computational studies (A) Mechanism in which the substrate has formed an initial covalent adduct with Cys159. (B) Mechanism in which the substrate has formed an initial covalent adduct with Cys96.

A New Mechanism for Carbon-Hg bond cleavage by MerB

In the first part of my thesis, I determined that the MerB D99S protein co-purifies with a Cu^{II} bound in the active site and based on this finding hypothesized that D99 plays a key role in regulating substrate binding specificity (Wahba *et al.* 2016). In subsequent work, I investigated the interaction of MerB with other organometal compounds and demonstrated that both organolead and organotin compounds initially bind to D99 followed by subsequent binding to C96 prior to cleavage of the carbon-metal bond. These results suggest that the initial binding of substrates to MerB occurs with the carboxylate anion of D99 and this is in contrast with all previously proposed mechanisms for carbon-mercury bond cleavage by MerB involving an initial reaction with a thiolate anion from either C96 or C159. Based on our results, we propose a new mechanism for carbon-metal bond cleavage by MerB that is initiated by binding of organometals to the carboxylate anion of D99 (**Figure 21**). In this mechanism, D99 is predominantly deprotonated given the typical pKa value for the side chain of an aspartic acid (3.80) and the partially positively charged mercuric atom from the organomercurial compound will initially bind to the negatively

charged carboxylate anion of D99. Given its close proximity to D99, there will be a subsequent nucleophilic attack of the organomercurial substrate by the thiol group of C96. We postulate that C96 will have a slightly lower than expected pK_a due to a helix dipole effect (C96 is in the α-helix between residues 95-107 of MerB) and it will be partially or fully deprotonated (**Figure 21**). The nucleophilic attach by C96 will be followed closely by a similar attack from the thiol group of C159. In addition, D99 will be stabilized by acquiring a proton from C159 (C159 must be deprotonated in order to function as the second thiolate ligand). In the transition state, the organomercurial substrate will be coordinated in a triganol geometry and the carbanion intermediate will be stabilized by a proton from D99. This mechanism is consistent with the work of Walsh demonstrating that MerB cleaves carbon-Hg bonds using an S_E2 mechanism because it involves a concerted reaction with release of the hydrocarbon moiety. In support to our mechanism, a dithiol containing peptide has been shown to cleave the alkyl groups of TMT through hydrolytic protonolysis (Buck-Koehntop *et al.* 2006). Our new proposal for the cleavage of carbon-metal bonds by MerB is different from all previous suggested proposals and we are currently pursuing computational calculations to examine carbon-metal bond cleavage based on the initial binding to the carboxylate anion of D99 with Dr. Pedro Silva.

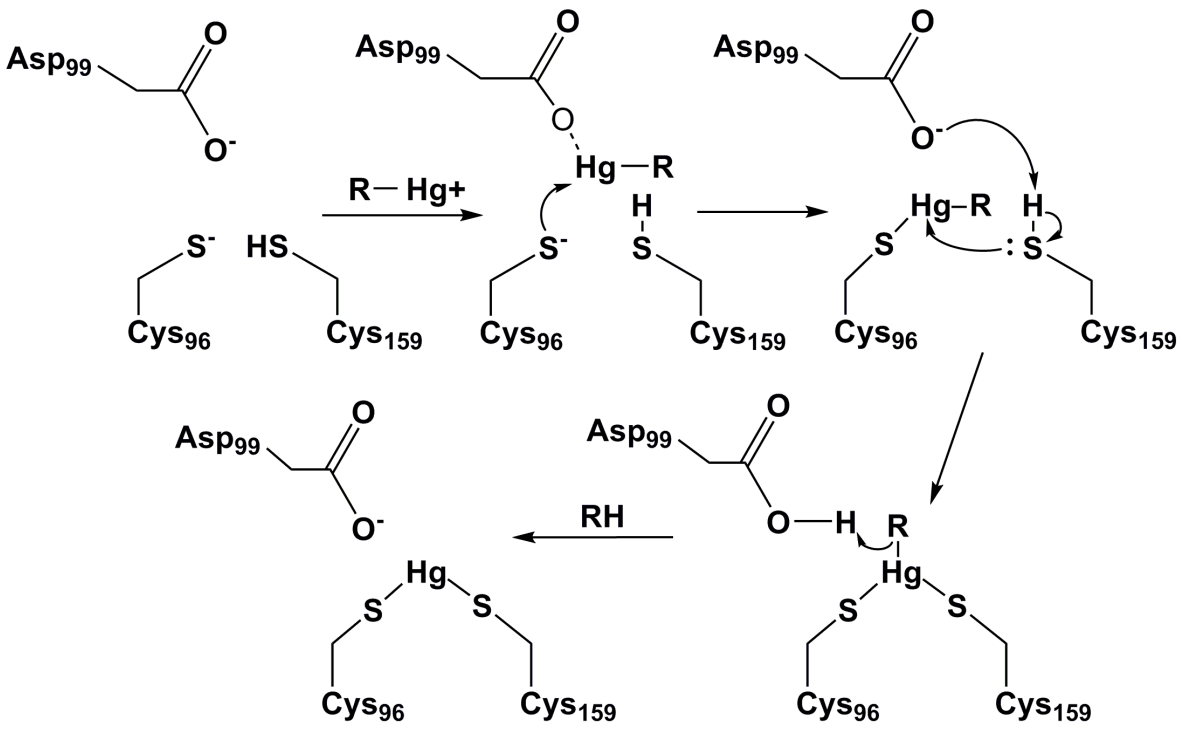

Figure 21: Proposed mechanism of carbon-Hg bond cleavage through initial binding to D99 based on results with organolead and organotin compounds. In this mechanism, the organomercurial cation initially binds to the carboxylate moiety of D99. Next, the thiolate of C96 binds the mercuric atom of the organomercurial compound to form the first Hg-thiol bond and D99 is in position to activate C159 through a proton abstraction. Once deprotonated, the thiolate of C159 forms the second Hg-thiol bond with the organomercurial substrates. In the final step, D99 donates a proton to the carbanion (CH_3-), which results in protonolysis of the carbon-Hg bond and formation of the two products. The carbon moiety product (RH) is released and the Hg^{II} product remains bound in the active site for transfer to MerA.

Two different mechanisms of inhibition by organotin compounds DMT and TET

Although DET and DEL are substrates for MerB, other organotin and organolead compounds were found to function as inhibitors. In our studies, the binding of organotin and organolead compounds to MerB indicate that there might be two different mechanisms for inhibition. Our structural studies show that tri-substituted organometals, like TML and TET, bind only to D99 and there is no indication for either cleavage of the alkyl groups or

binding to C96 or C159. In addition, these compounds bind to MerB with weaker affinity than MeHg. In contrast, DMT binds initially to D99, but also to C96 after longer soaking (1h or more). These results are also consistent with the higher affinity of DMT over TMT on binding to a dithiol containg peptide (Buck-Koehntop *et al.* 2006). Surprisingly, DMT binds with higher affinity to MerB than MeHg, and the binding of DMT to C96 causes a disruption of the cation-π interaction between R155 and W95 in the active site. This also leads to the displacement of C159 further away from the tin atom. Previous studies with organotin compounds determined that TET was a reversible inhibitor of MerB, but that DMT was an irreversible inhibitor. This appears to be consistent with the ITC results and suggests that TML would function as a weak inhibitor like TET. The structural studies also indicate that the conformational change in the active site through loss of the cation-π interaction between R155 and W95 plays an important role in the irreversible inhibition by DMT. Alternatively, the ITC studies indicate that DMT has a higher affinity for MerB than MeHg whereas TET binds with a lower affinity. Thus, the irreversible inhibition by DMT is most likely the result of two factors. First, DMT binds with higher affinity and second it remains bound in the active site in part due to the disruption of the cation- π interaction between W95 and R155.

The role of W95-R155 interaction for catalytic activity of MerB

The MerB-DMT complex indicates that the cation-π interaction between W95 and R155 plays an important role in the catalytic activity. The distance between C96 and C159 varies between 4.2 Å to 6.5 Å with and without the cation-π interaction and it seems that this interaction helps C159 maintain its position near C96 in the active site. From the crystal structures of the MerB complex with the various bound metals, we can see that C96 and W95 are at one side in the active site and C159 and R155 are on the other side. The residues are located within a loop (residues 93-97) and a helix (residues 153-162). The cation- π interaction between W95 and R155 brings the loop containing C96 and the helix containing C159 closer to each other in a position appropriate for cleaving carbon-metal bonds. The disruption of the cation- π interaction allows the helix to move far from the loop and this significantly increases the distance between the two crucial cysteine residues. Thus

our structure explains the possible inhibitory effect of DMT. The importance of the cation-π interaction for catalytic activity is further supported by the fact that W95 is conserved in all known variants of MerB and the R155 is conserved in all but four variants [*Bacillus megaterium* MerB2, *Bacillus subtillis* MerB2, *Bacillus sp*. (RC607) MerB2, *Clostridium butyricum* MerB2]. These four variants are the same four variants that contain the active site serine and the R155 is replaced by an alanine residue. Thus, the decrease in activity associated with these proteins could be due to either the presence of the serine in the active site or the absence of the cation-π interaction.

Possible utilization of mer system components in bioremediation effort of organolead and organotin

Several bacterial detoxification systems that provide microbial resistance to different inorganic ions, like Cd^{II}, Zn^{II} and Pb^{II}, function by using special transport systems to pump the toxic metals out of the cell. The *mer* system functions with a completely different objective where the goal is to bring the toxic mercurial compounds into the cytoplasm to be cleaved and/or reduced to the less toxic Hg^0 which is then expired by the cell due to its volatility. This same approach may also be an optimal mechanism for the detoxification of organolead compounds, like DEL. After the passive diffusion of DEL through the cell membrane due to its lipophilicity, MerB will cleave DEL to Pb^{IV}. Although Pb^{IV} is less toxic than DEL, it would not be ideal to release it inside the cell due to its reactivity. However, we have demonstrated that MerB has the capacity to directly transfer Pb^{IV} to NMerA. Although, it has not been confirmed that NMerA could transport Pb^{IV} to the active site MerA, the transport of Pb^{IV} from MerB to NmerA demonstrates that this is a possible detoxification route. The next question would be whether or not MerA has the capacity to reduce Pb^{IV} to Pb^{II}. Based purely on its reduction potential, Pb^{IV} would be easier to reduce to Pb^{II} than Hg^{II} to Hg^0 (reduction potential 1.65 E° for Pb^{IV} E° in comparision to 0.85 for Hg^{II}) However, the reduction of Pb^{II} to Pb^0 might be more challenging, as the Pb^{II} to Pb^0 reduction potential (-0.13 E°) is low in comparison to Hg^{II} to Hg^0.

The bacterial reduction of Pb^{IV} to the less toxic Pb^{II} (Sigel *et al.* 2010) could represent a distinct advantage for bacterial survival, because select bacteria (*Ralstonia metallidurans*

strain CH34) have a detoxification system for Pb^{II} but not Pb^{IV} (Hynninen *et al.* 2009). This detoxification system is encoded by the *pbrABCD* operon, which confers resistance to Pb^{II} as well to Cd^{II} and Zn^{II} by expressing four proteins (PbrA, PbrB, PbrC and PbrD) that sequester and remove Pb^{II} from the cell. More specifically, PbrA is a P-type ATPase, which pumps Pb^{II} from the cytosol to the periplasmic space. Once in the periplasmic space, PbrB is believed to assist in moving Pb^{II} from the periplasmic compartment to the extracellular environment. Although the function of PbrC is currently unknown, the PbrD protein is responsible for sequestering intercellular Pb^{II} (Hynninen *et al.* 2009). Although no structures have been solved for the proteins from the *pbrABCD* operon, the Pb^{II}-binding sites in all four proteins are predicted to consist of cysteine residues since these proteins all contain a significant number of cysteine residues in their sequences.

The one question that remains to be answered is whether or not MerB and MerA could be combined with proteins from the Pb^{II}-efflux system to remediate organolead compounds. In the case of Hg^{II} reduction by MerA, the resultant product is Hg^0, which can be directly expired from the cell due to its volatility. However, in case of Pb^{IV}, reduction by MerA would generate the reactive Pb^{II} as a product. It is not known whether or not MerA has the capacity to release Pb^{II} to the cytosol. Alternatively, it could directly transfer the product to the intracellular Pb^{II}-binding protein PbrD. It has been noted that biological rather than chemical processes contribute to the degradation of organolead compounds in the environment, but the microorganism(s) responsible for this detoxification has not been identified (Ou *et al.* 1994). Our results showing MerB cleavage of DEL indicate that the bacterial resistance to organolead compounds might be attributed in part to proteins of the *mer* system although this has not been investigated.

Engineering a microbial system to convert DEL to Pb^{II} and its subsequent efflux from the cell could represent a possible bioremediation system for the detoxification of organolead compounds. However, it would be more practical to collect and accumulate the toxic metals as opposed to redistributing them back in environment. This goal could be reached by expansion of an existing phytoremediation system. Select plants have a natural ability to grow and accumulate toxic level of metals, including Pb, Cd and Sn. These plants express high levels of cysteine-rich phytochelatin compounds that function as metals

chelators. After sequestering metals inside plant cells, the phytochelatin-metal complexes are stored safely in vacuoles to protect cellular proteins from the deleterious effect of these reactive metals and these metal-resistant plants accumulate the toxic metals without a further oxidation/reduction process (Rascio & Navari-Izzo 2011). Carbon-metal cleavage and metal-ion reduction are not commonplace in plants, but these functions could be engineered through preparation of transgenic plants containing the genes of interest. MerB and MerA could be encoded in these phytochelatin-expressing plants. This would allow cleavage of DEL and the accumulation of Pb^{II} inside plant cell bound to the phytochelatins. Alternatively, bacteria expressing just PbrD could enhance the capacity of the plant to hyperaccumulate the Pb^{II} product (Borremans *et al.* 2001). Improving phytoremediation system for cleaning up organolead contaminated sites could represent an efficient and ecological approach for removal of toxic compounds from contaminated site.

MerB binds to several other metals such as (Pb(II), Sn(II), Zn(II), Cd(II) As(II), but not (Cu, Ni, Fe, Co).

Given the possibility of utilizing MerB in phytoremediation efforts for cleaning up contaminated sites, it is important to screen the ability of MerB to bind other metals, which are present either naturally or as a common contaminant at a given site. Initially, our results with the organotin and organolead compounds suggest that the active site of MerB has high affinity for metals and in particular transition (Hg) and post transition metals (Pb and Sn). Recently, I have investigated MerB interaction with toxic metals like Pb^{II}, Sn^{II}, Cd^{II}, As^{II} as well as with essential metals like Zn^{II}, Cu^{II}, Ni^{II}, Fe^{II} and Co^{II} (unpublished results). Structural studies indicate MerB has the capacity to bind Pb^{II}, Cd^{II}, As^{II} and each coordinate with the three active site residues in a similar manner as Hg^{II}. On the other hand, Sn^{II} was found to bind D99 and C96 and this induced the disruption of the cation-π interaction between W95 and R155 in a similar manner as seen in the MerB-DMT complex. We have also initiated ITC studies with these various metals and the preliminary results indicate that the affinity for MerB is $Hg^{II} > Sn^{II} > Pb^{II}$. Interestingly, after soaking MerB crystals with high concentrations of several essential metals (2 mM), we saw no binding of Cu^{II}, Ni^{II}, Fe^{II} or Co^{II} in the active site of MerB crystals. The only essential metal that appears to bind to

MerB is Zn^{II}, but this is not surprising if one considers that it is postulated that MerB originated through duplication of a treble-clef zinc-finger domain as discussed earlier. However, the affinity of MerB for Zn^{II} is several orders of magnitude lower than their affinity to metals like Hg^{II}, Sn^{II} and Pb^{II} as determined by ITC (unpublished data). This lower affinity of Zn^{II} could be attributed to the conversion from a zinc-binding site to a mercury-binding site as well as the fact that the aspartic acid residue is not as common in zinc-binding domains as are cysteine and histidine. Taken together, these results suggest that MerB seems to have the ability to distinguish between toxic metals and essential metals. These findings are consistent with the role of MerB in detoxification of organomercurial compounds in MeHg-contaminated environments without competition from other essential metals for the ultimate goal of bacteria survival.

In general, metalloproteins recognize their target metal based on a number of factors, including size, charge, coordination geometry and functional conformation. Remarkably, MerB displays a biological strategy for selective metal ion recognition. It remains to be answered what factors regulate metal recognition by the active site of MerB. In our study with MerB D99S and MerB-DMT, we highlighted the importance of some of the structural determinants of the ligands which retain the specificity and activity of the catalytic triad. We believe also that the correct ligand set and the cation-π interaction between Arg155 and Trp95 are important in keeping the functional geometry of the active site residues to enable metal selectivity. Based on our initial results with several metals, we could classify them into two groups. MerB was unable to bind transition metals which are located near the center of the periodic table, but it binds post transition metals like Pb and Sn, as well as group 12 elements. Interestingly, group 12 elements are classified as non-transition metals but rather as main group elements because of their electronic configuration. Thus, the catalytic triad of MerB appears to be able to distinguish between transition metals and main group elements. This MerB-specific view of periodic table may provide important insights into the factors affecting metal selectivity. The ability of MerB to discriminate between these various metals highlights another potential advantage of employing MerB in phytoremediation efforts since it has the ability to selectively bind toxic metals and leave behind the essential metals.

References

Aldridge, W. N. (1976) The Influence of Organotin Compounds on Mitochondrial Functions, In *Organotin Compounds: New Chemistry and Applications*, pp 186-196, ACS.

Andreottola, G., Dallago, L., and Ferrarese, E. (2008) Feasibility study for the remediation of groundwater contaminated by organolead compounds, *J. Hazard. Mater. 156*, 488-498.

Ansari, A. Z., Bradner, J. E., and O'Halloran, T. V. (1995) DNA-bend modulation in a repressor-to-activator switching mechanism, *Nature 374*, 371-375.

Ansari, A. Z., Chael, M. L., and O'Halloran, T. V. (1992) Allosteric underwinding of DNA is a critical step in positive control of transcription by Hg-MerR, *Nature 355*, 87-89.

Aschner, M., and Clarkson, T. W. (1989) Methyl mercury uptake across bovine brain capillary endothelial cells in vitro: The role of amino acids, *Pharmacol. Toxicol. 64*, 293-297.

Bakir, F., Damluji, S. F., Amin-Zaki, L., Murtadha, M., Khalidi, A., al-Rawi, N. Y., Tikriti, S., Dahahir, H. I., Clarkson, T. W., Smith, J. C., and Doherty, R. A. (1973) Methylmercury poisoning in Iraq, *Science 181*, 230-241.

Ballatori, N., and Clarkson, T. W. (1982) Developmental changes in the biliary excretion of methylmercury and glutathione, *Science 216*, 61-63.

Barkay, T., Miller, S. M., and Summers, A. O. (2003) Bacterial mercury resistance from atoms to ecosystems, *FEMS Microbiol. Rev. 27*, 355-384.

Barnes, J. L., McDowell, E. M., McNeil, J. S., Flamenbaum, W., and Trump, B. F. (1980) Studies on the pathophysiology of acute renal failure. V. Effect of chronic saline loading on the progression of proximal tubular injury and functional impairment

following administration of mercuric chloride in the rat, *Virchows Arch. B. Cell Pathol. Incl. Mol. Pathol. 32*, 233-260.

Begley, T. P., Walts, A. E., and Walsh, C. T. (1986a) Bacterial organomercurial lyase: overproduction, isolation, and characterization, *Biochemistry 25*, 7186-7192.

Begley, T. P., Walts, A. E., and Walsh, C. T. (1986b) Mechanistic studies of a protonolytic organomercurial cleaving enzyme: bacterial organomercurial lyase, *Biochemistry 25*, 7192-7200.

Benison, G. C., Di Lello, P., Shokes, J. E., Cosper, N. J., Scott, R. A., Legault, P., and Omichinski, J. G. (2004) A stable mercury-containing complex of the organomercurial lyase MerB: Catalysis, product release, and direct transfer to MerA, *Biochemistry 43*, 8333-8345.

Berlin, M., Zalups, R. K., and Fowler, B. A. (2007) Chapter 33 - Mercury, In *Handbook on the Toxicology of Metals (Third Edition)*, pp 675-729, Academic Press, Burlington.

Bernhoft, R. A. (2012) Mercury toxicity and treatment: a review of the literature, *J. Environ. Public Health 2012*, 460-508.

Bizily, S. P., Kim, T., Kandasamy, M. K., and Meagher, R. B. (2003) Subcellular targeting of methylmercury lyase enhances its specific activity for organic mercury detoxification in plants, *Plant Physiol. 131*, 463-471.

Bizily, S. P., Rugh, C. L., and Meagher, R. B. (2000) Phytodetoxification of hazardous organomercurials by genetically engineered plants, *Nat. Biotechnol. 18*, 213-217.

Borremans, B., Hobman, J. L., Provoost, A., Brown, N. L., and van der Lelie, D. (2001) Cloning and Functional Analysis of the pbr Lead Resistance Determinant of Ralstonia metallidurans CH34, *J. Bacteriol. 183*, 5651-5658.

Brown, N. L., Camakaris, J., Lee, B. T., Williams, T., Morby, A. P., Parkhill, J., and Rouch, D. A. (1991) Bacterial resistances to mercury and copper, *J. Cell. Biochem. 46*, 106-114.

Brown, N. L., Shih, Y. C., Leang, C., Glendinning, K. J., Hobman, J. L., and Wilson, J. R. (2002) Mercury transport and resistance, *Biochem. Soc. Trans. 30*, 715-718.

Brown, N. L., Stoyanov, J. V., Kidd, S. P., and Hobman, J. L. (2003) The MerR family of transcriptional regulators, *FEMS Microbiol. Rev. 27*, 145-163.

Buck-Koehntop, B. A., Porcelli, F., Lewin, J. L., Cramer, C. J., and Veglia, G. (2006) Biological chemistry of organotin compounds: Interactions and dealkylation by dithiols, *J. Organomet. Chem. 691*, 1748-1755.

Chang, C. C., Lin, L. Y., Zou, X. W., Huang, C. C., and Chan, N. L. (2015) Structural basis of the mercury(II)-mediated conformational switching of the dual-function transcriptional regulator MerR, *Nucleic Acids Res. 43*, 7612-7623.

Chien, M. F., Narita, M., Lin, K. H., Matsui, K., Huang, C. C., and Endo, G. (2010) Organomercurials removal by heterogeneous merB genes harboring bacterial strains, *J biosci bioeng 110*, 94-98.

Clarkson, T. W. (2002) The three modern faces of mercury, *Environ. Health Perspect. 110 Suppl 1*, 11-23.

Clarkson, T. W., and Magos, L. (2006) The toxicology of mercury and its chemical compounds, *Crit. Rev. Toxicol. 36*, 609-662.

Condee, C. W., and Summers, A. O. (1992) A mer-lux transcriptional fusion for real-time examination of in vivo gene expression kinetics and promoter response to altered superhelicity, *J. Bacteriol. 174*, 8094-8101.

Depew, D. C., Burgess, N. M., and Campbell, L. M. (2013) Spatial patterns of methylmercury risks to common loons and piscivorous fish in Canada, *Environ. Sci. Technol. 47*, 13093-13103.

Di Lello, P., Benison, G. C., Omichinski, J. G., and Legault, P. (2004a) 1H, 15N, and 13C resonance assignment of the 23 kDa organomercurial lyase MerB in its free and mercury-bound forms, *J. Biomol. NMR 29*, 457-458.

Di Lello, P., Benison, G. C., Valafar, H., Pitts, K. E., Summers, A. O., Legault, P., and Omichinski, J. G. (2004b) NMR structural studies reveal a novel protein fold for MerB, the organomercurial lyase involved in the bacterial mercury resistance system, *Biochemistry 43*, 8322-8332.

Dltri, F. M. (1991) Mercury contamination-what we have learned since Minamata, *Environ. Monit. Assess. 19*, 165-182.

Dltri, P. A., and Dltri, F. M. (1978) Mercury contamination: A human tragedy, *Environ. Manage. 2*, 3-16.

Dorea, J. G., Farina, M., and Rocha, J. B. (2013) Toxicity of ethylmercury (and Thimerosal): a comparison with methylmercury, *J. Appl. Toxicol. 33*, 700-711.

Dubalska, K., Rutkowska, M., Bajger-Nowak, G., Konieczka, P., and Namieśnik, J. (2013) Organotin Compounds: Environmental Fate and Analytics, *Crit. Res. Analyt. Chem. 43*, 35-54.

Eisler, R. (1988) Lead Hazards to Fish, Wildlife, and Invertebrates: A Synoptic Review, In *Contaminant Hazard Reviews*, Laurel, MD.

Fox, B., and Walsh, C. T. (1982) Mercuric reductase. Purification and characterization of a transposon-encoded flavoprotein containing an oxidation-reduction-active disulfide, *J. Biol. Chem. 257*, 2498-2503.

Furukawa, K., and Tonomura, K. (1971) Enzyme System Involved in the Decomposition of Phenyl Mercuric Acetate by Mercury-resistant Pseudomonas, *Agric. Biol. Chem. 35*, 604-610.

Garnier, R., Fuster, J. M., Conso, F., Dautzenberg, B., Sors, C., and Fournier, E. (1981) [Acute mercury vapour poisoning (author's transl)], *Toxicol. Eur. Res. 3*, 77-86.

Gopinath, E., and Bruice, T. C. (1987) Assistance of protodemercuration by bis-thiol ligation and nucleophilic catalysis. A model study which relates to the organomercurial lyase reaction, *J. Am. Chem. Soc. 109*, 7903-7905.

Greenwood, M. R. (1985) Methylmercury poisoning in Iraq. An epidemiological study of the 1971-1972 outbreak, *J. Appl. Toxicol. 5*, 148-159.

Griffin, H. G., Foster, T. J., Silver, S., and Misra, T. K. (1987) Cloning and dna-sequence of the mercuric-resistance and organomercurial-resistance determinants of plasmid PDU1358, *Proc. Natl. Acad. Sci. U. S. A. 84*, 3112-3116.

Hobman, J. L., and Crossman, L. C. (2015) Bacterial antimicrobial metal ion resistance, *J. Med. Microbiol. 64*, 471-497.

Hong, B., Nauss, R., Harwood, I. M., and Miller, S. M. (2010) Direct measurement of mercury(II) removal from organomercurial lyase (MerB) by tryptophan fluorescence: NmerA domain of coevolved gamma-proteobacterial mercuric ion reductase (MerA) is more efficient than MerA catalytic core or glutathione, *Biochemistry 49*, 8187-8196.

Huang, C. C., Narita, M., Yamagata, T., and Endo, G. (1999) Identification of three merB genes and characterization of a broad-spectrum mercury resistance module encoded by a class II transposon of Bacillus megaterium strain MB1, *Gene 239*, 361-366.

Hursh, J. B., Clarkson, T. W., Cherian, M. G., Vostal, J. J., and Mallie, R. V. (1976) Clearance of Mercury (Hg-197, Hg-203) Vapor Inhaled by Human Subjects, *Archives of Environmental Health: Inter. J. 31*, 302-309.

Hussein, H. S., Ruiz, O. N., Terry, N., and Daniell, H. (2007) Phytoremediation of mercury and organomercurials in chloroplast transgenic plants: enhanced root uptake, translocation to shoots, and volatilization, *Environ. Sci. Technol. 41*, 8439-8446.

Hynninen, A., Touze, T., Pitkanen, L., Mengin-Lecreulx, D., and Virta, M. (2009) An efflux transporter PbrA and a phosphatase PbrB cooperate in a lead-resistance mechanism in bacteria, *Mol. Microbiol. 74*, 384-394.

Jarvie, A. W. P., Markall, R. N., and Potter, H. R. (1981) Decomposition of organolead compounds in aqueous systems, *Environ. Res. 25*, 241-249.

Ji, G., and Silver, S. (1995) Bacterial resistance mechanisms for heavy metals of environmental concern, *J. Ind. Microbiol. 14*, 61-75.

Johs, A., Harwood, I. M., Parks, J. M., Nauss, R. E., Smith, J. C., Liang, L., and Miller, S. M. (2011) Structural characterization of intramolecular Hg(2+) transfer between flexibly linked domains of mercuric ion reductase, *J. Mol. Biol. 413*, 639-656.

Kaur, G., and Subramanian, S. (2014) Repurposing TRASH: Emergence of the enzyme organomercurial lyase from a non-catalytic zinc finger scaffold, *J. Struct. Biol. 188*, 16-21.

Kot, F. S., Rapoport, V. L., and Kharitonova, G. V. (2007) Immobilization of soil mercury by colloidal sulphur in the laboratory experiment, *Cent. Europ. J. .Chem. 5*, 846-857.

Kreevoy, M. M. (1957) Acid Cleavage of Methylmercuric Iodide, *J. Am. Chem. Soc. 79*, 5927-5930.

Kucharski, R., Zielonka, U., Sas-Nowosielska, A., Kuperberg, J. M., Worsztynowicz, A., and Szdzuj, J. (2005) A method of mercury removal from topsoil using low-thermal application, *Environ. Monit. Assess. 104*, 341-351.

Kulkarni, R. D., and Summers, A. O. (1999) MerR cross-links to the alpha, beta, and sigma 70 subunits of RNA polymerase in the preinitiation complex at the merTPCAD promoter, *Biochemistry 38*, 3362-3368.

Laddaga, R. A., Chu, L., Misra, T. K., and Silver, S. (1987) Nucleotide sequence and expression of the mercurial-resistance operon from Staphylococcus aureus plasmid pI258, *Proc. Natl. Acad. Sci. U. S. A. 84*, 5106-5110.

Lafrance-Vanasse, J., Lefebvre, M., Di Lello, P., Sygusch, J., and Omichinski, J. G. (2009) Crystal structures of the organomercurial lyase merb in its free and mercury-bound forms Insights into the mechanism of methylmercury degradation, *J. Biol. Chem. 284*, 938-944.

Leaner, J. J., and Mason, R. P. (2002) Methylmercury accumulation and fluxes across the intestine of channel catfish, Ictalurus punctatus, *Comparative Biochemistry and Physiology Part C: Toxi. Pharm. 132*, 247-259.

Ledwidge, R., Hong, B., Dotsch, V., and Miller, S. M. (2010) NmerA of Tn501 mercuric ion reductase: structural modulation of the pKa values of the metal binding cysteine thiols, *Biochemistry 49*, 8988-8998.

Ledwidge, R., Patel, B., Dong, A., Fiedler, D., Falkowski, M., Zelikova, J., Summers, A. O., Pai, E. F., and Miller, S. M. (2005) NmerA, the metal binding domain of mercuric ion reductase, removes Hg2+ from proteins, delivers it to the catalytic core, and protects cells under glutathione-depleted conditions, *Biochemistry 44*, 11402-11416.

Lee, D. J., Minchin, S. D., and Busby, S. J. W. (2012) Activating Transcription in Bacteria, *Annu. Rev. Microbiol. 66*, 125-152.

Lello, P. D., Lafrance-Vanasse, J., and Omichinski, J. G. (2010) The Organomercurial Lyase MerB, In *Handbook of Metalloproteins*, pp 1-13, John Wiley & Sons, Ltd.

Liu, J., Valsaraj, K. T., Devai, I., and DeLaune, R. D. (2008) Immobilization of aqueous Hg(II) by mackinawite (FeS), *J. Hazard. Mater. 157*, 432-440.

Lund, B. O., Miller, D. M., and Woods, J. S. (1993) Studies on Hg(II)-induced H_2O_2 formation and oxidative stress in vivo and in vitro in rat kidney mitochondria, *Biochem. Pharmacol. 45*, 2017-2024.

Lyyra, S., Meagher, R. B., Kim, T., Heaton, A., Montello, P., Balish, R. S., and Merkle, S. A. (2007) Coupling two mercury resistance genes in Eastern cottonwood enhances the processing of organomercury, *Plan. Biotech. J. 5*, 254-262.

Mailman, M., Stepnuk, L., Cicek, N., and Bodaly, R. A. (2006) Strategies to lower methyl mercury concentrations in hydroelectric reservoirs and lakes: A review, *Sci. Total Environ. 368*, 224-235.

Mason, R. P., and Benoit, J. M. (2003) Organomercury Compounds in the Environment, In *Organometallic Compounds in the Environment*, pp 57-99, John Wiley & Sons, Ltd.

Mason, R. P., Fitzgerald, W. F., and Morel, F. M. M. (1994) The biogeochemical cycling of elemental mercury: Anthropogenic influences, *Geochim. Cosmochim. Acta 58*, 3191-3198.

Mason, R. P., and Sheu, G. R. (2002) Role of the ocean in the global mercury cycle, *Global Biogeochem Cy 16*, 40-41-40-14.

Massacci, P., Piga, L., and Ferrini, M. (2000) Applications of physical and thermal treatment for the removal of mercury from contaminated materials, *Miner. Engineer. 13*, 963-967.

McGrath, S. P., Lombi, E., Gray, C. W., Caille, N., Dunham, S. J., and Zhao, F. J. (2006) Field evaluation of Cd and Zn phytoextraction potential by the hyperaccumulators Thlaspi caerulescens and Arabidopsis halleri, *Environ. Pollut. 141*, 115-125.

McGuirl, M. A., Bollinger, J. A., Cosper, N., Scott, R. A., and Dooley, D. M. (2001) Expression, purification, and characterization of NosL, a novel Cu(I) protein of the nitrous oxide reductase (nos) gene cluster, *J. Biol. Inorg. Chem. 6*, 189-195.

Meagher, R. B. (2000) Phytoremediation of toxic elemental and organic pollutants, *Curr. Opin. Plant Biol. 3*, 153-162.

Melnick, J. G., and Parkin, G. (2007) Cleaving mercury-alkyl bonds: a functional model for mercury detoxification by MerB, *Science 317*, 225-227.

Melnick, J. G., Yurkerwich, K., and Parkin, G. (2009) Synthesis, Structure, and Reactivity of Two-Coordinate Mercury Alkyl Compounds with Sulfur Ligands: Relevance to Mercury Detoxification, *Inorg. Chem. 48*, 6763-6772.

Merkle, S. A. (2006) Engineering forest trees with heavy metal resistance genes, *Silvae Genetica 55*, 263-268.

Miller, S. M. (1999) Bacterial detoxification of Hg(II) and organomercurials, *Essays. Biochem., Vol 34, 1999 34*, 17-30.

Miller, S. M. (2007) Cleaving C-Hg bonds: two thiolates are better than one, *Nat. Chem. Biol. 3*, 537-538.

Miller, S. M., Ballou, D. P., Massey, V., Williams, C. H., Jr., and Walsh, C. T. (1986) Two-electron reduced mercuric reductase binds Hg(II) to the active site dithiol but does not catalyze Hg(II) reduction, *J. Biol. Chem. 261*, 8081-8084.

Moore, M. J., Distefano, M. D., Zydowsky, L. D., Cummings, R. T., and Walsh, C. T. (1990) Organomercurial lyase and mercuric ion reductase: nature's mercury detoxification catalysts, *Acc. Chem. Res. 23*, 301-308.

Moore, M. J., Miller, S. M., and Walsh, C. T. (1992) C-terminal cysteines of Tn501 mercuric ion reductase, *Biochemistry 31*, 1677-1685.

Morby, A. P., Hobman, J. L., and Brown, N. L. (1995) The role of cysteine residues in the transport of mercuric ions by the Tn501 MerT and MerP mercury-resistance proteins, *Mol. Microbiol. 17*, 25-35.

Morel, F. M. M., Kraepiel, A. M. L., and Amyot, M. (1998) The chemical cycle and bioaccumulation of mercury, *Annu. Rev. Ecol. Syst. 29*, 543-566.

Nagata, T., Morita, H., Akizawa, T., and Pan-Hou, H. (2010) Development of a transgenic tobacco plant for phytoremediation of methylmercury pollution, *Appl. Microbiol. Biotechnol. 87*, 781-786.

Nascimento, A. M., and Chartone-Souza, E. (2003) Operon mer: bacterial resistance to mercury and potential for bioremediation of contaminated environments, *Genet. Mol. Res. 2*, 92-101.

Nesci, S., Ventrella, V., Trombetti, F., Pirini, M., and Pagliarani, A. (2011) Tributyltin (TBT) and mitochondrial respiration in mussel digestive gland, *Toxicol. In Vitro 25*, 951-959.

Ni, B., Kramer, J. R., Bell, R. A., and Werstiuk, N. H. (2006) Protonolysis of the Hg−C Bond of chloromethylmercury and dimethylmercury. A DFT and QTAIM Study, *J.Phys..Chem. A 110*, 9451-9458.

Nriagu, J., and Becker, C. (2003) Volcanic emissions of mercury to the atmosphere: global and regional inventories, *Sci. Total Environ. 304*, 3-12.

Olushola Sunday, A., Abdullahi Alafara, B., and Godwin Oladele, O. (2012) Toxicity and speciation analysis of organotin compounds, *Chemical Speciation & Bioavailability 24*, 216-226.

Omichinski, J. G. (2007) Biochemistry - Toward methylmercury bioremediation, *Science 317*, 205-206.

Osborn, A. M., Bruce, K. D., Strike, P., and Ritchie, D. A. (1997) Distribution, diversity and evolution of the bacterial mercury resistance (mer) operon, *FEMS Microbiol. Rev. 19*, 239-262.

Ou, L.-T., Thomas, J. E., and Jing, W. (1994) Biological and chemical degradation of tetraethyl lead in soil, *Bull. Environ. Contam. Toxicol. 52*, 238-245.

Ou, L. T., Jing, W., and Thomas, J. E. (1995) Biological and chemical degradation of ionic ethyllead compounds in soil, *Environ. Toxicol. Chem. 14*, 545-551.

Pagliarani, A., Bandiera, P., Ventrella, V., Trombetti, F., Pirini, M., Nesci, S., and Borgatti, A. R. (2008) Tributyltin (TBT) inhibition of oligomycin-sensitive Mg-ATPase activity in mussel mitochondria, *Toxicol. In Vitro 22*, 827-836.

Parkhill, J., Ansari, A. Z., Wright, J. G., Brown, N. L., and O'Halloran, T. V. (1993) Construction and characterization of a mercury-independent MerR activator (MerRAC): transcriptional activation in the absence of Hg(II) is accompanied by DNA distortion, *EMBO J. 12*, 413-421.

Parks, J. M., Guo, H., Momany, C., Liang, L. Y., Miller, S. M., Summers, A. O., and Smith, J. C. (2009) Mechanism of Hg-C Protonolysis in the Organomercurial Lyase MerB, *J. Am. Chem. Soc. 131*, 13278-13285.

Pennella, M. A., and Giedroc, D. P. (2005) Structural determinants of metal selectivity in prokaryotic metal-responsive transcriptional regulators, *Biometals 18*, 413-428.

Picaud, T., and Desbois, A. (2006) Interaction of Glutathione Reductase with Heavy Metal: The Binding of Hg(II) or Cd(II) to the Reduced Enzyme Affects Both the Redox Dithiol Pair and the Flavin, *Biochemistry 45*, 15829-15837.

Pitts, K. E., and Summers, A. O. (2002) The roles of thiols in the bacterial organomercurial lyase (MerB), *Biochemistry 41*, 10287-10296.

Qian, H., Sahlman, L., Eriksson, P. O., Hambraeus, C., Edlund, U., and Sethson, I. (1998) NMR solution structure of the oxidized form of MerP, a mercuric ion binding protein involved in bacterial mercuric ion resistance, *Biochemistry 37*, 9316-9322.

Quinn, C. F., Carpenter, M. C., Croteau, M. L., and Wilcox, D. E. (2016) Chapter One - Isothermal Titration Calorimetry Measurements of Metal Ions Binding to Proteins, In *Methods Enzymol.* (Andrew, L. F., Ed.), pp 3-21, Academic Press.

Rascio, N., and Navari-Izzo, F. (2011) Heavy metal hyperaccumulating plants: How and why do they do it? And what makes them so interesting?, *Plant Sci. 180*, 169-181.

Rossy, E., Seneque, O., Lascoux, D., Lemaire, D., Crouzy, S., Delangle, P., and Coves, J. (2004) Is the cytoplasmic loop of MerT, the mercuric ion transport protein, involved in mercury transfer to the mercuric reductase?, *FEBS Lett. 575*, 86-90.

Rugh, C. L., Wilde, H. D., Stack, N. M., Thompson, D. M., Summers, A. O., and Meagher, R. B. (1996) Mercuric ion reduction and resistance in transgenic Arabidopsis thaliana plants expressing a modified bacterial merA gene, *Proc. Natl. Acad. Sci. U. S. A. 93*, 3182-3187.

Ruiz, O. N., and Daniell, H. (2009) Genetic engineering to enhance mercury phytoremediation, *Curr. Opin. Biotechnol. 20*, 213-219.

Saint-Amour, D., Roy, M. S., Bastien, C., Ayotte, P., Dewailly, E., Despres, C., Gingras, S., and Muckle, G. (2006) Alterations of visual evoked potentials in preschool Inuit children exposed to methylmercury and polychlorinated biphenyls from a marine diet, *Neurotoxicology 27*, 567-578.

Satoh, M., Nishimura, N., Kanayama, Y., Naganuma, A., Suzuki, T., and Tohyama, C. (1997) Enhanced renal toxicity by inorganic mercury in metallothionein-null mice, *J. Pharmacol. Exp. Ther. 283*, 1529-1533.

Schartup, A. T., Balcom, P. H., Soerensen, A. L., Gosnell, K. J., Calder, R. S. D., Mason, R. P., and Sunderland, E. M. (2015) Freshwater discharges drive high levels of methylmercury in Arctic marine biota, *Proc. Natl. Acad. Sci*. *112*, 11789-11794.

Schiering, N., Kabsch, W., Moore, M. J., Distefano, M. D., Walsh, C. T., and Pai, E. F. (1991) Structure of the detoxification catalyst mercuric ion reductase from Bacillus sp. strain RC607, *Nature 352*, 168-172.

Schottel, J. L. (1978) The mercuric and organomercurial detoxifying enzymes from a plasmid-bearing strain of Escherichia coli, *J. Biol. Chem. 253*, 4341-4349.

Schuster, P. F., Krabbenhoft, D. P., Naftz, D. L., Cecil, L. D., Olson, M. L., Dewild, J. F., Susong, D. D., Green, J. R., and Abbott, M. L. (2002) Atmospherc mercury deposition during the last 270 years: a glacial ice core record of natural and anthropogenic sources, *Environ. Sci. Technol. 36*, 2303-2310.

Selin, N. E. (2009) Global Biogeochemical Cycling of Mercury: A Review, *Annu. Rev. Environ. Resour. 34*, 43-63.

Serre, L., Rossy, E., Pebay-Peyroula, E., Cohen-Addad, C., and Coves, J. (2004) Crystal structure of the oxidized form of the periplasmic mercury-binding protein MerP from Ralstonia metallidurans CH34, *J. Mol. Biol. 339*, 161-171.

Shewchuk, L. M., Helmann, J. D., Ross, W., Park, S. J., Summers, A. O., and Walsh, C. T. (1989) Transcriptional switching by the MerR protein: activation and repression mutants implicate distinct DNA and mercury(II) binding domains, *Biochemistry 28*, 2340-2344.

Sigel, A., Sigel, H., and Sigel, R. O. (2010) Alkylated compounds and their environmental toxicology, In *Organometallics in Environment and Toxicology* pp 153-162, RCS publishing.

Silver, S., and Phung, L. T. (2005) A bacterial view of the periodic table: genes and proteins for toxic inorganic ions, *J. Ind. Microbiol. Biotechnol. 32*, 587-605.

Smith, P. J., Langolf, G. D., and Goldberg, J. (1983) Effect of occupational exposure to elemental mercury on short term memory, *Br. J. Ind. Med. 40*, 413-419.

Steele, R. A., and Opella, S. J. (1997) Structures of the reduced and mercury-bound forms of MerP, the periplasmic protein from the bacterial mercury detoxification system, *Biochemistry 36*, 6885-6895.

Summers, A. O. (1986) Organization, Expression, and Evolution of Genes for Mercury Resistance, *Annu. Rev. Microbiol. 40*, 607-634.

Syversen, T., and Kaur, P. (2012) The toxicology of mercury and its compounds, *J. Trace Elem. Med. Biol. 26*, 215-226.

Taubner, L. M., McGuirl, M. A., Dooley, D. M., and Copie, V. (2006) Structural studies of Apo NosL, an accessory protein of the nitrous oxide reductase system: insights from structural homology with MerB, a mercury resistance protein, *Biochemistry 45*, 12240-12252.

Taugner, R., Winkel, K. z., and Iravani, J. (1966) [On the localization of mercuric chloride concentration in the rat kidney], *Virchows Arch. Pathol. Anat. Physiol. Klin. Med. 340*, 369-383.

Tezuka, T., and Tonomura, K. (1976) Purification and properties of an enzyme catalyzing the splitting of carbon-mercury linkages from mercury-resistant Pseudomonas K-62 strain. I. Splitting enzyme 1, *J. Biochem. 80*, 79-87.

Tezuka, T., and Tonomura, K. (1978) Purification and properties of a second enzyme catalyzing the splitting of carbon-mercury linkages from mercury-resistant Pseudomonas K-62, *J. Bacteriol. 135*, 138-143.

Ullrich, S. M., Tanton, T. W., and Abdrashitova, S. A. (2001) Mercury in the Aquatic Environment: A Review of Factors Affecting Methylation, *Critic. Rev. Environ. Sci. Technol. 31*, 241-293.

UNEP. (2013) Global Mercury Assessment 2013: Sources, Emissions, Releases and Environmental Transport., (Chemicals Branch, G., Switzerland, Ed.), UNEP Division of Technology, Industry and Economics, Chemicals Branch International Environment House.

Wagner-Dobler, I., von Canstein, H., Li, Y., Timmis, K. N., and Deckwer, W. D. (2000) Removal of mercury from chemical wastewater by microoganisms in technical scale, *Environ. Sci. Technol. 34*, 4628-4634.

Wahba, H. M., Lecoq, L., Stevenson, M., Mansour, A., Cappadocia, L., Lafrance-Vanasse, J., Wilkinson, K. J., Sygusch, J., Wilcox, D. E., and Omichinski, J. G. (2016) Structural and Biochemical Characterization of a Copper-Binding Mutant of the Organomercurial Lyase MerB: Insight into the Key Role of the Active Site Aspartic Acid in Hg–Carbon Bond Cleavage and Metal Binding Specificity, *Biochemistry 55*, 1070-1081.

Walsh, C., Distefano, M., and Moore, M. (1988a) Mutagenesis of paired cysteine residues in the disulphide-containing flavoprotein mercuric ion reductase from mercury-resistant bacteria, *Biochem. Soc. Trans. 16*, 90-91.

Walsh, C. T., Distefano, M. D., Moore, M. J., Shewchuk, L. M., and Verdine, G. L. (1988b) Molecular basis of bacterial resistance to organomercurial and inorganic mercuric salts, *FASEB J. 2*, 124-130.

Walts, A. E., and Walsh, C. T. (1988) Bacterial organomercurial lyase: novel enzymic protonolysis of organostannanes, *J. Am. Chem. Soc. 110*, 1950-1953.

Wang, J., Feng, X., Anderson, C. W., Xing, Y., and Shang, L. (2012) Remediation of mercury contaminated sites - A review, *J. Hazard. Mater. 221-222*, 1-18.

Wang, Q., Kim, D., Dionysiou, D. D., Sorial, G. A., and Timberlake, D. (2004) Sources and remediation for mercury contamination in aquatic systems--a literature review, *Environ. Pollut. 131*, 323-336.

Wang, Y., Moore, M., Levinson, H. S., Silver, S., Walsh, C., and Mahler, I. (1989) Nucleotide-sequence of a chromosomal mercury resistance determinant from a bacillus sp with broad-spectrum mercury resistance, *J. Bacteriol. 171*, 83-92.

Warkany, J. (1966) Acrodynia--postmortem of a disease, *Am. J. Dis. Child. 112*, 147-156.

Wilhelm, M., Deeken, S., Berssen, E., Saak, W., Lützen, A., Koch, R., and Strasdeit, H. (2004) The First Structurally Authenticated Organomercury(1+) Thioether Complexes − Mercury−Carbon Bond Activation Related to the Mechanism of the Bacterial Enzyme Organomercurial Lyase, *Eur. J. Inorg. Chem. 2004*, 2301-2312.

Wu, Z., Wang, B., He, J., and Chen, T. (2016) Synthesis of tunable-band-gap "Open-Box" halide perovskites by use of anion exchange and internal dissolution procedures, *J. Colloid Interface Sci. 461*, 162-167.

Yin, Z., Jiang, H., Syversen, T., Rocha, J. B. T., Farina, M., and Aschner, M. (2008) The methylmercury-L-cysteine conjugate is a substrate for the L-type large neutral amino acid transporter, *J. Neurochem. 107*, 1083-1090.

Zachariadis, G. A., and Rosenberg, E. (2012) Speciation analysis of triethyl-lead and tributyl-tin compounds in human urine by liquid-liquid extraction and gas chromatography microwave-induced plasma atomic emission detection, *J Sep Sci 35*, 1132-1137.

Zalups, R. K. (2000) Molecular Interactions with Mercury in the Kidney, *Pharmacol. Rev. 52*, 113-144.

Zhu, R., Gao, C., Sun, T., Shen, L., Sun, D., and Li, X. (2016) Surface decorating of CHNHPbBr nanoparticles with the chemically adsorbed perylenetetracarboxylic diimide, *Langmuir*, 3294–3299.